MEASUREMENT METHODS OF ACOUSTICAL PROPERTIES OF MATERIALS

SESSIONS

A state-of-the-art of in situ measurement of the sound absorption coefficient of road pavements

Michel Bérengier[(1)], Massimo Garai[(2)]

[(1)] L.C.P.C. - Centre de Nantes, Route de Bouaye, BP 4129, 44341 Bouguenais Cedex, France
[(2)] DIENCA - University of Bologna, Viale Risorgimento 2, 40136 Bologna, Italy

In complement to noise barriers, low-noise pavements are effective tools to control traffic noise. In addition to their good qualities regarding tyre/noise generation, they also have interesting sound absorption properties which contribute to their acoustic efficiency. To measure the sound absorption coefficient, an ***in situ*** test method is required. Several techniques based on impulsive methods have been tested. They can be used both for the determination of the absorption coefficient of road surfaces currently in use, as well as for the comparison of design specifications with current performance data after completion of the construction work.
First, the paper presents the various methods developed up to now and compares the results with those of other techniques like Kundt tube and propagation test at grazing incidence. Finally, the current method included in the ISO standard 13472-1, based on the use of a sequence of impulses is detailed. This allows the acquisition of the impulse response of the material under test in situ. Depending on the selected test signal, it is possible to obtain valid results in presence of high level of non-stationary background noise. Results obtained for various road porous pavements will be presented and compared to the last theoretical models.

INTRODUCTION

Since the development of new low-noise pavements, the sound absorption coefficient has always been considered as one of the most important physical parameter to measure in order to characterise the acoustical efficiency of a road pavement. This characteristic can be measured independently *in labo*, on bore cores extracted from the wearing course, by the Kundt tube technique [1] or *in situ* using various non destructive testing procedures. These procedures based on an impulse approach have been progressing for about twenty years according to the signal processing techniques evolution. Depending on the different measuring methods detailed in this paper, the sound absorption coefficient can be estimated under normal, oblique or grazing incidences. When possible, results obtained under perpendicular incidence will be directly compared to the impedance tube values.

THE SOUND ABSORPTION COEFFICENT MEASUREMENTS

Whatever the method used, the sound absorption coefficient is estimated through the sound reflection coefficient measurement. If $R_p(f)$ is the frequency dependent sound reflection factor, the sound absorption coefficient $\alpha(f)$ is identified by the following equation:

$$\alpha(f) = 1 - \left| R_p(f) \right|^2 \qquad (1)$$

A sound source and one or two microphones (depending on the technique) are located over the road surface under test. The sound source produces a transient sound wave which travels past the microphone position to the surface under test and is reflected. Each microphone receives both the direct sound pressure wave travelling from the sound source to the road surface and the sound pressure wave reflected by the road surface under test. These signals are processed in different ways, depending on the techniques used, as detailed in the following.

The measurement must take place in an essentially free field, i.e. a field free from reflections coming from surfaces other than the road surface to be tested. For this reason, depending on the techniques, a very short time signal (around 1 ms) or the acquisition of an impulse response having peaks as sharp as possible are recommended. Thus, the reflections coming from other surfaces than the road pavement can be identified from their time delay and rejected. To ensure an accurate averaged result, the test impulses emitted by the sound source must be as reproducible as possible.

Propagation technique under grazing incidence

This technique requires a set of two microphones located 4 m away from the impulse sound source. The first one (reference) is directly put on the road surface under test and the second one is situated at the same height as the source with respect to the road surface (0.60 m) (see figure 1). According to this measuring

procedure, the sound reflection factor of the road surface is determined from the estimation of its complex impedance Z.

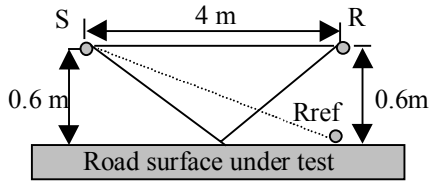

FIGURE 1. Measurement under grazing incidence : Geometrical set-up

This estimation is obtained through a Levenberg-Marquardt inverse fitting algorithm applied to the excess attenuation between the two microphones R and R_{ref}. To run this computing programme, the knowledge of an accurate propagation model together with adapted impedance models representative of various road pavements behaviour are required.

The different kinds of pavements are treated as finite or infinite layers of extended (porous pavement) or local (dense pavement) reaction materials. In this condition, and assuming an exp(-iωt) time dependence, the sound pressure level for a point source is given by the approximate solution of the Helmholtz equation :

$$\frac{p(f)}{p_0} = \frac{A_d}{r_d} exp(ik_d r_d) + \frac{Q(f) A_r}{r_r} exp(ik_r r_r) \quad (2)$$

where r_d and r_r represent the source/receiver and image-source/receiver distances respectively, A_d and A_r the amplitudes of the direct and reflected waves and k_d and k_r the corresponding wavenumbers. The function $Q(f)$ is the spherical reflection coefficient of the ground [3] function of the sound reflection factor $R_p(f)$ which can be expressed as a function of the surface impedance $Z(f)$.

For local reacting materials, $Z(f)$ is computed using the Delany and Bazley model [4]:

$$Z(f) = \left[1 + 0.051\left(\frac{f}{\sigma}\right)^{-0.75}\right] + i\left[0.077\left(\frac{f}{\sigma}\right)^{-0.73}\right] \quad (3)$$

For this model, only the airflow resistance of the material σ is required. For dense pavements (asphalt concrete, cement concrete, etc.), values between 2.10^4 and 10^5 $kNsm^{-4}$ are found.

For porous pavements, $Z(f)$ can be computed through a phenomenological model developed in France [5]. This model takes into account the thermal and viscous exchanges inside the structure. It needs the knowledge of the main four physical characteristics of the structure : the airflow resistance σ, the connecting porosity Ω, the tortuosity q^2 and the thickness ℓ. In most cases, the bottom layer underneath the porous layer has an infinite impedance Z_T. Under this condition, the surface impedance can be expressed as :

$$Z = \frac{Z_c}{\chi} coth(-ik\ell\chi) \quad (4)$$

where Z_c is the characteristic impedance, and $\chi = \left(1 - \left(\frac{k_0}{k}\right)^2 cos^2\varphi\right)^{1/2}$. φ is the angle between the incident wave and the road surface and k_0 is the wave number in the air.

For typical porous pavements, the fitting results give $\sigma \approx 10$ $kNsm^{-4}$, $\Omega \approx 15$ %, $q^2 \approx 2$ with a thickness $\ell = 0.04$ m, while for a porous pavement with a high void content, we obtain : $\sigma \approx 2$ $kNsm^{-4}$, $\Omega \approx 25$ %, $q^2 \approx 3.5$ for the same thickness ℓ.

Knowing $Z(f)$, $R_p(f)$ can be expressed by the equation :

$$R_p(f) = \frac{Z(f)\sin\varphi - \chi}{Z(f)\sin\varphi + \chi} \quad (5)$$

and then $\alpha(f)$ is calculated from equation 1.

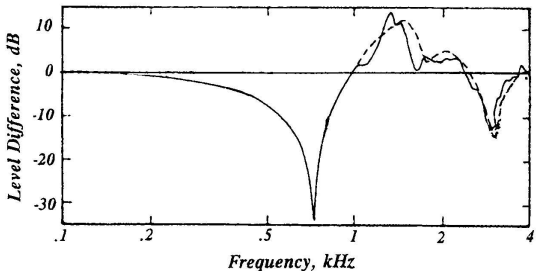

FIGURE 2. Result of the fitting procedure (——) : Experimental result, (----) : Prediction model

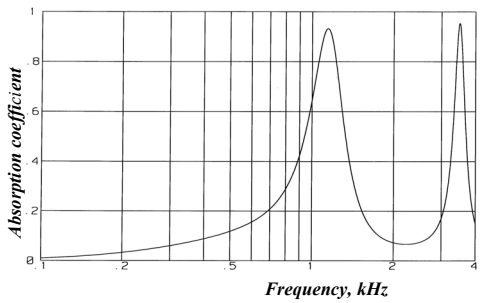

FIGURE 3. Predicted absorption coefficient from the fitted values of the physical parameters of the porous surface

In the case of a high porous drainage asphalt, figures 2 and 3 illustrate the various steps of the procedure. Figure 2 shows the result of the fitting procedure while figure 3 represents the computed values of $\alpha(f)$. The values of the fitted physical parameters are the following : $\sigma = 2$ kNsm^{-4}, $\Omega = 30$ %, $q^2 = 3.3$ with a thickness $\ell = 0.04$ m.

Local techniques under normal incidence

The direct and the reflected wave, received by the same microphone, are corrected for the path length difference; the power reflection factor of the road surface is then given by the ratio between the direct and reflected waves power spectra.

$$\left|R_p(f)\right|^2 = 1 - \frac{1}{K_r^2}\left|\frac{P_r(f)}{P_d(f)}\right|^2 \qquad (6)$$

where: K_r is the geometrical spreading factor [2,9] accounting for the path length difference between the direct and the reflected sound pressure wave. $P_r(f)$ is the spectrum of the sound pressure wave reflected by the road surface, as detected by the microphone and $P_d(f)$ the spectrum of the direct sound pressure wave travelling from the sound source to the road surface, as detected by the microphone.

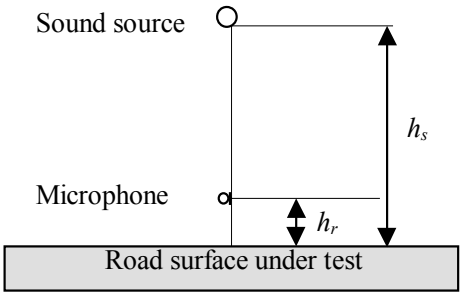

FIGURE 4. Measurement under normal incidence : Geometrical set-up

The basis of this technique has been developed in the years 1980 and standardised for the first time by the French standard organisation AFNOR in 1990 [6]. At that time, the impulse source was an 8 mm alarm pistol. Afterwards, this system has been progressively modified in order to integrate the last evolution of the signal processing techniques. Currently, the sound source is a loudspeaker fed by sequences of repeatable impulses. In both techniques, the general measurement set-up is identical and displayed on figure 4 and the active area which contributes to the reflection is about 3 m² [2,6].

Technique using a mechanical impulse

With this kind of source (alarm pistol shot), the signal characteristics were the following : very short impulse (around 1 ms), peak level close to 130 dB at 1 m, good energy distribution between 250 Hz and 3 kHz and rather good omnidirectionality (± 2 dB) in the perpendicular plane to the pistol barrel.

With this system, $R_p(f)$ is calculated from equation 6 after a windowing operation on the direct and reflected signals as shown on figure 5, and an averaging over 10 shots. Due to the delay between the two signals, function of the system geometry ($h_s = 2$ m and $h_r = 0.50$ m), the window size is about 3 ms. Considering this, the low frequency resolution is around 300 Hz. In addition, the high level of the shots induces some non-linearities in the high frequency domain (up to 2 kHz). In spite of these restrictions, some correct results have been found for various road pavements in the frequency range (400 Hz – 2 kHz). Figure 6 shows a comparison between measurements obtained following this method, the Kundt tube standard [1] on bore cores and the phenomenological theoretical model [5].

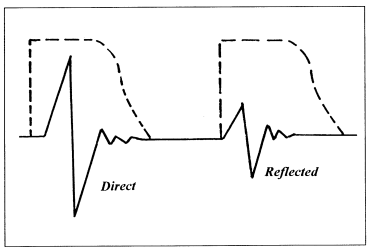

FIGURE 5. Temporal window

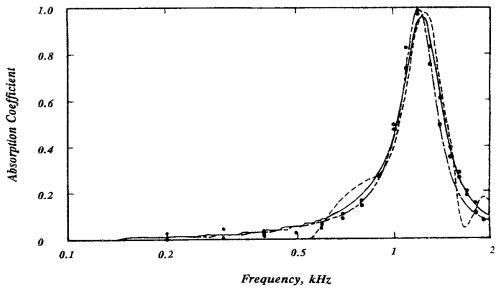

FIGURE 6. Comparison between measurements (--- : impulse technique ; ● ● ● : Kundt tube) and prediction (——)

Technique using sequences of repeatable impulses

The overall impulse response measured over the road surface consists of direct sound, reflection from the surface and other parasitic reflections. For further processing, the direct and the reflected sound wave

from the surface must be separated. This can be done in the time domain by a simple time windowing, identical to the previous method, when the time delay between the direct and reflected signals is sufficient or by cancellation of the direct sound wave from the overall impulse response by subtraction of an identical signal [7]. For this operation, the incident sound wave must be exactly known in shape, amplitude and time delay. In principle, this can be obtained performing a free-field measurement with the same geometrical configuration of the set-up keeping the distance between the microphone and the sound source strictly constant. This signal subtraction technique allows to position the microphone very close to the road surface and to take a temporal window for the reflected sound wave as large as allowed by the time delay between the reflected sound wave from the surface and the first parasitic reflection.

Whatever the road pavement structure, very small absorption values are measured in the low frequency range. Accurate values in this range are very difficult to obtain. Small variations of the sound pressure levels both of the direct and reflected signal can induce high discrepancies on the sound absorption values. This is due to the approximation concerning the frequency response of the system, which is assumed to be linear and frequency independent. In practice, this is not completely true. In order to avoid this problem, and to improve the accuracy of the method, a reference measurement performed on a totally-reflecting surface such as a smooth dense continuous concrete is used [8]. From the two measurements, one on the reference surface ($R_{p,ref,meas}(f)$) and the other on the road surface ($R_{p,road,meas}(f)$), the true sound pressure reflection factor of the road surface to be used in eq. 1 is computed as:

$$R_{p,road}(f) = \frac{R_{p,road,meas}(f)}{R_{p,ref,meas}(f)} \qquad (7)$$

For the measurement, an electro-acoustical source is used. This, receives an input electrical signal consisting of an impulse or a sequence of repeatable impulses. The crest factor of each impulse shall not be so high as to force the loudspeaker to operate in a non-linear manner. The usage of a maximum-length sequence (MLS) is recommended [9] to get the maximum noise rejection [9], but other signals can be used, provided that the *S/N* is not compromised. The *S/N* ratio can be improved by repeating the same test signal and synchronously averaging the microphone response.

Results can be given both in the 1/3 octave bands from 250 Hz to 4 kHz or in narrow bands if necessary.

Figure 7 shows a 1/3 octave bands comparison between a MLS and a sweep burst signals while figure 8 shows a narrow band comparison between a MLS and a mechanical impulse technique.

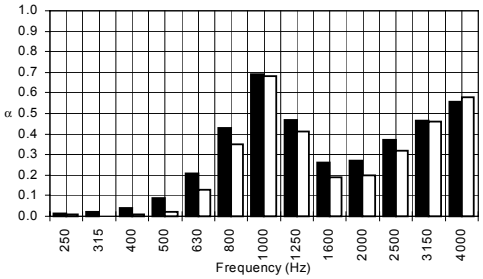

FIGURE 7. MLS (■) and sweep burst (□)

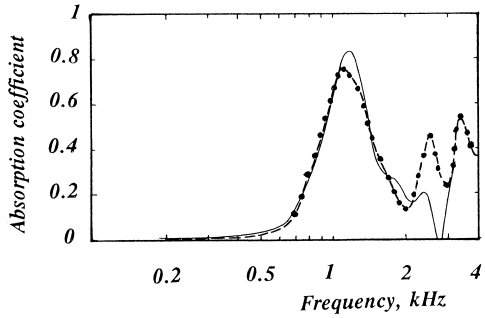

FIGURE 8. MLS (● - ●) and mechanical impulse (----)

CONCLUSION

The last method is robust enough and easy to use to be performed directly *in situ*. It is included in ISO standard 13472-1. Experimental results compare fairly well with the last theoretical model predictions concerning the acoustic behaviour of porous surfaces. With the various methods detailed in this paper, it is also possible, after some modifications in the post-processing software, to determine the acoustic impedance representative of the acoustic properties of road surfaces relevant to traffic noise prediction.

REFERENCES

1. ISO 10534-1, Acoustics - Determination of sound absorption coefficient and impedance in impedance tubes- Part 1: Method using standing wave ratio.
2. M. Bérengier, Y. Delanne, Bull. liaison Labo P. et Ch. **139**, 113-118 (1985).
3. M. Bérengier, M.R. Stinson, G.A. Daigle, J.F. Hamet, J. Acoust. Soc. Am. **101** (1), 155-162 (1997).
4. M.E. Delany, E.N. Bazley, Appl. Acoust. **3**, 105-116 (1970).
5. J.F. Hamet, M. Bérengier, Internoise 93, 641-646 (1993).
6. AFNOR 31089, Acoustique – Code d'essai pour la détermination de caractéristiques acoustiques installés en champ libre.
7. E. Mommertz, Appl. Acoust. **46**, 251-263 (1995).
8. M. Bérengier, ICA 95 (1995).
9. M. Garai, Appl. Acoust. **39**, 119-139 (1993).

Evaluation of Free Field Techniques for the Measurement of the Surface Impedance of Sound Absorbing Materials.

W.Lauriks[a], G.Jansens[a], J.F.Allard[b], L. De Geetere[a], G. Vermeir[a].

[a] *Laboratorium voor Akoestiek en Thermische Fysica, Universiteit Leuven, Celestijnenlaan 200D, Heverlee, Belgium.*

[b] *Institut d'Acoustique et de Méchanique, Université du Maine, Avenue Olivier Messiaen, Le Mans, France*

Measurements of the reflection coefficient or surface impedance of sound absorbing materials often require free field conditions since the behaviour of the material can be influenced by edge constraints (for instance in an impedance tube). Most methods extract the impedance from the measurement of the sound pressure in a few points using a model for the reflection of sound waves on the material. The accuracy of the method depends on the assumptions made in the model -for instance, several models require the material to be local reacting, others require a sound source located far from the surface-. In the low frequency region, diffraction from the edges of the sample under investigation will ultimately cause a bias in the measured sound pressures and hence result in a low frequency limit of the method. Different techniques to evaluate the surface impedance of sound absorbing materials will be discussed and compared in accuracy and ease-of-use. Possible sources of errors and methods to increase the frequency interval in which reliable results can be obtained will be discussed. Some of these techniques have a potential as an in situ technique to evaluate the surface impedance of building constructions in large rooms.

INTRODUCTION

Using the impedance tube for evaluating the acoustic impedance of sound absorbing materials may lead to erroneous results when the elasticity of the sample contributes to the sound field [1]. This is often the case with porous materials with medium and high flow resistivity or with materials covered with an impervious screen or a resistive membrane. Moreover, the current state-of-the-art of the software predicting the acoustic climate in rooms requires data for the impedance or absorption coefficient at oblique incidence. There is also an increasing demand for a technique to evaluate material performance in-situ.

The most versatile technique to evaluate the impedance at oblique incidence of a surface in the free field is the Near Field Acoustic Holographic Technique, introduced by Tamura [2] and developed further by several other laboratories [3,4]. This technique can even be used for the study of surface waves, propagating parallel to the surface [5]. However, the technique is time-consuming and can hardly be used in-situ conditions.

In the second half of the 80's, several laboratories developed free field techniques, based on the measurement of the sound pressure in two points above the sample (see e.g. [6]). This technique can be used in-situ under certain conditions [7]. More recently, the use of MLS sequences has led to a series of 'impulse techniques' [8,9] that give good results in-situ situations.

PROBLEM STATEMENT

In most situations, the sample dimensions are limited and obtaining good measurements requires two microphones and sound source to be placed *close* to the surface. Only in this way can unwanted reflections from the edges of the sample be adequately removed. However, placing the source and the receivers close to the surface means that the sound field cannot be modeled as a simple incident and reflected spherical wave. We want to evaluate the effect of short source-sample distances on the measuring conditions.

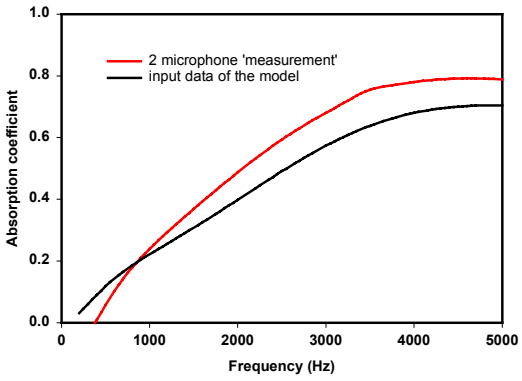

Figure 1. Simulation of the result of the two mictophone technique with the source at 20 cm from the surface, compared to absorption coefficient of the surface.

Figure 1 shows a numerical simulation of the impact of the position of the source on the result obtained with the two-microphone technique. The source was located at 20 centimeters above the surface, the sound field was calculated using the Sommerfeld integral and the absorption coefficient used as input for the calculation is also shown in the Figure.

THREE MICROPHONE TECHNIQUE

The reflected sound field can be written in integral form using the Sommerfeld integral:

$$p_r = \frac{ik}{2}\int_{-\infty}^{+\infty} R(q)\frac{qdq}{\mu}H_0^1(kqr)\exp(i\mu k(z+z_0))$$

where: $\mu = \sqrt{1-q^2}$, $\mathrm{Im}(\mu) > 0$, r is the horizontal distance between source and receiver and z and z_0 are the height of the source and the receiver and H_0^1 is the zero order Hankel function. For *locally reacting* materials, this expression depends only on the (constant) surface impedance Z_s and a procedure can be designed to find the best impedance that matches the experimental data [7].

However, a lot of materials are not locally reacting and this method cannot be applied in a general way. If the source is not too close to the surface, an approximation of the Sommerfeld equation can be obtained [10]:

$$p_r = \frac{\exp(ikr_1)}{r_1}\left[R(\theta_0) - \frac{iN}{kr_1}\right],$$

where θ_0 is the angle of specular reflection. This gives the possibility to extract the reflection coefficient as a function of the angle of incidence by measuring the sound pressure in three points above the surface [10]. Figure 2 below shows the reflection coefficient of a foam at normal incidence, measured with the traditional two-microphone technique, the Near Field Acoustic Holographic technique (NAH) and this three microphone technique. The results from the three microphone technique are satisfactory and the method allows the source to be placed closer to the sample than the two microphone technique.

However, this new method seems to be very sensitive to noise.

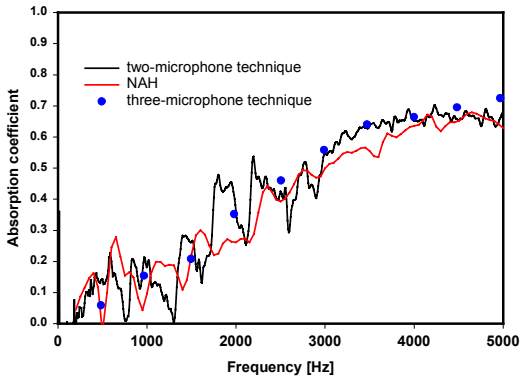

Figure 2. Comparison of the Near Field Acoustic Holographic technique with the traditional two microphone technique and the three microphone technique.

GRAZING INCIDENCE TECHNIQUE

When the material is non locally reacting, a technique similar to the one used by Chien and Soroka [11] can by used but the constant surface impedance must be replaced by the impedance at grazing incidence [12,13]. The surface impedance at grazing incidence can than be obtained for non-locally reacting surfaces at very short source-receiver distances. First results can be found in [12] and further results will be presented.

REFERENCES

1. Vigran, T. E., Kelders, L., Lauriks, W., Leclaire, Ph., and Johansen, **T. F.** *Acustica/Acta Acustica* **83,**419-423 (1997
2. M. Tamura, *J. Acoust. Soc. Am.* **88**, 2259-2264 (1990)
3. Verhaegen, C., Lauriks, W., and Cops, A *Proceedings InterNoise,* 241 - 246 . (1992)
4. J. Tizianel, F.F. Allard, W. Lauriks, L. Kelders *J.Sound and Vibration* **202**, 600-604 (1997)
5. L. Kelders, J.F. Allard, W. Lauriks *J. Acoust. Soc. Am.* **103**, 882-889 (1998)
6. Allard, J. F., Cops, A, and Lauriks, W. *Proceedings InterNoise* **1099** - 1102 . (1988)
7. Allard J. F. , Champoux Y., *Noise Control Engineering Journal* **32**, 15-23 (1989)
8. Garai M., *Applied Acoustics* **39**, 119-139 (1993)
9. Mommertz E., *Applied Acoustics* **46**, 251-263 (1995)
10. G.Jansens, W.Lauriks, G.Vermeir, J.F.Allard, *submitted to JASA,* 2001
11. C.F. Chien, W.W. Soroka *J.Sound and Vibration* **43**, 9-20 (1975)
12. J.F. Allard, M. Henry, V. Gareton, G. Jansens, W. Lauriks. *submitted to JASA,* 2001
13. C. Nocke, H.V. Fuchs, V.Mellert *Acustica united with Acta Acustica* **85**, 586-590 (1999)

A Method for Measuring Oblique Incidence Absorption Coefficient of Absorptive Panels by Stretched Pulse Technique

K. Kimura and K. Yamamoto

Kobayasi Institute of Physical Research, 3-20-41 Higashi-motomachi, Kokubunji, Tokyo, 185-0022 Japan

It is important to reduce noise reflected from highway structures such as the ceiling of double deck viaducts, where absorptive materials can be installed for this purpose. The potential effectiveness of such materials can be estimated using the oblique incidence absorption coefficient in a semi-anechoic room. The method for measuring oblique incidence absorption coefficient was proposed for optimum Aoshima's time-stretched pulse (OATSP). It is also very important to use this technique in *in-situ* measurement of absorption coefficient for sound absorbing materials attached to structures such as noise barriers and ceilings of double deck viaducts. Using this method, field measurements are carried out at four different sites where absorptive panels are mounted to the underside of upper decks of elevated roads. It is shown that oblique incidence absorption coefficient measured in the field shows good agreement with the results in the laboratory.

INTRODUCTION

In order to decrease the sound reflected from the underside of the upper decks of elevated roads with a double deck structure, highly absorptive materials have been attached to areas of reflection. Based upon a time-stretched pulse technique, a practical method for measuring oblique incidence absorption coefficient was proposed[1]. The oblique incidence absorption coefficient is estimated from insertion loss, which is determined by the ratio of sound energy reflected from a sample surface to that reflected from a concrete floor. The measurements for a fibrous material shows good agreement with theoretical values which were calculated from the surface impedance of the material.

Oblique incidence absorption coefficient is measured for the purpose of estimating the acoustical performance of absorptive panels, installed in locations such as ceilings of double deck viaducts. It is very important that the acoustical performance of the absorptive panels be verified in field study, displaying noise reduction ability in the field similar to that shown in the semi-anechoic room. It is therefore essential to select and produce materials with consistent noise reduction ability.

Measurement of oblique incidence absorption coefficient

Optimum Aoshima's time-stretched pulse (OATSP) is applied to the measurement of a reflected wave. Figure 1 shows an example of the test signal waveform of OATSP. Figure 2 shows the compressed waveform which is obtained after being passed through a inverse filter.

FIGURE 1. The time domain of the test signal for this measurement.

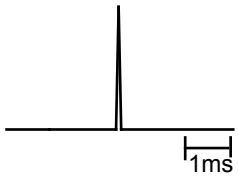

FIGURE 2. A compressed waveform where the test waveform where the test signal is passed through a inverse filter.

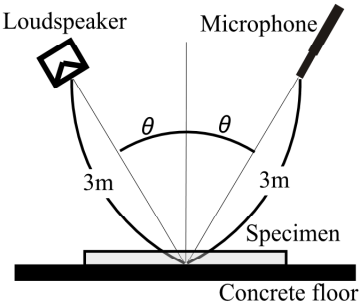

FIGURE 3. Geometrical arrangement of Loudspeaker and Microphone in the semi-anechoic room.

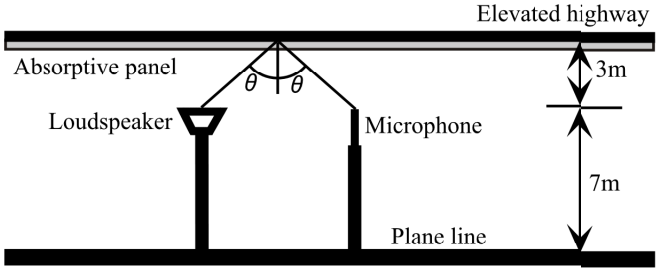

FIGURE 4. Geometrical arrangement of Loudspeaker and Microphone *in-situ.*

The measurement of absorptive panels attached at road structures were taken using the same method used in the semi-anechoic room for the verification of acoustical performance of absorptive panels as shown in Fig.3. A loudspeaker and a microphone were arranged at specular symmetric positions in relation to the underside of the upper deck of double deck viaducts as shown in Fig.4. The measurement point was a median in the center of the road. The loudspeaker and the microphone were each clamped to the tips of poles. The height of underside of upper deck was about 10m. The height of the loudspeaker and the microphone was about 7m from ground level. The distance from both the loudspeaker and the microphone to the center of the floor was 3m in the measuring room. On site, the loudspeaker and the microphone were moved parallel to the overhead surface. Thus, the distance from both the loudspeaker and the microphone to the underside of upper deck was about 3m. The angles of both the loudspeaker and the microphone in relation to the test panel were changed. The angle of sound incidenceθ was varied from 0° to 45° in intervals of 15° in the measuring room. However, it is difficult to set the loudspeaker and the microphone at the angleθ=0° on site. The loudspeaker and the microphone were both set at 5° .

RESULTS

The measurements were taken in four different sites of the underside of the upper decks of elevated roads. The panels which have been attached to these surfaces have the ability to reduce reflected noise by 10dB or more. A reduction of 10dB is equal to 0.90 at the averaged oblique incidence absorption coefficient. The averaged oblique incidence absorption coefficient, which is averaged over incident angles and weighted on the representative spectrum of A-weighted road traffic noise, is proposed as a single number index for the evaluation of noise control design at highways.

Random samples of the panels were inspected in the laboratory before being installed at the site. Figure 5 shows the comparison of the measurements taken in the laboratory and in the field. The averaged oblique incidence absorption coefficient is in good agreement with both measurement sites. When testing is done on absorptive panel with a noise reduction ability of 0.95 and over for averaged oblique incidence absorption coefficient, there are good results at any angle. However, when testing is done on panels with an ability of 0.9 to 0.95, results of the laboratory and on site measurements began to diverge. This error of margin is decreased when testing is done on absorptive panels of high quality, as the results are calculated from insertion loss based on dB.

CONCLUSION

The noise reduction ability of absorptive panels to be attached on the underside of the upper decks of elevated roads can be accurately estimated using the oblique incidence absorption coefficient. The measurement *in-situ* was the same method as in a semi-anechoic room. The field measurements were carried out in four different sites of the underside of the upper decks of elevated roads. In this case, oblique incidence absorption coefficient measured in the field shows good agreement with results from the laboratory.

REFERENCE

1. Kimura K., Yamamoto K. A method for measuring oblique incidence absorption coefficient of absorptive panels by stretched pulse technique. Applied Acoustics 2001;62: 617-632.

Table 1. Averaged oblique incidence absorption coefficient of absorptive panel

	Site-A	Site-B	Site-C	Site-D
Measured in the room	0.93	0.96	0.95	0.96
Measured in the field	0.91	0.97	0.96	0.97

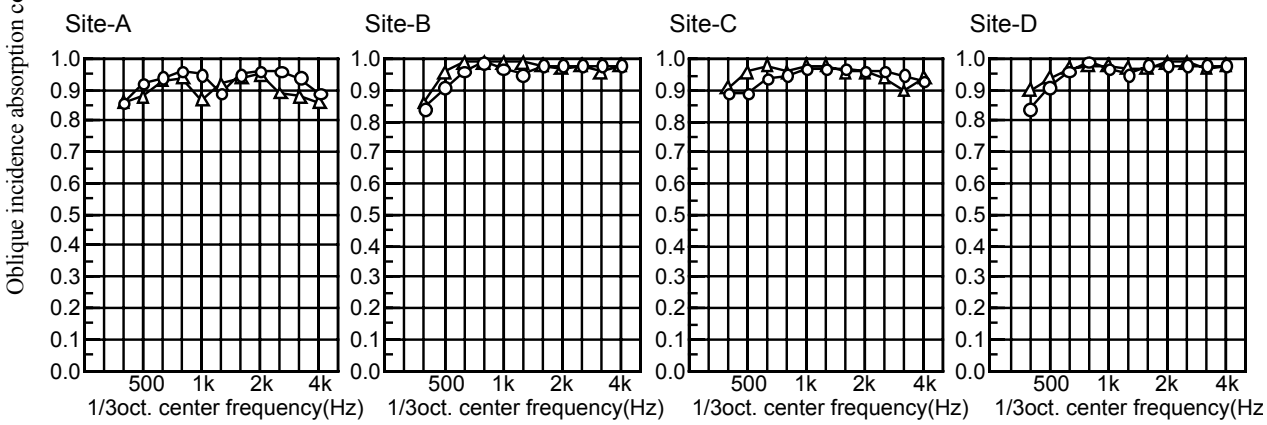

FIGURE 5. The comparison of the average value of the absorption coefficients in the measuring room and in the field.
○－○ Measured in the measuring room; △－△ measured in the field

Measurement of non-uniform impedance surface by the two microphone method

T.Wu, Y.W.Lam and T.J.Cox

School of Acoustics and Electronic Engineering, University of Salford, M5 4WT, UK

Characterising the acoustical properties of a surface, in terms of surface impedance is important. The two microphone method has been applied successfully to the measurement of the absorption coefficient of uniform impedance surface. However, its ability to measure non-uniform impedance surfaces has not been fully explored. In the project described in this paper, the two microphone method was used to measure the absorption coefficient of a non-uniform impedance surface. The sample was a profiled absorber and measurements were made in an anechoic chamber under oblique incidence. The results are compared with predictions. Good agreement has been found in low and middle frequency ranges, where specular reflection dominates the scattered sound field. Significant deviations appear when there is more than one dominating reflected wave; possible solutions to this will be presented.

INTRODUCTION

Two microphone methods has been developed for measuring absorption coefficients of uniform impedance surfaces in the free field. The importance of the sound absorption of non-uniform impedance surfaces, such as noise-barriers, profiled absorbers *etc.* is widely acknowledged, however, the ability to characterise this kind of structure by the two microphone technique has not been fully investigated. Garai[1] has investigated the measurement of the sound absorption of non-flat barriers under oblique incident conditions by the two microphone system, and the results showed a higher absorption coefficient than expected, which was due to the scattering of sound in non-specular directions.

In this paper, the absorption coefficient of a profiled absorber, which contains a non-uniform impedance surface, has been measured using oblique incident sound by the two microphone system in an anechoic chamber. The results showed good agreement in low and middle frequency ranges, where specular reflections dominated the scattered sound field.

DESCRIPTION OF THE METHOD

The two microphone method is illustrated in Figure 1. Let d_1, and d_2 be the distances between the panel and the microphones M_1, M_2 respectively. Let p_1 and p_2 be the pressure at M_1 and M_2. k is the sound propagation number, ϑ is the sound incident angle.

The two microphone technique is based on the flat uniform impedance surface, where only specular reflections exist. The sound field at i point in front of the panel will be:

$$p_i = Ae^{-jk_x x_i - jk_y y_i} + RAe^{+jk_x x_i - jk_y y_i} \qquad (1)$$

where R is the reflection coefficient of the sample, $k_x = k\cos\theta$ and $k_y = k\sin\theta$. So R could be derived from measurements data at point M_1 and M_2:

$$R = \frac{p_1/p_2\, e^{jkd_2\cos\theta} - e^{jkd_1\cos\theta}}{e^{-jkd_1\cos\theta} - p_1/p_2\, e^{-jkd_2\cos\theta}} \qquad (2)$$

the absorption coefficient $\alpha = 1 - |R|^2$

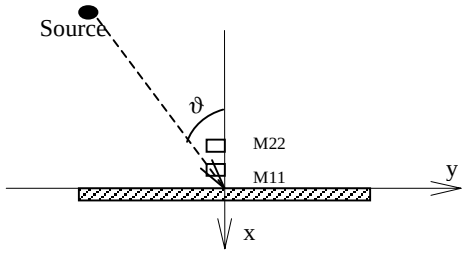

Figure 1. Description of two microphone system

SOUND FIELD IN FRONT OF A PROFILED ABSORBER

The profiled absorber tested here, as shown in Figure 2, is a periodic surface structure with rigid construction and a resistive layer on the top. The elements of the structure are wells of the same width separated by thin fins. Within one period, the depth sequence has been optimised to give the optimal absorption performance over the frequency range of interest [2]. It is a non-uniform, periodic impedance structure. For the one-dimensional absorber, the sound field in front of the absorber is decomposed into the incident plane wave $p_e(x,z)$ and scattered field $p_s(x,z)$

$$p(x,z) = p_e(x,z) + p_s(x,z)$$
$$p_e(x,z) = P_e e^{j(xk_x + zk_z)} \quad (3)$$
$$p_s(x,z) = \sum A_n e^{j(-x\beta_n - z\gamma_n)}$$

where $k_x = k\sin\theta_e, k_z = k\cos\theta_e$,and $\beta_n = k_x + n\frac{2\pi}{T}$

$\gamma_n = -jk\sqrt{(\sin\theta_e + n\frac{\lambda}{T})^2 - 1}$, T is the width of one period. Details of the prediction method used to calculate the absorption coefficient on the surface of the profiled absorber is in reference 2.

$$\alpha(\theta_e) = 1 - \left|\frac{A_0}{P_e}\right|^2 - \frac{1}{\cos\theta_e}\sum\left|\frac{A_{n_s}}{P_e}\right|^2\sqrt{1-(\sin\theta_e + n_s\lambda/T)^2} \quad (4)$$

where n_s is the radiating index in the far field.

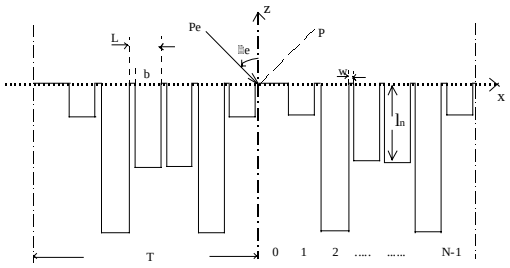

Figure 2. A one dimensional profiled absorber

TWO MICROPHONE SIMULATION

Two samples have been tested in simulations. They have the same depth sequence as in one period, but different width and top resistant layer. The incident angle is 30° vertical. The simulation results are shown in Figure 3. It can been seen in a), that the two microphone simulation worked for sample one even for the frequency range above 1.7kHz, where two reflection terms occur. This is because the specular reflection term dominated the sound field and made the biggest contribution. For example, at frequency f=2kHz, A_0=0.46, A_{-1}=0.09. A big difference has been shown in b) with sample two simulation at frequency range above 1.7kHz, where more than one reflection terms are significant. For example, at f=2kHz, A_0=0.29, A_{-1} =0.47.

In order to solve the more component problems, three microphone simulation has been tried for sample two, and the result shown in Figure 3b) has a very good agreement with prediction.

MEASUREMENT VERIFICATION

A 1x1m example of sample 1 was made, which contains 7 periods. The measurements have been carried out in an anechoic chamber under 30° vertical incident sound. The result is shown in Figure 3a), the good agreement can been seen between the prediction, measurement and simulation.

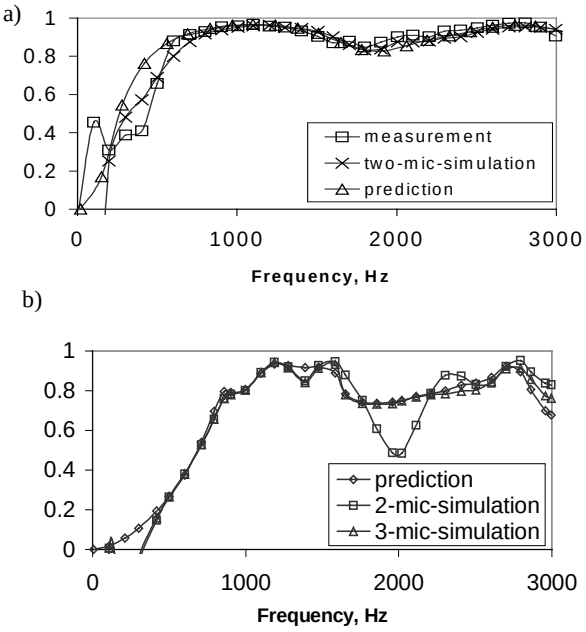

Figure 3. Absorption comparison of the simulation, prediction and measurement. a) Sample one; b) Sample two

CONCLUSION

This investigation showed that the two microphone method could be applied to a non-uniform impedance surface to measure the absorption coefficients, provided that the specular reflection dominates the sound field. When specular reflections do not dominate the sound field, the multiple microphone method can be used to solve the strong scattering problems. This method has been investigated, and the results will be published in the future paper.

ACKNOWLEDGMENTS

This work was funded by Engineering and Physical Sciences Research Council (EPSRC) of Britain, under Grant No. GR/L34396.

REFERENCES

1. M. Garai and A. Cocchi, Inter-noise **96**, 757-762 (1996).
2. T. Wu, T.J.Cox and Y.W.Lam, J. Acoust. Soc. Am. **108** (2), 643-650 (2000).

An Intercomparison of Laboratory Measurements of Flow Resistance

M. Garai, F. Pompoli

D.I.E.N.C.A., University of Bologna, Viale Risorgimento 2, 40136 Bologna, Italy

This paper presents the results of an Inter-Laboratory Test (ILT) of airflow resistance measurements on acoustic materials following the ISO 9053 Standard. Each of nine European laboratories received two sheets of melamine foam of different thickness, taken from the same factory batch. The laboratories cut the test samples from the supplied sheets and carried out measurements in repeatability conditions, either on a single sample either on different samples in order to take into account also the influence of the sample cutting and dishomogeneity of the foam. The main result of this European ILT is the determination of the repeatability and reproducibility standard deviation values typical of these measurements. The data show that most of the laboratories have a good internal repeatability, even if some measurement devices seem to give a better performance than others. On the other hand, the overall reproducibility is only fair, mainly due to systematic deviations inherent in the current laboratory practice; it is suggested that more attention on the calibration of the measurement procedures could lead to better values.

INTRODUCTION

The airflow resistance of porous materials is an important parameter, that gives information on their structural and acoustical properties. Its measurement is standardised in ISO 9053 [1], which contemplates two different methods: the direct airflow method is characterised by the passing of an unidirectional airflow through a test specimen; the alternating airflow method is characterised by a sinusoidal airflow with a frequency of 2 Hz. The Standard only specifies the accuracies for the direct measurements of differential pressure between the two sides of the specimen, the volumetric airflow rate and the thickness of the specimen. The overall accuracy of the measurement is not specified; an inter-laboratory precision experiment was planned but not yet accomplished.

The purpose of the present ILT is the determination of the repeatability and reproducibility standard deviation values (s_r and s_R), applying the statistical procedures recommended for this kind of projects by ISO 5725-2 Standard [2]. The ILT was co-ordinated by the Engineering Department of the University of Ferrara and D.I.E.N.C.A. of the University of Bologna and was performed during the year 2000.

TEST DESCRIPTION

The participation to the project was opened to all laboratories having a flow resistance measurement apparatus; the test material was sent to eleven European laboratories, nine of which sent back their results (Tab.1). Nearly all the laboratories adopted the continuos airflow method; two laboratories repeated the measurements using two different devices. In these cases only the results of one apparatus have been utilised for the calculation of s_r and s_R, in order to keep the conditions for a "blind test". For confidentiality reasons, all results are reported here without reference to the laboratory. From preliminary tests melamine foam has resulted a material with an homogeneous airflow permeability, so it has been selected as test specimen; in fact, the lack of homogeneity can be a cause of relevant errors for these kind of test.

For this ILT panels with planar surfaces, a nominal density of $10 \pm 1{,}5$ Kg/m^3 and two different thicknesses (40mm and 60mm) have been used. For each thickness, a sheet of material, large enough to cut 5 samples, has been sent to each laboratory. The cutting operation was left to the operators of each laboratory, because this is included in the error factors that influence the measurement. For each thickness, two different tests in repeatability conditions have been

Table 1: ILT laboratories and measurement methods.

Laboratory	*Method*
BRE - Acoustics Centre (UK)	Direct
Danish Technological Institute - Building Components - Teknologiparken (D)	Direct
Department of Physics-University of Leuven (B)	Direct
DETEC- University of Napoli (I)	Direct
DIF, University of Ferrara & DIENCA, University of Bologna (I)	Alternating
DITEC, University of Genova (I)	Direct
Muller-BBM (D)	Direct
Turku regional institute of occupational health (FIN)	Direct
Versucht und Forschungsanstalt WIEN - MA 39 - VFA (AUT)	Direct

conducted: 1) on the same sample, measured five times, each time mounted and dismounted from the sample holder; 2) on five different samples, to evaluate also the effect of sample cutting and material dishomogeneity.

Some discrepancies were found among the test reports, but at the moment it has been decided to use all data for the statistical calculation, leaving to a successive critical analysis the observations on the different test procedures adopted by the laboratories.

RESULTS

The test results were sent by participants to the ILT supervisor, at the Engineering Department of the University of Ferrara. They were analysed according to the ISO Standard [2] for the determination of repeatability and reproducibility of a measurement method. This permitted to obtain the repeatability and reproducibility standard deviations s_r and s_R.

The repeatability values s_r are very low for the repeated measurements on a single sample (2,4-2,8%)

Table 2: final results of the ILT: for each test, the general mean m, the repeatability and reproducibility standard deviation (s_r and s_R) and their relative values with reference to the general mean m are reported.

	60mm 1 Sample	*60mm 5 Samples*	*40mm 1 Sample*	*40mm 5 Samples*
m (Ns/m^4)	11.425	11.107	10.096	9763
s_r (Ns/m^4)	273	606	279	574
s_R (Ns/m^4)	1.949	1.923	1.018	1.211
s_r (%)	2,4	5,5	2,8	5,9
s_R (%)	17,1	17,3	10,1	12,4

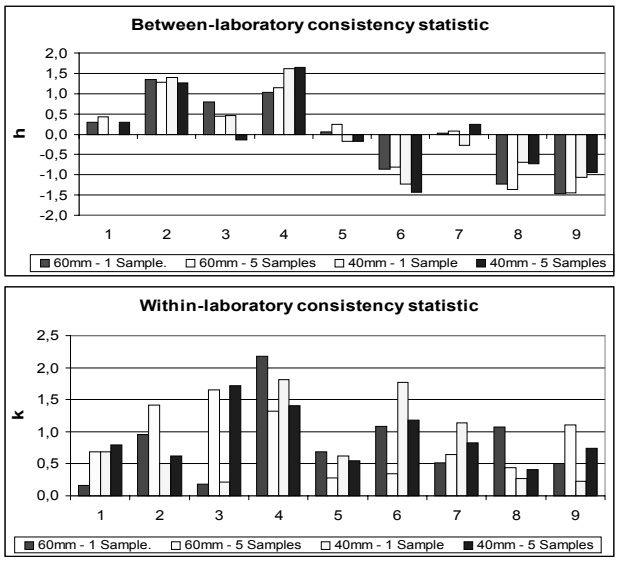

FIGURE 1: statistical consistency test according to ISO 5725-2 Standard (graphical technique): graphs of h (between-laboratory consistency statistic) and k (within-laboratory consistency statistic).

and slightly higher for the test with five specimens (5,5-5,9%), while the reproducibility values s_R are considerably higher, ranging from 10,1% to 17,3%. Statistical tests were also conducted, with graphical and numerical (Cochran's test [2]) methods, to evaluate the consistency of data; the graphs of the h and k parameters where obtained: they indicate the statistical consistency between laboratories and within a laboratory, respectively (Fig.1); upper limiting values of h and k for nine laboratory and five measurements are h=2,13 and k=1,73 (1% significance level); it can be seen that just one laboratory reaches these limits in one test; also Cochran's test gives evidence to this small anomaly. Excluding these data doesn't conduct to significant differences on s_r and s_R values.

DISCUSSION AND CONCLUSIONS

It is possible to deduce some observations:

- The internal laboratory repeatability is good, both for the 1-sample and 5-samples tests. The standard method shows a good s_r, varying from 2,1 to 2,8% (1 sample) and 5,5 to 5,9% (5 samples). Among laboratories, the repeatability is not constant (0,4-5,6%) for 1 sample, 1,5-10,2% for 5 samples); this indicates that some apparatus are more accurate than the others.
- The reproducibility of measurements is fair (10,1-17,1% for 1-sample, 12,4-17,3% for 5-sample tests). Fig.1 shows that mean values of single laboratories are really different; h graph shows that the between laboratories consistency has the same sign and similar values in the four tests for most laboratories; this indicates a similar difference from the general mean and gives evidence to systematic errors in the different devices. In fact, it can be noticed that the Standard [1] describes a calibration system only for the alternating airflow method; it seems appropriate to introduce a calibration procedure also for the direct airflow method.
- The examination of test reports reveals that some laboratories use high airflow velocities, not following the Standard [1]. This is due to the difficulty to measure low pressure differences but can increase internal dissipative phenomena. In fact these laboratories exhibit a tendency to give higher airflow resistance values.

REFERENCES

1. ISO 9053: 1991
2. ISO 5725-2: 1994

The participating laboratories and Prof. Roberto Pompoli, co-ordinator of this project, are gratefully acknowledged.

Applications of a free-field transfer function method to measure the acoustic impedance

C. Nocke, V. Mellert

University of Oldenburg, Physics Department- Acoustics, D - 26111 Oldenburg, Germany

Several in-situ methods have been suggested to investigate the acoustic performance of absorbing or reflecting materials. After a short review of historical methods one of these modern methods, the transfer function method [1], will be briefly described and some results will be presented. These results compare well with other methods for many materials.

GENERAL INTRODUCTION

Apart from standardised methods like standing wave tube and reverberation chamber measurements there have been several approaches to deduce the absorption coefficient or impedance under approximated free-field conditions. Many of the existing procedures assume plane wave propagation and can thus be referred to as geometrical procedures.

BRIEF HISTORICAL REVIEW

One of the earliest set-ups to measure the absorption of a material in-situ has been proposed by CREMER [2] in 1933 by investigating standing waves in front of a reflecting surface. In 1934 SPANDÖCK [3] presented a method using short tones with 800 Hz and 4000 Hz of only 1/200 s duration. By this he was able to separate the reflected signal from the incident signal in front of a reflecting surface. Similar to CREMER'S approach INGARD/BOLT [4] investigated the sound field in front of a surface and compared it with the sound field in front of a perfectly reflecting surface. This comparison allowed to deduce the absorption coefficient and the impedance respectively. For small angles of incidence these authors give a clear hint that the influence of sphericity of the sound waves might influence the result especially at low frequencies. Further methods have been described by DAVIES/MULHOLLAND [5] and KINTSL [6] also using a comparison of two measurements, one without reflection and the other with reflections at the surface investigated. KINTSL [6] deduces a formula later quoted by GARAI [8] and in [10] to calculate the area influencing the reflection. HEINZ/WILMS [7] and GARAI [8] show the first applications of modern MLS-based measurement equipment to deduce absorption coefficients in-situ. A MLS-based procedure similar to SPANDÖCKS [3] method is introduced by MOMMERTZ [9] as subtraction technique. This method has been modified to be used as a standard procedure described in draft ENV 1793 [10], part 5. All these methods assume plane waves, e.g. k r should be sufficiently high. So an alternative method (transfer function method) has been proposed relying on spherical wave propagation above an absorbing plane [1, 11, 12]. In the following the method will be described very briefly and results are shown.

TRANSFER FUNCTION METHOD

Fig. 1 shows the two steps needed for the measurement of the excess attenuation function, e.g. transfer function between source and receiver normalised to free-field propagation. First a pseudo-free-field measurement between source and receiver is carried out as reference. Parasitic reflections are removed by applying time windows. The same time window is used when investigating the reflection close to the surface. The spectra of both time windowed signals are calculated.

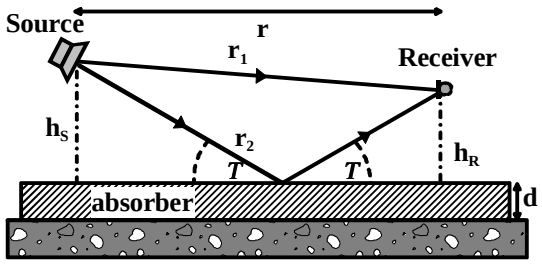

FIGURE 1. Set-up for reflection measurement close to the surface under investigation.

Dividing the reflection measurement spectrum by the reference spectrum yields the wanted complex excess attenuation function or normalised transfer function [11, 12]. Magnitude and phase of this transfer function are used as input to a numerical inversion procedure as described in [11, 12] to deduce the acoustic impedance of the surface. The impedance Z allows to calculate the absorption coefficient for normal ($\Delta_{90°}$) or diffuse incidence (Δ_{diff})[1, 9, 11, 12].

EXPERIMENTAL RESULTS

Several measurements have been carried out above different surfaces. A typical experimental set-up for determining the absorption properties of a wall surface in a room is shown in Fig. 2.

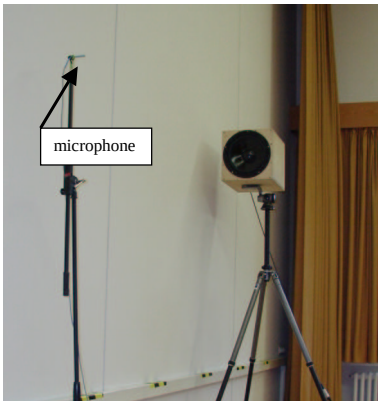

FIGURE 2. Set-up of microphone and loudspeaker for reflection measurement close to wall surface, distance r = 1.8 m.

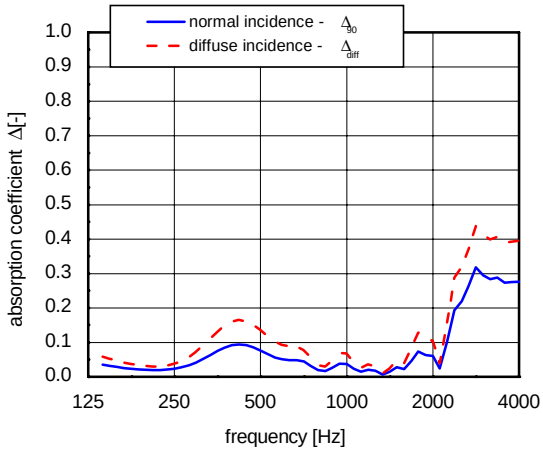

FIGURE 3. Result for the measurement of the wall in Fig. 2.

Fig. 3 shows the result for the absorption coefficient for a gypsum board wall (Fig. 2) as calculated from the measured impedance values for normal and diffuse incidence [12]. The lower frequency limit of this measurement was 133 Hz according to the time window length of 7.5 ms applied in the measurement. Up to 2000 Hz the absorption coefficient is below 0.15 as could be expected for such a material of this kind.

Fig. 4 shows the result for the impedance of a 5 cm thick layer of a mineral fibre. The corresponding absorption coefficient agrees well with measurements in a standing wave tube. The influence of different measurement geometries is given by the error bars drawn.

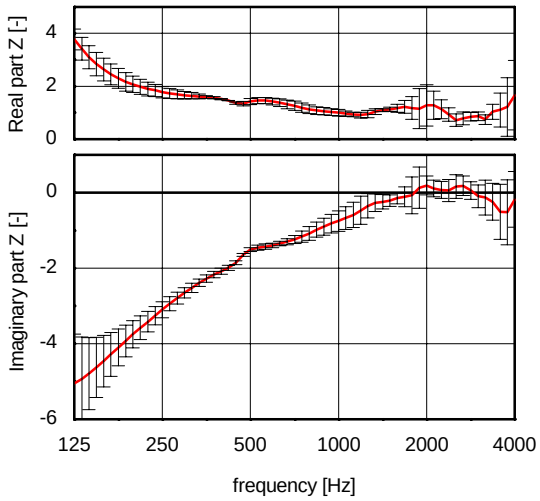

FIGURE 4. Result for the complex impedance measurement above an absorbing material. Error bars result from different measurement geometries.

FUTURE WORK

Other materials and linings of walls have been investigated. The results agree well with literature values and other measurements. For some absorbing structures like plate-like resonators further investigations are needed. Results from strongly diffusing surfaces should be interpreted with care, further investigations will concentrate on this aspect that might be explained with the concept of an effective impedance as suggested in [13].

REFERENCES

1. C. Nocke, *Appl. Acoustics*, **59(3)**, 253-264 (2000).
2. L. Cremer, *Elektr. techn. Nachrichten*, **10(7)**, 302-315 (1933).
3. F. Spandöck, *Annalen der Physik*, **5(20)**, 328-344 (1934).
4. U. Ingard and R. H. Bolt, *J. Acoust. Soc. Am.*, **23(5)**, 329-335 (1951).
5. J. C. Davies and K. A. Mulholland, *J. Sound Vib.*, **67(1)**, 135-149 (1979).
6. Z. Kintsl, *Sov. Phys. Acoust.*, **21(1)**, 30-32 (1983).
7. U. Wilms and R. Heinz, *Acutsica.*, **75(1)**, 28-29 (1991).
8. M. Garai, *Appl. Acoustics*, **39(1/2)**, 119-139 (1993).
9. E. Mommertz, *Untersuchung akustischer Wandeigenschaften und Modellierung der Schallrückwürfe in der binauralen Raumsimulation*, Dissertation RWTH Aachen, Shaker Verlag, 1996
10. Draft European Standard Pr ENV 1793-5, *Road traffic noise reducing devices – test method for determining the acoustic performance – Part 5: Intrinsic characteristics In situ values of sound reflection and airborne sound insulation*, Version 5.1 (2000).
11. S. Taherzadeh and K. Attenborough, *J. Acoust. Soc. Am.*, **105(3)**, 2039-2042 (1999).
12. C. Nocke, *In-situ Messung der akustischen (Wand-)Impedanz*, Dissertation Universität Oldenburg, Shaker Verlag, 2000
13. K. M. Li and T. Waters-Fuller and K. Attenborough, *J. Acoust. Soc. Am.*, **104(2)**, 679-685 (1998).

Visco-elastic Properties of Liquids Measured by Acoustical Method at 40 kHz

B.B. Damdinov

Buryat Scientific Center, 670047, Ulan-Ude, Russia

Experimental research of dynamical shear properties of liquids was conducted in order to study low frequency visco-elastic relaxation in liquids. Experiment with different organic liquids (glycoles, oils, alcohols) was carried out. An experimental procedure for investigation of visco-elastic properties of liquids by acoustical resonance method at 40 kHz has been worked out.

INTRODUCTION

Important direction of studies in the molecular physics of liquids is connected with acoustic measurements of their shear visco-elastic characteristics [1,2]. Measurement of dynamic shear characteristics of liquids is one of the direct methods of liquid investigation and studying. According to generally accepted beliefs about the nature of liquids shear elasticity must be observed at periods of shift fluctuations comparable to a time of settled existence of separate particles of liquid, which is identified with a time of relaxation of non-equilibrium condition. Time of relaxation is valued on velocities of self-diffusion, and calculations give the value of order 10^{-10} - 10^{-12} sec for low viscosity liquids. Consequently, shear elasticity of such liquids must be observed at frequencies of shift fluctuations of order 10^{10} - 10^{12} Hz. However in work [3,4] it was uniquely shown that all liquids without any exceptions at the frequency 10^5 Hz possess shear elasticity. Given fact shows that in liquids there exists unknown earlier low frequency visco-elastic relaxation process, explained by, probably, collective interactions of groups of molecules. Time of relaxation of groups of molecules is much higher than that of settled existence of separate molecules. One of the distinctive pecularities of shear mechanical characteristics of usual liquids is a small value of tangent of mechanical loss angle ($tan\theta < 1$). According to Maxwell's rheological model this means that frequency of relaxation of observed process is at below frequency, used in the experiment, which formed in work [3,4] 74 kHz. So, valuable information on the nature of given process can give studies of low-frequency shear elasticity of liquids at lower frequencies.

Visco-elastic characteristics of different organic liquids have been carried out by acoustical resonance method at frequency 40 kHz.

EXPERIMENTAL METHOD

Studying of dynamical properties of liquids was carried out by resonance method with using an piezoquartz. The resonance method for measuring the shear elasticity consists in the following: a piezoquartz crystal performs longitudinal (axial) oscillations at the basic resonance frequency, and its horizontal surface performing tangential oscillations supports a liquid interlayer covered by a solid cover plate. The cover plate with the liquid film is disposed on one end of the piezoquartz crystal. In this case, the liquid interlayer undergoes a shear deformation, and standing shear waves should be induced in it. The parameters of the resonance curve of the piezoquartz crystal vary depending on the interlayer thickness.

The complex shift, Δf^*, of the resonance frequency of the piezoquartz crystal due to its interaction with the liquid interlayer has the form [4].

$$\Delta f^* = \frac{SG^* \kappa^*}{4\pi^2 M f_o} \cdot \frac{1 + cos(2\kappa^* H - \varphi^*)}{sin(2\kappa^* H - \varphi^*)}, \quad (1)$$

where S is the area of the base of the cover plate; $k^* = \beta - i\alpha$ is its complex wave number; $G^* = G' + iG''$ is the complex shear elasticity modulus of liquid; H is the thickness of the liquid interlayer; φ^* is the complex shift of the phase when the wave is reflected from the liquid – cover plate interface; M is the mass of the piezoquartz crystal; f_0 is its resonance frequency. The expressions for the real $\Delta f'$ and the imaginary $\Delta f''$ components of the shift of the resonance frequency will be as follows (when the cover plate is at rest because of a weak bond with the piezoquartz crystal):

$$\Delta f' = \frac{S}{4\pi^2 M f_0} \times \times \frac{(G'\beta + G''\alpha)\sin 2\beta H + (G'\alpha - G''\beta) Sh 2\alpha H}{ch 2\alpha H - \cos 2\beta H}, \quad (2)$$

$$\Delta f' = \frac{S}{4\pi^2 M f_0} \times \times \frac{(G''\beta \quad G'\alpha)\sin 2\beta H + (G''\alpha + G'\beta) Sh 2\alpha H}{ch\ 2\alpha H \quad \cos 2\beta H} \quad (3)$$

Analysis of the expressions (2) and (3) gives three methods for measurement of the shear modulus of liquids. The first method, more accurately, is realized with small thickness of the liquid interlayer, when $H<<\lambda$ (wavelength). In this case, both the real and the imaginary components of the resonance frequency shift are proportional to the inverse value of the liquid interlayer thickness. For the real shear modulus, G', and for the mechanical losses angle, $tan\theta$, the following calculating formulas are derived [4]:

$$G' = \frac{4\pi^2 M f_0 \Delta f' H}{S}, \quad (4)$$

$$tg\ \theta = \frac{G''}{G'} = \frac{\Delta f''}{\Delta f'}. \quad (5)$$

EXPERIMENTAL RESULTS

Studying of shear elasticity of liquids in the broad range of frequencies is possible undertaking the measurements on one installation. Each range requires making the separate installation. Experiment on 40 kHz was made by the resonance method using piezocrystal with the mass 13.81 gr. Area of contact was 0.2 sm^2. Important value of the resonance method is that it has no restrictions in viscosity of investigated liquids [5].

Table 1. Visco-elastic properties of liquids at 40 kHz

Liquids	G', Mpa	tanθ
Ethylen glycole	0.040	0.76
Diethylen glycole	0.051	0.44
Triethylen glycole	0.074	0.65
Dibutylphtalate	0.065	0.29
Butil alcohole	0.094	0.22
Olein acid	0.076	0.23
Tetradecane	0.056	0.28
Pentadecane	0.063	0.13
Hexadecane	0.066	0.12
Vaseline oil	0.113	0.61

Figure 1 shows the experimental dependencies of the real and imaginary components of the frequency shift on the inverse value of the liquid interlayer thickness for vaseline oil. Obtained linear dependencies confirm the liquid to have constant shear elasticity modulus, according to the formula (4). The real shear modulus and the mechanical losses angle were measured for vaseline oil (G' = 0.113 MPa and $tan\theta$ = 0.61) correspondingly.

Similar results are also obtained for other investigated liquids. The calculated by formulas (4) and (5) values of G' and $tan\theta$ are reported in Table 1.

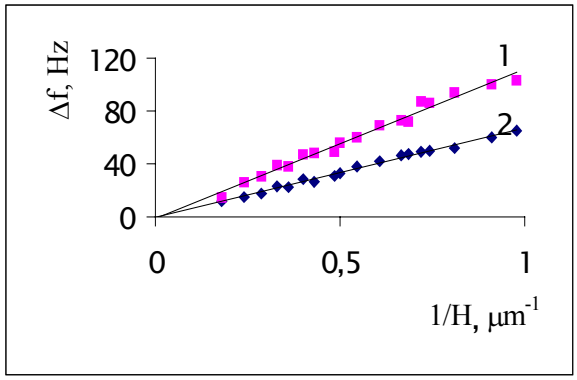

FIGURE 1. Experimental dependencies of $\Delta f'$ (1) and $\Delta f''$ (2) on $1/H$ for vaseline oil.

ACKNOWLEDGMENTS

This work was supported by the Russian Foundation for Basic Research, grant №98-01-503 and Acoustical Society of America, grant №1210/2

REFERENCES

1. S. Ernst, E. Zorebski, K. Bebek, Acustica. **72**, 81-89 (1990)
2. T.G. Mason, Rheol. Acta. **39**, 371-378 (2000)
3. U.B. Bazaron, B.V. Derjaguin, A.V. Bulgadaev, Docl. Acad. nauk SSSR. **160**, 799- 803 (1965)
4. B.V. Derjaguin, B.B. Badmaev, U.B. Bazaron, Kh.D. Lamazhapova and O.R. Budaev, Phys. Chem. Liq. **29**, 201-209 (1995)
5. B.B. Badmaev, B.B. Damdinov, Sov. Phys. Acoust. **47**, (2001) (in print)

Study on the Reflectance of Ultrasonic Plane Wave from Sand Surface

L. Tao, M. Ojima and S. Motooka

Department of Electronics Engineering, Chiba Institute of Technology,
2-17-1, Tsudanuma, Narashino, Chiba, 275-0016, Japan

A method of discriminating the water content of sand by ultrasonic pulse-echo signals of sensor array was studied in our previous work. The reflectance of ultrasound measured from dry sand surface was rather weaker than that calculated from the general impedance of sand. In order to explain this property, this paper estimates the reflectance by theoretical analysis of reflection from dry sand surface, with the assumptions of plane wave and simple sphere model sand grain. The result shows that the reflectance is independent with the radius of sand grain, if it is small enough than wavelength. The estimation is verified by the reflectance of two kinds of sand with different sizes measured by using plane transmitter-receiver array.

INTRODUCTION

River sand is an important material for the production of concrete, and the water content of sand for mixing with the cement during the manufacture influences the quality of the concrete produced. In our previous work, a water content discrimination method by ultrasonic pulse-echo signal was studied [1,2]. And the reflectance of ultrasound measured from dry sand surface was rather weaker than that calculated from the general impedance of sand. In order to explain this property, this paper estimates the reflectance by theoretical analysis of reflection from dry sand surface, with the assumptions of plane wave and simple sphere model sand grain. The result shows that the reflectance is independent with the radius of sand grain, if it is small enough than wavelength. The estimation is verified by the measured reflectance of two kinds of sand with different sizes.

CALCULATION

As shown in Fig. 1.(a), a pyramidal packing model using spheres with the same size as sand grains is employed as a simple approximation for reflectance calculation, though the shape of sand grains is not uniform actually. And a perpendicular incident plane wave is assumed. The reflectance is defined as

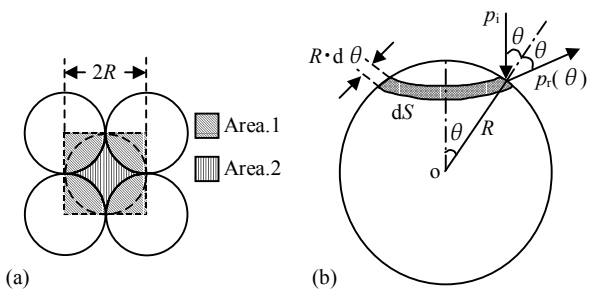

FIGURE 1. Model of sand grains.

$$r = \frac{|p_{\text{sand}}|}{|p_{\text{ideal}}|} \tag{1}$$

where p_{sand} and p_{ideal} denote the sound pressure reflected from the sand surface and that from an ideal rigid surface, respectively. It is known that p_{ideal} should be same as the pressure of incident wave in the condition of plane wave.

The sand surface can be regarded as the repeat of the shadow part shown in Fig. 1.(a), in the condition of regular arrangement of grains with same size. In this section the reflectance will be estimated in this square part. The analysis is divided into two areas illustrated in the figure, where Area 1 includes four quarter parts of the sand grains in the upper layer, and Area 2 a sand grain in the lower layer which is covered partly by Area 1. Moreover, because the dimension of sand grains is far small than the wavelength of the sound wave, in this microstructural model, the reflect pressure of the sand surface is treated quasi-statically as the average pressure in this square area, without the consideration of the phase difference of the reflection from differential parts of the sand grains with different depths.

The 4 quarter parts of sand grains in Area 1 is equivalent to a whole sand grain shown in Fig. 1.(b), where p_i is the pressure of the incident wave. The differential composed force contributed by the reflection from the differential area dS shown in the figure is,

$$dF = \left[p_r(\theta) \cdot (dS \cdot \cos\theta)\right] \cdot \cos 2\theta \tag{2}$$

where $dS = (2\pi R \cdot \sin\theta) \cdot (R \cdot d\theta)$. The reflection from differential areas where θ is larger than $\pi/4$ are omitted in our estimation for they make no direct contribution to the overall reflection of sand surface, but bring forth rather complicated multi-reflections between sand grains. Moreover, considering that both the sound

impedance of the sand grain and that of the ideal rigid material are far larger than that of air, $p_i=p_r(\theta)=p_{ideal}$ is assumed approximately. The composed force by the reflection in Area 1 is derived as

$$F_1 = 2\pi R^2 p_{ideal}\int_0^{\frac{\pi}{4}} \cos\theta \cdot \cos 2\theta \cdot \sin\theta \, d\theta \qquad (3)$$
$$= 0.196(2R)^2 p_{ideal}$$

In Area 2, which includes a single sand grain shown in Fig. 1.(b), the composed force can be derived similarly besides excluding the reflection from the hidden parts covered by Area 1. The result is

$$F_2 = 0.144(2R)^2 p_{ideal} \qquad (4)$$

The average pressure of reflection should be

$$p_{sand} = \frac{F_1 + F_2}{(2R)^2} = 0.34 p_{ideal} \qquad (5)$$

Substituting into eq.1, the final estimation result of the reflectance of sand surface is 0.34.

MEASUREMENT

Figure 2 shows the experimental system. All the four ultrasonic transmitters and four receivers are PZT type with a resonance frequency of 39.75kHz. A 10 periods (252μs) AC pulse of 39.75kHz electric wave with 10Vp-p amplitude is transformed by four transmitters to an incident sound wave at meantime. The echo signal that reflected from the measuring surface is

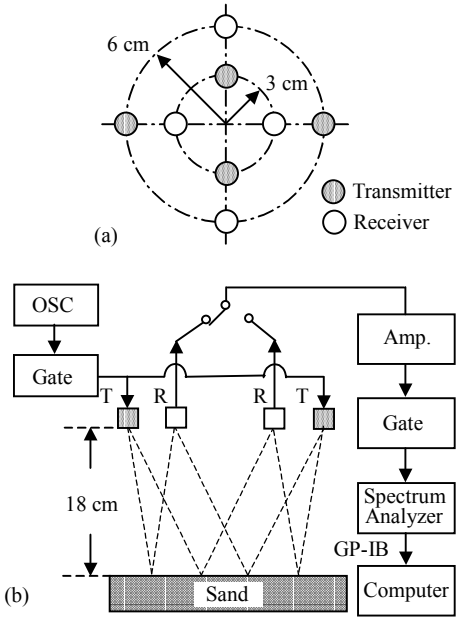

FIGURE 2. (a) Transmitter-Receiver array; (b) Measurement system.

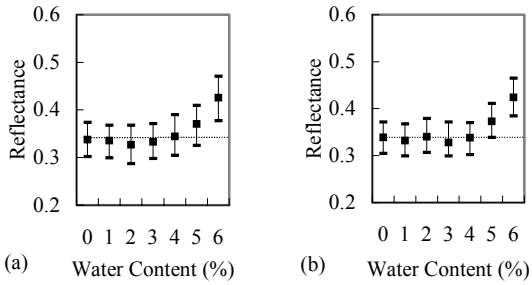

FIGURE 3. Measurement results of reflectance of (a) River sand; (b) Mountain sand.

amplified (40dB) and then analyzed by a spectral analyzer. Finally, the amplitude of 39.75kHz amplified signal is read into computer as reflection data.

Water surface is employed as ideal rigid reflect plane for its natural horizontal feature and its far larger impedance than that of the air. Two kinds of sand (river sand and mountain sand) differing in average grain size (about 0.37 mm and 0.23 mm respectively) with different water content (mass percentage of water in moist sand) are employed as the specimen for measurement.

Figure 3 is an example of the measured results of the distribution of 40 reflectance data of one receiver. The results of both the two kinds of sands agree well with the estimated reflectance that is independent with the grain size. And the reflectance remains constantly till the water content is 4%. It is supposed that the water in the sand is absorbed water only, and the microstructure remains same as that of dry sand.

CONCLUSION

The reflectance of sand surface is estimated to be 0.34, with the assumptions of plane wave and simple sphere model sand grain. The measurement results of river sand and mountain sand are similar though they are different in grain size, and agree well with the estimation. Furthermore, the reflectance of moist sand surface keeps same as that of dry sand surface while the water content is lower than 4%.

REFERENCES

1. S. Motooka, M. Sakata, N. Takano and T. Watanabe, "Measurement of moisture in sand using pulse echo method", in *Proc. 15th Int. Congress on Acoustics,* Trondheim, Norway, 1995, Volume I, pp. 285-288.
2. N. Takano, M. Fujimoto, L. Tao and S. Motooka, Jpn. J. Appl. Phys. **39**, 3112-3116 (2000)

Ultrasonic and X-ray diffraction measurements of acoustical properties of materials under extreme conditions of pressure and temperature

R. Debord, F. Decremps, D. Lheureux°, J.P. Itie,
G. Syfosse, M. Fischer and A. Zarembowitch

PMC(UMR 7602 CNRS), Tour 13 E4, 4 Place Jussieu 75252 Paris Cedex 05 (France)
°Miller Institute, Earth and Planetary Science Department U.C.Berkeley, 415 Mc Cone Hall, Berkeley(USA)

A new experimental set-up which permits to carry out simultaneously ultrasonic and X-ray diffraction measurements under high pressure and temperature has been developed. We illustrate the performances of this device by showing the elastic behavior under high pressure and temperature of different oxides.

INTRODUCTION

The determination of the elastic moduli of materials under extreme conditions of pressure and temperature is of major importance for geophysics as well as for condensed-matter physics. It is well known that most of our knowledge on the earth's interior comes from acoustic seismology: refracted and reflected elastic waves can probe the earth and gather information on the elastic structure and eventually the physics and chemistry of inaccessible regions down to the center of our planet. To extract from transit time of elastic waves consistent information on the earth's interior, one need to know the values of physical parameters of high pressure and high temperature phase of the mineral constitutive of the earth's interior corresponding to depths between 30 and 2900 km. This finalized research has side-effects on fundamental physics since it enlarges our understanding of physics under "ordinary" conditions of pressure and temperature. For condensed-matter physicists changes in crystal structure or electronic properties of materials are often revealed much more clearly through changes in elastic properties than by other means. So, we have developed a new experimental set-up using a "Paris-Edinburgh cell", which is a high pressure vessel that contains relatively large samples. This set-up permits to perform simultaneous X-ray diffraction measurements at high pressure (P~10GPa) and high temperature (T~ 1000K). We illustrate the performances of this device by showing the elastic behavior under high pressure and high temperature of two oxides for which such measurements shed some light on the mechanism of their phase transitions.

EXPERIMENTAL

High pressure experimental set-up

Originally the Paris-Edinburgh cell (fig. 1) was developed for high pressure neutron diffraction measurements [1]. We adapted this press to simultaneously perform ultrasonic and X-ray diffraction measurements. The samples are compressed between two opposite tungsten carbide flat anvils. The hydraulic press which generates the necessary thrust, is connected to the lower part of the cell. The experimental cell and the sample surroundings are shown in fig. 1. The crystal sample was encased in a boron nitride (h-BN) cylinder, which was used as a pressure-transmitting medium. Compressed NaCl powder was located below and around the sample. This set-up was put into a boron epoxy gasket (5:1 in mass) which has a low X-ray absorption coefficient.
The pressure value was determined by measuring the sodium chloride lattice parameters using the Decker's equation of state [2]. The measurement accuracy was ± 0.1 GPa.

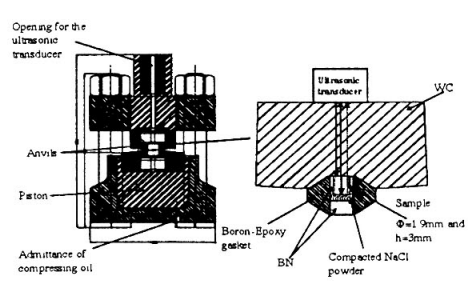

Figure 1. Ultrasonic cell assembly of the Paris-Edinburgh press

High temperature cell

A graphite furnace surrounding the sample is used in order to obtain the high temperature by Joule effect. The electric contacts are realised in inox. A thermocouple which is in contact with the single crystal and the Nacl powder is used to measure temperature.

Ultrasonic measurements

The longitudinal and shear ultrasonic waves were generated by plates of $LiNbO_3$, which were sticked to the rear face of the upper anvil with indium. The ultrasonic wave frequency was of the order of 20 MHz. The transit time values were estimated with an accuracy of approximately 1ns.

RESULTS

High pressure elastic constants of $SrTiO_3$

$SrTiO_3$ is a "model" perovskite which undergoes a cubic-quadratic structural phase transition at 105K. This transition has been extensively studied at ordinary pressure but less information concerns the transition which occurs when the pressure is increased from zero to about 9 GPa[3]. Using the Paris -Edinburgh set-up, we have determined the pressure dependence of the elastic constants at room temperature. The results are shown in Fig. 2.

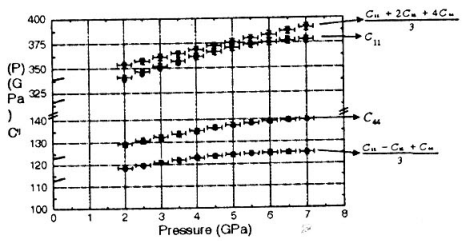

Figure 2. Elastic constant of $SrTiO_3$ under pressure.

From Fig.2, we see that the elastic constants of $SrTiO_3$ do not show any discontinuity around 6 GPa[4] neither up to 7 GPa as it has been sometimes reported.

High pressure and temperature elastic constants of ZnO

If most of covalent II-VI compounds crystallize at room condition in a zinc blende or cinnabar structure, ZnO possesses an hexagonal wurtzite structure that transforms to a sixfold-rocksalt structure at P_T = 9 GPa.

In spite of considerable numerical efforts, its particular electronic properties cannot still be fully evaluated by ab initio calculations. The energetic separation between the p and d valence electrons is known to be tiny. The precise measurements at different temperature and pressure of the elastic moduli is expected to give insight into the transformation mechanism by which the structure changes.

In situ acoustic measurements as well as X-ray diffraction experiments were performed simultaneously in the furnace placed inside the "Paris-Edinburgh" cell.

The first results obtained with that "light" equipment (the weight of the cell is less than 50kg) seems to be in agreement with those obtained previously by one of us (F.D) with a heavy uniaxial apparatus (USCA-1000)[5]. The results previously reported are shown in Fig. 3.

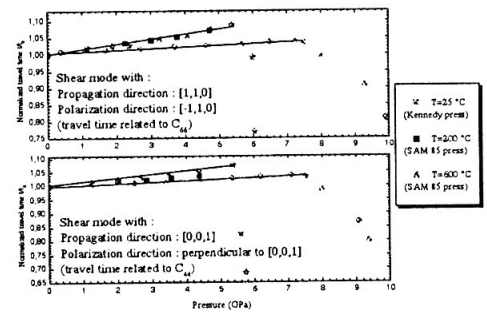

Figure 3. Normalized travel times versus pressure for the transverse pure modes corresponding to C_{44} and C_{66}.

The present experimental results show that ZnO becomes softer against shear-type acoustic distortions under pressure. At high temperature, the pressure derivatives of the elastic shear modes become more negative: the elastic shear softening observed at room temperature is enhanced at elevated temperature.

REFERENCES

1. Besson, J.M., Nelmes, M.J., Hamel, G., Loveday, J.S., Weill, G., Hull,S., Physica B, 180/181 , 907 (1992)
2. Decker, D.L., J.Appl.Phys, 36, 157, (1957)
3. Lheureux, D., Thèse de l'Université P.et M. Curie (2000)
4. Lheureux, D., Polian, A., Fischer, M., Gauthier, M., Itie, J.P, Proc. of the 2000 IEEE Internaional Ultrasonics symposium,, Porto Rico,(under press)
5. Decremps, F., Zhang, J., Li, B., Lieberman, R.C,. Phys. Rev. B, 63, 2241 (2001)

Nonlinearity Parameter Measurement in Liquids and Gels using the Parametric Interaction

Christophe Barrière, Xavier Jacob and Daniel Royer

Laboratoire Ondes et Acoustique, Université Paris 7, CNRS UMR 7587,
ESPCI, 10 rue Vauquelin, 75005 Paris, France.

In order to measure the acoustic nonlinearity parameter, a method based on the parametric interaction of two ultrasonic waves has been developed. The interaction of a high frequency continuous wave with a low frequency pulse is equivalent to a phase modulation of the high frequency wave. Thus, the nonlinearity parameter is determined by demodulating the continuous-wave phase. This technique circumvents the diffraction effects. Measuring nonlinearity parameters of well-known liquids validates the measurement principle. Absolute measurements require the low frequency transducer calibration with an optical interferometer. They are given with a 5-% uncertainty and are in good agreement with those found in literature. By comparing two media, relative measurements are also achievable without any transducer calibration, with a 2-% precision. This technique is applied for measuring nonlinearity parameters of gelatin gels mimicking biological tissues.

INTRODUCTION

The commonest ways of measuring nonlinearity parameters are the thermodynamic method and the finite amplitude method [1]. The thermodynamic method is based on measurements of sound speed variations induced by changes in the hydrostatic pressure and in the temperature of the medium. This method is accurate (1%), but it is not easy to implement in industrial cases or *in vivo* studies. The finite amplitude method consists in measuring the second harmonic components, whose amplitude is proportional to the coefficient of nonlinearity. This method gives a precision of 5 to 10 %, because of the transducer calibrations and the nonlinear diffraction effects. However, this technique has been successfully employed for *in vivo* nonlinearity parameter determination. We present results from experiments based on parametric interaction in liquids and gels. We can also make a comparison between two media and measure nonlinearity parameters without any transducer calibration.

THEORETICAL ANALYSIS

Classically, the parametric interaction of two primary waves (frequencies f_1 and f_2) gives rise to nonlinearly induced waves at sum and difference frequencies ($f_\pm = f_1 \pm f_2$). Nonlinear acoustic wave propagation in a viscous fluid is governed by Kuznestov's equation [2]. On this theoretical basis, we derived an integral expression of the velocity potentials $y_\pm$ of the secondary waves, under an approximation of weak nonlinearity [3]. This model has been validated with experiments carried out in water. It was shown that diffraction acts in a similar way on the two secondary waves, when the two primary waves have a high frequency ratio ($f_1 > 10\ f_2$). Moreover, the secondary wave diffraction profiles are very close to the high frequency (HF) primary wave one. Thus, a measurement method, which compares the secondary wave amplitudes to the HF primary wave one, does not yield any diffraction problem.

Applying these theoretical results to the interaction of a low frequency (LF) pulse with a HF continuous wave, we have shown that the HF potential $y_{HF} = y_1 + y_+ + y_-$ can be written as a phase modulation of the carrier, even if diffraction is taken into account:

$$y_{HF}(\mathbf{r},t) = y_1(\mathbf{r})\mathrm{e}^{-j(w_1 t + \Delta\Phi_p)} \qquad (1)$$

$\mathbf{r}$ and t denote respectively the spatial and temporal coordinates. The index of modulation

$$\Delta\Phi_p(z,t) = b\,\frac{w_1}{c_0^2} z\,\mathrm{e}^{-a_2 z} v_2\left(t - \frac{z}{c_0}\right) \qquad (2)$$

is proportional to the surface velocity v_2 of the LF transducer and to the nonlinearity parameter $b = 1+B/2A$. c_0 and a are the sound speed and the absorption coefficient of the undisturbed fluid and z is the interaction distance of the primary waves.

MEASUREMENTS

A block diagram of the experimental setup is shown in Fig. 1. The HF planar transducer, driven by a stable 30-MHz frequency source, is immersed in a small vessel, whose bottom is the surface of the LF transducer (f_2 = 2.5 MHz).

The reflected HF acoustic wave is phase-modulated by the pulse launched by the LF transducer. The HF signal is extracted by a 180°-hybrid junction and is processed by a digital filter, which compares the secondary waves amplitudes to the HF primary wave one, to obtain the phase modulation $\Delta\Phi_P$.

According to Eq. (2), the output signal is a linear function of the amplitude of the LF surface velocity. The absolute measurement of v_2 with an optical interferometer allows the determination of the nonlinearity parameter from the slope of the experimental curve $\Delta\Phi_P$ versus v_2 (fig. 2). An experiment carried out with water gives the value: $b_{water} = 3.45 \pm 0.06$ (20°C), very close to the generally accepted ones [1].

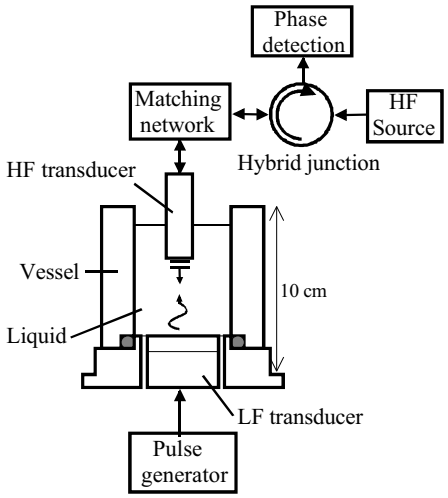

Fig. 1: Experimental set-up used to measure acoustic nonlinearity parameters of liquids and gels.

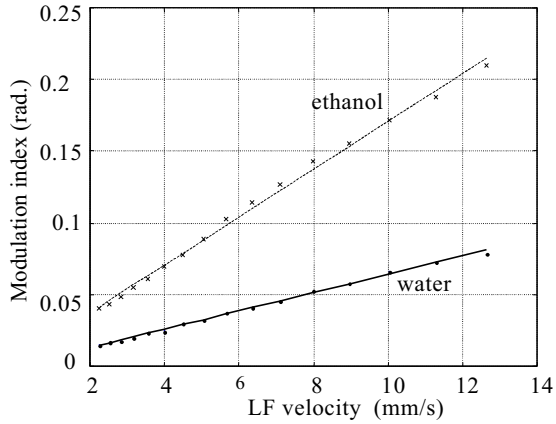

Fig. 2: Index of modulation of the HF signal for water (—) and ethanol (····) versus the amplitude of the LF transducer surface velocity. The interaction distance is $z = 22$ mm.

The uncertainty on this absolute measurement is about ± 5 %. It is almost due to the systematic error (± 4 %) on the interferometer calibration factor. The phase modulation is extracted with a numerical method, which provides only a ± 0.5 % uncertainty. In order to improve the measurement accuracy, a relative method was developed. Since the LF transducer is designed to operate in contact with a solid, its acoustic impedance is much higher than a liquid or gel one and its peak surface velocity does not depend on the loading liquid or gel.

Then, the nonlinearity parameter of ethanol is obtained by comparing the slopes of the two experimental curves, without any transducer calibration. Assuming that the nonlinearity parameter of water is known with a ± 1 % with a thermodynamic method, the nonlinearity parameter of ethanol is given with a ± 2 % uncertainty: $b_{\text{ethanol}} = 6.14 \pm 0.12$. Using the same method, experiments carried out in coupling gel and gelatin gel (fig. 3) give the values: $b_{\text{coupling}} = 3.45 \pm 0.07$ and $b_{\text{gelatin}} = 3.7 \pm 0.07$.

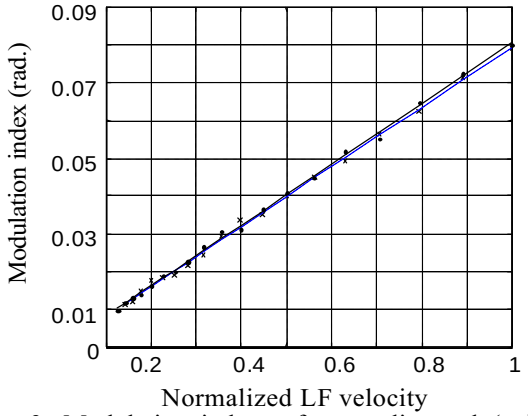

Fig. 3: Modulation indexes for coupling gel (—) and gelatin gel based (---) versus the normalized LF velocity.

CONCLUSION

The phase modulation resulting from the parametric interaction between two acoustic waves with a high frequency ratio has been used to measure nonlinearity parameters of liquids and gels. Our measurements do not need corrections based on diffraction models. This method provides absolute and relative measurements with respective accuracies of 5 and 2 %. It will now be employed to characterize the nonlinearity of biological tissues and to measure nonlinearity parameters of solids for Non Destructive Evaluation.

REFERENCES

[1] T. R. Beyer, Nonlinear Acoustics, Academic Press, New York, 1998.

[2] V.P. Kuznetsov, “Equations of nonlinear acoustics”, Sov. Phys. Acust., 16, p. 467, 1971.

[3] C. Barrière and D. Royer, “Diffraction effects in the parametric interaction of acoustic waves: application to measurements of the nonlinearity parameter *B*/*A* in liquids", to be published in IEEE Trans. Ultrason. Ferro. and Freq. Control.

Experimental study of a magnetoelastic device for the low-ultrasonic testing of elongated structures

L. Laguerre [a], J.-C. Aime [a, b], M. Brissaud [b]

[a] *Laboratoire Central des Ponts et Chaussées, Route de Bouaye, BP 4129, 44341 Bouguenais Cedex, France.*
[b] *Laboratoire de Génie Electrique et de Ferroélectricité, Institut National des Sciences Appliquées de Lyon, Bâtiment Gustave Ferrié, 8 rue de la Physique, 69621 Villeurbanne Cedex, France.*

A simple magnetoelastic device for the low-frequency ultrasonic testing of elongated ferromagnetic structures is presented. From experimental observations, the nonlinear behavior of the magnetoelastic transduction versus the polarizing field and amplitude of the driving field is illustrated for different material samples. Concurrently, the noncontact magnetoelastic device is used to study the guided wave propagation in structures. Finally, defect detection is performed using pulse compression technique.

INTRODUCTION

The magnetoelastic-based pulse–echo device generates and detects mechanical waves using the direct and inverse magnetostrictive effect [1]. In our case, this non-contact device is tested on steel members of civil engineering structures in laboratory-based experiments for the flaws detection. The steel material acts both as a part of the transducer and medium of propagation. The proposed method is alternative to conventional ones.

EXPERIMENTAL ARRANGEMENT

The magnetoelastic device is constituted by one transmitter and one detector. Each transducer is composed of a static part (solenoïdal coil), a dynamic part (small coil) and a magnetic core (the specimen under evaluation). The small coil is in the middle of the solenoidal coil to superimpose locally the dynamic magnetic field to the static field. The axisymmetric device configuration imposes axial magnetic fields. So the device is mainly sensitive to longitudinal-polarized mechanical waves. A DC adjustable power supply allows to vary the solenoidal coil intensity (*i.e.* the specimen magnetization). The transmitter is piloted by a controlled-current amplifier driven by a low radio-frequency burst voltage (with variable amplitude and center–frequency f_c , $\Delta f = f_c$). The detected time voltage signal is filtered and amplified by 60 dB. The detector SNR is improved with time-averaging of N emission/detection cycles (N<1000). Data are collected and processed with a PC and Labview software.

MAGNETOELASTIC EMISSION

Both magnetic and magnetoelastic nonlinearities as well as hysteretic effects influence the magnetoelastic transduction. These effects mainly depend on the nature of the material, the polarizing field and driving field strengths, the operating frequency. Experimental measurements were made on different cylindrical ferromagnetic specimens. Magnetoelastic emission is assessed from the measurement of the characteristics (amplitude and spectrum) of the first mechanical wave arrival. Figure 1 (TOP) shows for both specimen, the magnetoelastic emission rms increases to an optimum for a given range of polarizing current strengths to level off as the current increases. The magnetoelastic emission rms voltage increases with the driving current amplitude (Idyn). Figure 1 (BOTTOM) illustrates the polarizing current strength influence on the distorsion of the magnetoelastic-generated wave for two Idyn.

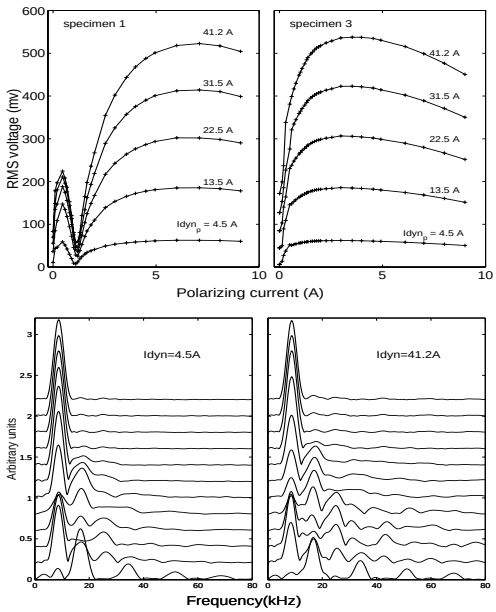

FIGURE 1: f_c = 9 kHz (TOP) Variation of magnetoelastic emission rms voltage with increasing dynamic current amplitude at different polarizing intensities (specimens 1 and 3) (BOTTOM) Variation of the magnetoelastic emission amplitude spectrum (specimen 1) with increasing polarizing current (from 0 to 9A) for 2 Idyn (4.5 et 41.2A)

Hence, the selection of the polarizing current intensity allows to linearize and enhance the magnetoelastic emission. It allows the control of the magnetoelastic source which is critical in the application of guided waves to non-destructive evaluation (NDE).

PROPAGATION

The dispersive nature of a cylindrical waveguide [2] are examined. Experiments on a cylindrical bar were performed for different f_c. The time-frequency representation of Figure 2 (TOP) is an example of the time evolution of the frequencies composing a pulse excitation with f_c=150 kHz. It depicts the dispersion of modes L01 and L02. Figure 2 (BOTTOM) shows the experiment agree well with the theoretical curves.

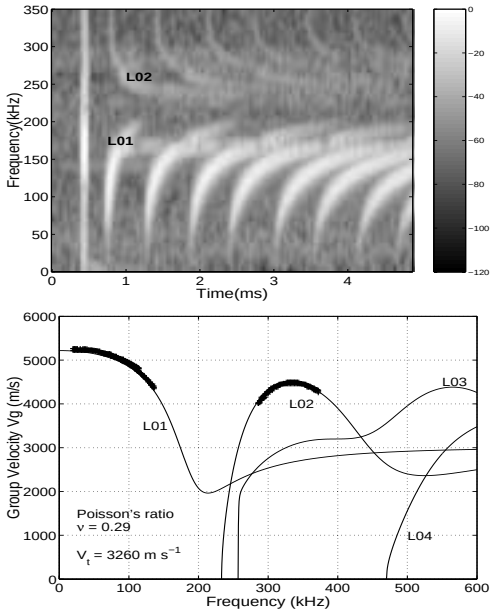

FIGURE 3: f_c= 150 kHz, steel cylindrical bar, diameter 15.5 mm, length 6m (TOP) Time-frequency transform of the echogram of the bar (BOTTOM) Theoretical versus experimental dimensionless longitudinal group velocities

DEFECT DETECTION

Artificial flaws were made in two common civil engineering structures samples (*i.e.* a bar and a prestressing strand) for specimens 1 and 3. The excitation frequency content is chosen for a monomodal weak dispersive propagation and a satisfactory spatial resolution over several meters of propagation. Figure 4 (TOP) shows the reflected wave D11 due to the interaction between the direct wave and the flaw. Arrival (1) is the direct wave, (2) and (3) are relative to the end-echo. D12, D13 and D14 are relative to the successive multiple reflections of direct transmitted wave between the flaw and the nearest bar-end. Measurements have shown attenuation in a prestressing strand is higher than for same diameter bar [3]. Modulated-frequency signals are a solution to improve both SNR and time resolution. Figure 4 (BOTTOM) shows the strand cross-correlogram, for different chirp excitations of constant duration and increasing frequencies. The two artificial flaws (one surrounding wire broken at 680mm from the end and 150mm of one surrounding wire cut off from the same end) are detected (D1 and D2) and time resolution is improved with frequency. The near-end flaw detection was not possible with a classical pulse.

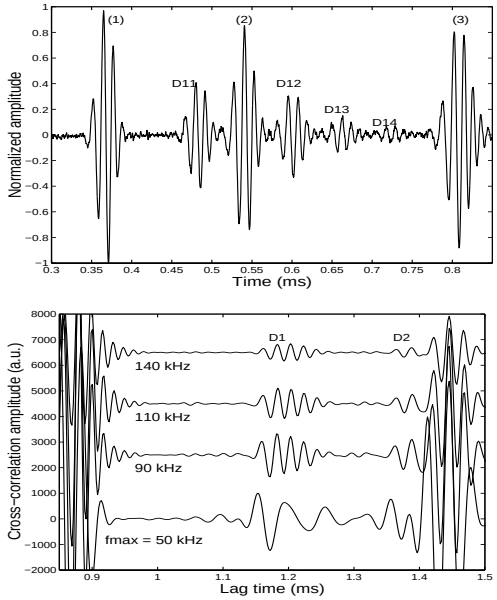

FIGURE 4: (TOP) Echogram of a cylindrical steel bar (diameter 14 mm, length 2.9m), f_c= 80kHz with a radial hole of 5mm in diameter at 150mm from the bar-end.(BOTTOM) Crosscorrelogram of the strand with flaws, for different product duration-bandwidth chirp excitations (the higher frequency is from 50 to 140kHz).

The experimental study has shown the potentialities of the magnetoelastic device for the NDE of elongated steel cylindrical structures illustrating technical aspects of generation, propagation and detection.

REFERENCES

1. Bozorth R. M., *Ferromagnetism*, Van Nostrand Company Inc., New York, 1951
2. Achenbach J. D., *Wave propagation in elastic solids*, North Highland Publi., Amsterdam, 1984.
3. Laguerre L., J.-C. Aime and M. Brissaud, "Generation and detection of elastic guided waves with magnetoelastic device for the NDE of steel cables and bars", 15th WCNDT, Roma, 2000 (www.ndt.net)

Mechanical characterization of poroelastic materials

R. Panneton, C. Langlois, and N. Atalla

Groupe d'Acoustique de l'Université de Sherbrooke, Department of Mechanical Engineering, Université de Sherbrooke, Sherbrooke (Quebec) J1K 2R1, Canada

In this paper, polynomial relations in terms of Poisson's ratio and shape factor are developed to link the apparent Young's modulus to the true Young's modulus of an isotropic poroelastic disc-shaped sample under quasi-static compression. The method leads to a system of two equations and two unknowns. The unique admissible solutions to the system are the true Young's modulus and Poisson's ratio of the material. Also, using the quasi-static measurements of the compression mechanical impedance, the structural loss factor of the material can be deduced. The method is applied successfully to characterize the three elastic parameters of a poroelastic foam sample. It is shown that the method leads to a unique set of elastic parameters known as the true values of the material and not the apparent values.

INTRODUCTION

Following theoretical models based on the Biot theory [1], the solid phase of an isotropic elastic porous material is defined by three vacuum elastic properties: Young's modulus, Poisson's ratio and loss factor. However, under vacuum conditions, closed cells trapped in the materials may burst and change the properties of the material. To prevent this problem and for the sake of simplicity, current techniques based on static or dynamic measurements with compression, shear or torsion tests are performed in air at low frequencies to characterize the elastics properties [2-4].

In the classical compression test shown in figure 1, boundary conditions, initial strain, and the air saturating the material may affect the transfer function measurement ($F(L)/x_0$) used to compute the elastic properties of an open-cell porous material. The objective of this paper is to analyze one of these effects, namely the boundaries conditions, and to derive a measurement method for the three elastic parameters.

BOUNDARY CONDITIONS EFFECTS

For the compression test sketches in figure 1, the shape factor of the porous test specimen is defined by the ratio of its cross-sectional area (A) to the total area of the stress-free surfaces ($2\pi rL$). For samples of large shape factor, the transfer function is strongly dependent on the shape factor if the ends of the sample are bonded. That is, under compression, the sample bulges sideways as shown in figure 2.

Since the bulge out effect is related to the geometry of the sample (its shape factor) and its Poisson's ratio, some works have taken advantage of this effect and used two different shape factors to compute both the Poisson's ratio and the Young's modulus [2]. However, they generally led to the development of

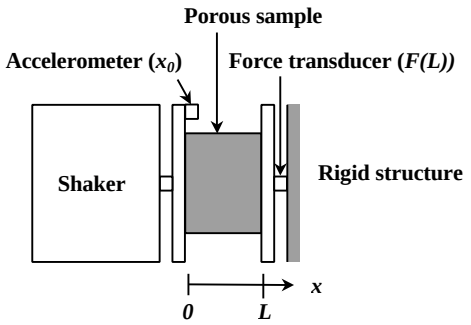

FIGURE 1. Sketch of the vibration compression test.

methods requiring one rod-like sample (very small shape factor) and one disc shaped sample (large shape factor). The rod-like sample is usually an inconvenient shape since it is subjected to buckling and difficult to cut from commercially available porous materials.

Our investigation with an axisymmetrical FEM model showed that the measured compression stiffness K (or $\mathrm{Re}(F(L)/x_0)$) can be correlated to the shape factor s of the test specimen for different Poisson's ratios ν. This correlation takes the form of polynomial relations amongst the measured compression stiffness, the Young's modulus, the Poisson's ratio, and the shape factor. By defining the apparent Young's modulus E' of the sample by its 1D compression stiffness

$$K = \frac{E'A}{L} \tag{1}$$

the polynomial relations can be used to link the apparent Young's modulus to the true Young's modulus of the material:

$$E = \frac{E'}{P(s,\nu)}. \tag{2}$$

The development of the polynomials is beyond the scope of this paper and may be found elsewhere [5]. In the following, it is shown how these polynomial expressions can be used to determine both the Young's modulus and Poisson's ratio of the material.

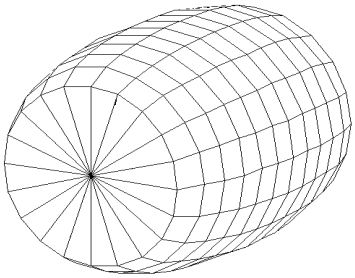

FIGURE 2. Representation of the bulge out effect of the specimen under compression test with bonded ends.

MEASUREMENT METHOD

The method proposed here is to measure the compression stiffness (real part of the transfer function) on two disc-shaped specimens of different shape factors s_1 and s_2, respectively. Using Eq.(2), the following equalities are written:

$$E = \frac{E_1'}{P(s_1,n)} \quad \text{and} \quad E = \frac{E_2'}{P(s_2,n)} \tag{3}$$

Since the apparent Young's moduli of samples 1 and 2 are directly obtained from measurements and Eq.(1), the only unknowns are the true Young's modulus and Poisson's ratio. Since the true Young's modulus is unique for the tested material, the following equation can be drawn from Eq.(3):

$$\frac{E_1'}{P(s_1,n)} - \frac{E_2'}{P(s_2,n)} = 0 \tag{4}$$

Here, the unique admissible zero of Eq.(4) is the Poisson's ratio of the tested material.

Once the Poisson's ratio of the material is found, one of the two equations in (4) can be used to retrieve the true Young's modulus of the material.

Finally, the low frequency structural loss factor can directly be approximated from the measured quasi-static transfer function:

$$h(w) \cong \frac{\mathrm{Im}(TF(w))}{\mathrm{Re}(TF(w))}. \tag{5}$$

RESULTS

To verify the validity of the method and the uniqueness of the solution, a quasi-static compression test is performed on two disc-shaped foam samples of shape factors 0.6519 and 0.1946, respectively. The measured transfer function for sample 1 is given in Figure 3.

Figure 4 plots the variations of Eq.(4) in function of the Poisson's ratio at 32.5 Hz. It is noted that Eq.(4) falls to zero at 0.45 that is the unique admissible solution. For this value of the Poisson's ratio, the true Young's modulus given by Eq.(3) is 108 kPa.

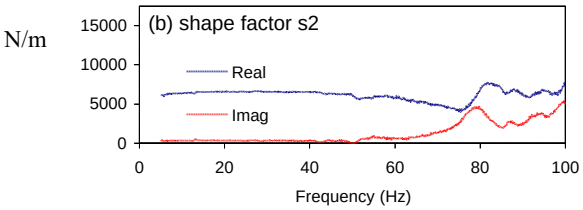

FIGURE 3. Typical measured transfer function $F(L)/x_0$.

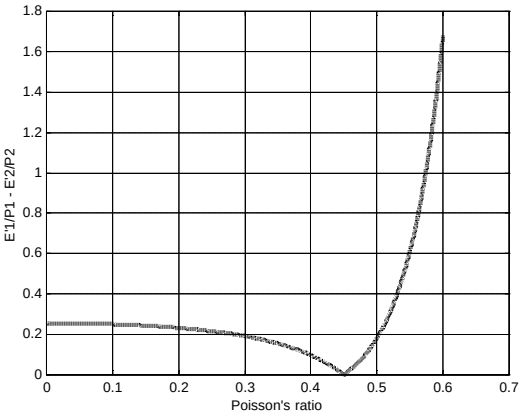

FIGURE 4. Variation of Eq.(4) in function of Poisson's ratio.

Also, using the transfer function given in figure 3, Eq.(5) yields a value of 0.047 for the structural loss factor.

Finally, using the elastic parameters measured with the proposed method, good numerical predictions of the acoustic behaviour of the material can be obtained compared to standing wave tube measurements. Such comparisons and further validations will be presented at the conference. See also reference 6.

ACKNOWLEDGMENTS

This research was supported by the National Sciences and Engineering Research Council of Canada (NSERC).

REFERENCES

[1] J.F. Allard, *Propagation of sound in porous media: modeling sound absorbing materials*, Elsevier Applied Science, London, UK, 1993.
[2] T. Pritz, Applied Acoustics **60**, 279-292 (2000).
[3] S. Sim and K.-J. Kim, Journal of Sound and Vibration **141**, 71-82 (1990).
[4] M. Mariez *et al*, Proc. of Internoise 96, 951 (1996).
[5] C. Langlois, R. Panneton, and N. Atalla, submitted for publication in J. Acoust. Soc. Am. (2001).
[6] D. Pilon, R. Panneton, and F. Sgard, to be presented at 17th I.C.A., Rome, Italy (2001).

Study on the Acoustic Transmission Loss of a Rigid Perforated Screen Backed with Porous Granular Material

P. Ricciardi

D.I.T.E.C.,Università di Genova, Via all'Opera Pia 15A, 16145 Genova, Italy

In this paper the calculation of the sound transmission loss of a perforated screen backed with granular porous media have been discussed. Theoretical models have been analysed. Laboratory measurements in coupled reverberant rooms have been carried out from 125 to 5000 Hz aiming to validating the models. Different model variations have been applied to be more compatible with the analysed granular material and results have been compared with laboratory measurements. The paper clearly shows that the calculation of acoustic transmission loss of the studied panel well agrees with measurements at frequencies below 2000 Hz.

INTRODUCTION

Theoretical analysis and experimental measurements of the sound transmission loss of a perforated screen using two ranges of diameters of granular porous media are discussed. The analysed structure is weatherproof, and, in some cases, is able to resist to high temperatures, up to 600 - 700 C. Sound transmission through rigid perforated screen backed with porous material is an important problem for building acoustics, noise reduction in transport vehicles and other engineering applications. This has been the subject of intensive investigation for many years and various theories have been developed by several authors. In 1949, Beranek and Work [1] studied the transmission of sound through double partitions. They did not consider the damping term and they deal only with normal incidence, which was extended to the diffusive sound field by London [2]. The analysis given by White and Powel [3] did not include the cavity absorption. The theory of Mulholland et al. [4] was restricted to cases where absorbing material with unity absorption is placed only at the edges of the cavity. In recent years Trochidis et al. [5] discussed the sound transmission through double partitions with cavity absorption and Chen [6] developed a model for perforated screens.

THEORETICAL MODELS

Among the various theoretical models the most suitable for the considered structure in diffusive field are the ones of Trochidis et al. [5] and Chen [6].

Trochidis Model

The model considers two infinite thin elastic plates, containing sound absorption material between them and with no connection between the plates. The excitation is a plane acoustical wave incident at angle θ. The acoustic transmission coefficient τ is related to the angle of incidence θ, the air impedance $\rho_0 c_0$, the complex wave number of air K_0, the radian frequency ω, and the Fourier transform of the normal displacement w_2 of the inner plate, by the following equations:

$$\tau(\theta) = \frac{\rho_0 c_0}{4\pi \cos\theta} \int_{-k_0}^{k_0} \frac{\rho_0 \omega^3 |w_2(s)|^2}{\sqrt{k_0^2 - s^2}} ds \qquad (1)$$

Chen Model

Chen proposes a two dimensional plane wave theory for the calculation of perforated screens. The mean transmission loss for all possible angles of incidence can be determined by the following equation:

$$TL = -10 \log \int_0^{\frac{\pi}{2}} \left| \left[\frac{1}{(A\cos\theta)+1} \right]^2 \right| sin2\theta d\theta \qquad (2)$$

where A is the ratio between the impedance of the perforated screen to twice the characteristic acoustic impedance of a plane wave propagating in open air.

EXPERIMENTAL RESULTS

To validate the considered models, measurements of the transmission loss were carried out in a coupled room in accordance with standard ISO 140-10 [7]. A containing structure (thickness of 5 cm) with a screen with perforation of 22%, (diameters of holes of 1.2 mm and thickness of 0.75 mm) on the source side, and a rigid metal screen on the other side (same thickness), has been filled by four different components: (A) foamed leaked clay with diameter of 2-3mm; (B) foamed leaked clay with diameter of 8-15 mm; (C) glass ball with diameter of 2-3mm (D); glass ball with diameter of 8-15 mm. Since the foamed clay presents a dual porosity, the glass balls have been tested in order to evaluate the effect of porosity. Results are plotted in figure 1.

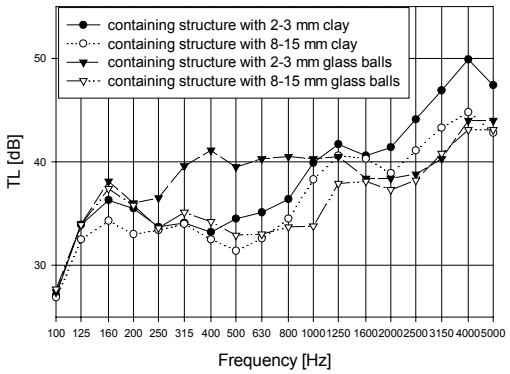

FIGURE 1- Transmission loss of the absorbent structure with four different materials versus frequency

DISCUSSION

Trochidis and Chen theories have been calculated for the experimental absorbent structure. Since they were not completely satisfying in simulating the transmission loss of the analysed granular material, different model variations have been applied. Trochidis formulation has been modified applying the complex wave-number K_b in the absorptive materials of Mechel [8] and of Delaney and Bazley [9]. Comparison between the model of Trochidis with the two different K_b and experimental data of clay with diameter of 8-15 mm are presented in figure 2. Input data for the absorptive materials have been presented in a previous work [10].

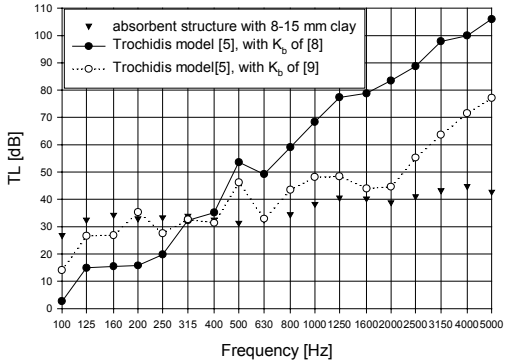

FIGURE 2- Comparison between experimental data of the analysed structure with 8-15 mm clay and Trochidis model [5] with complex wave-number of Mechel [8] and of Delaney and Bazley [9]

Further on the term A of the Chen model [6] have been modified with the impedance of the whole structure, evaluated as of sum of impedances of the three components. For the impedance of the absorptive material the models of Mechel [8], of Delaney and Bazley [9] and of Hamet [11], with structure factor equal to 3, flow resistance and porosity [10], have been applied and compared.

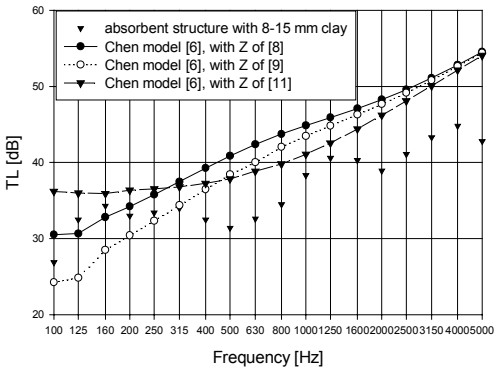

FIGURE 3- Comparison between experimental data of the analysed structure with 8-15 mm clay and Chen model [6] with different values of foam clay impedance [8, 9, 11].

CONCLUSIONS

Among models variations, Trochidis with the approximate formula of Delaney and Bazley and Chen with Hamet impedance seems to agree better with the considered granular porous media. Comparison between the two models have been carried out. The statistical factor used for this comparison is the Intraclass Correlation Coefficient (ICC), as the ratio of variance between subjects to total variance (variance within subjects plus variance between subjects) [12]. The modified Chen model values show a better agreement (ICC=0.77), then Trochidis (ICC=0.70), but both the models present a systematic error for frequency above 2000 Hz. The analytical models can be extended to develop the dependence of the transmission loss on the thickness, the percentage of perforation, porosity and flow resistance. Further work in this direction is current under way.

REFERENCES

[1]. L.L Beranek, G.A. Work, *J. Acou. Soc. Am*., **21**, 419-428, (1949).
[2]. A. London, *J. Acou. Soc. Am*, **22**, 280-288, (1950).
[3]. P. White, A. Powell, *J. Acou. Soc. Am*, **40**, 821-832, (1966).
[4]. K.A. Mullholland,, H.D. Parbrook, *J. Sound & Vibrations*, **6**, 324-334, (1968).
[5]. A. Tronchidis, A. Kalaroutis, *J. Sound & Vibrat*, **107**, 321-327, (1986).
[6]. K.T Chen, *App. Acoustics*, **46**, 131-151, (1995).
[7]. ISO 140-10, "Measurements of sound insulation in buildings and of building elements –1993, pp-1.11.
[8]. F. P. Mechel, *J. Acou. Soc. Am*, **83**, 1002-1013, (1988).
[9]. M. E. Delany, E. N. Bazley, *Applied Acoust*., **3**, 105-116, (1980).
[10] R. Bartolini, P. Ricciardi, C. Schenone, *XXVII Convegno AIA*, Genova, Italy, 1999, pp.139-143.
[11]. J.F. Hamet, *Rapport INRETS* n.159, 1-65, (1992).
[12] M.J.Bland, D.G.Altman *Lancet,* 307-10 (1986).

Global Inverse Methods for determining the Acoustical Parameters of Porous Materials

J. Tran-van[a,b,c], X. Olny[b], F.C. Sgard[b] and Y. Gervais[c]

[a]*Saint-Gobain Isover France, "les Miroirs",18 Avenue d'Alsace 92096 LA DEFENSE CEDEX*
[b]*Elaboratoire des Sciences de l'Habitat, Département Génie Civil et Bâtiment, URA CNRS 1652 Ecole Nationale des Travaux Publics de L'Etat,rue M. Audin, 69518 Vaulx-en Velin Cedex*
[c]*Laboratoite d'Etudes Aérodynamiques, Université de Poitiers, 40 Av. du recteur Pineau,86022 Poitiers Cedex*

Most of insulating or absorbing passive systems used in buildings acoustics involve porous materials. In order to predict their vibroacoustic behavior, it is necessary to determine their intrinsic acoustical parameters. Direct measurement of all parameters is however difficult. To alleviate this difficulty, a recent study has shown that inverse identification methods can be used to find out these parameters. In particular, tortuosity, viscous and thermal lengths can be evaluated from acoustical measurements in a standing wave tube combined with a direct measurement of porosity and resistivity. In this paper, global inverse methods are presented to characterize the acoustical parameters of anisotropic porous materials. The performance of these global inverse methods is discussed in isotropic case.

INTRODUCTION

The various models established to predict absorption coefficient and impedance of absorbing materials introduce some acoustical parameters. The inverse identification method[1] is a way to obtain these parameters using for example the absorption coefficient measurement of the material. Various optimization algorithms may be used, from the easiest one consisting in sweeping of each set of parameters (for example, the impedance for 10000 different combination of parameters is computed and the set giving the low difference between impedance calculation and measurement is selected) to more complex ones like genetic algorithms, cost function optimization…
In this paper is investigated a method using neural networks to determine three of the five acoustics parameters of the Biot-Allard model[2] from the measurements of the dynamic equivalent compressibility Keq and dynamic equivalent density ρeq.

USING NEURAL NETWORKS IN THE CASE OF ISOTROPIC MATERIALS

BIOT-ALLARD Model

Biot-Allard's model uses five parameters to determine completely the impedance and absorption of a porous material saturated by air. Dynamic compressibility and density of the equivalent fluid equivalent media are expressed as:

For the thermal effects, the dynamic compressibility is:

$$Keq = \frac{\gamma P_0 \phi^{-1}}{\left[\gamma - (\gamma-1)\left[1 + \frac{\sigma'\phi}{j\,\mathrm{Pr}^2\,\omega.\rho_0\alpha_\infty} G_J'\left(\mathrm{Pr}^2\,\omega\right)\right]^{-1}\right]}$$

with $G_J'(\mathrm{Pr}^2\,\omega) = \left(1 + \frac{4j\alpha_\infty^2\eta.\rho_0\omega\,\mathrm{Pr}^2}{\sigma'^2\Lambda'^2\phi^2}\right)^{1/2}$

and $\sigma' = \frac{8\alpha_\infty\eta}{\Lambda^2\phi}$

For the viscous effects, the dynamic density is:

$$\rho eq = \alpha_\infty\rho_0\phi^{-1}\left[1 + \frac{\sigma.\phi}{j\alpha_\infty\rho_0\omega} G_J(\omega)\right]$$

with $G_J(\omega) = \left(1 + \frac{4j\alpha_\infty^2\eta.\rho_0\omega}{\sigma^2\Lambda^2\phi^2}\right)^{1/2}$

These dynamic properties are obtained using the surface impedance of a porous material for example a rigid backing.

$$Zs = -j\left(Keq.\rho eq\right)^{1/2} \cot\left[\omega\left(\frac{Keq}{\rho eq}\right)^{1/2} d\right]$$

According this model, porosity, resistivity, tortuosity, viscous and thermal characteristic lengths allow to completely determine the acoustic behavior of the porous material considered as an equivalent fluid.

Design of the neural network adapted for inversion problem

A method based on neural network is proposed to solve the inverse problem consisting in finding the set of acoustic parameters which minimize a cost function equal to the difference between the measured and computed values for dynamic compressibility and density.

Neural network principle

A neural network is composed of differents layers of neurons. Each of the neuron of a layer is characterized by a weight and a bias. Each neuron is connected to all neurons of the previous layer and has one output which corresponds of the input of all neurons of the next layer. The network type used here is a radial basis network[3]. It uses two neurons layers with as many neurons as input vectors for the training and as many output as searched parameters.

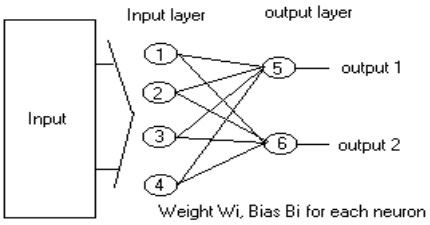

Data used for training phase

The neural network is trained with compressibility Keq and density ρeq of the equivalent medium as input data, and the five parameters as output. Training was tested with data corresponding to a number of materials between 32 to 1024. Dynamics compressibility and density were calculated for a number of frequencies comprised between 25 and 2500. Time calculation for the training p increases with the number of materials selected for the learning. Once trained, the network efficiency is evaluated by testing some materials which were not included in the training data base. Table1 displays some results:

Table 1. Parameters values calculation, N=243.

Parameter	Neural network value	Selected value
Porosity ϕ	0.94	0.95
Resistivity σ ($Nm^{-4}s^{-1}$)	50000	55000
Tortuosity α_∞	1.28	1.32
Viscous characteristic lenght Λ (m)	5e-4	4e-4
Thermal characteristic lenght Λ' (m)	1e-3	8e-4

Method limitation and comparison with other methods

The main problem encountered using neural network is the training step. In order to be efficient, and representative, it requires a large calculation calculation. The data selected should be numerous enough to allow the network to give corrects results. But once trained, the network can provide output values very quickly.
When it is compared to the try of a determined set of parameters, the neural network allows, to identify the parameters of a given material in a very short time. Compared to an optimization on three parameters simultaneously, and using just one set of parameters as initial condition, the neural network avoid local minimum.

CONCLUSION

Numerical inversion methods can be efficient in the determination of the parameters. These methods may be adapted to the determination of acoustical parameters of porous materials. The interest is to carry out measurements using a stranding wave tube to obtain values which are difficult to measure directly.

REFERENCES

1. Y. Atalla, R. Panneton, Inverse problem for a complete characterization of rigid porous materials using a standing wave tube, Acoustics Week in Canada 2000, september 28-29,2000

2. J.F. Allard, Propagation of sound in porous media. London and New-york: Elsevier Applied Science, 1993. 284 p.

3. J.M. Renders, Algorithmes génétiques et réseaux de neurones, publication Hermès Sciences 1995 336p.

An Acoustic Measurement of a Typical Parameter for the Porous Rigid Materials

M. A. Picard[a] , P. E. Solana[a] and J. V. Arizo[b]

[a]*Department of Applied Physics, Universidad Politécnica, 46022 Valencia, Spain*
[b]*Departament of Ing. e Infraest. De los Transportes, Universidad Politécnica, 46022 Valencia, Spain*

The porous rigid materials, by means of an electric or an equivalent fluid analogy, can be analysed. These media of rigid structure or lower coupling between the structure and the fluid that is contained in the pores. It is habitual to characterise them by physical parameters, as they are the density of the sample, the porosity, the flow resistivity and acoustic properties, as the characteristic impedance, the complex constant of propagation, the density and the compressibility of an equivalent fluid. And the compressibility of the equivalent fluid or their inverse one the bulk modulus, by theoretical, thermodynamic, and microscopic models is usually obtained. In this work this parameter is calculated and contrasted from acoustic hypothesis and the acoustic measure of the flow impedance for very thin samples.

INTRODUCTION

The porous materials with small coupling between the air and the structure can be studied by means of empiric approaches as the one of Delany [1] and that later on it was improved for Miki [2]. With them the characteristic impedance of the media and the constant of complex propagation can be obtained. The most representative parameter is the flow resistivity that in stationary régime under conditions of régime of slow flow (Poiseuille) it can be determinated, so that it is not it an acoustic parameter. You can also proceed acoustically by means of the measure of the specific flow impedance [3]. This last parameter is of great utility for the study of the other acoustic properties of these media like we will see next.

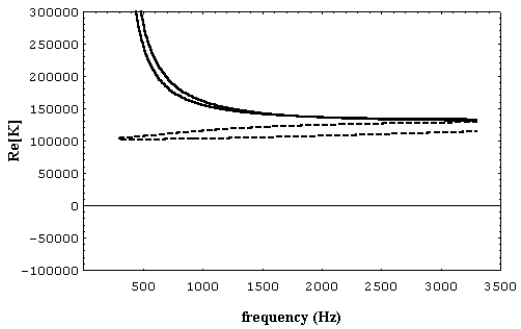

FIGURE 1. Theoretical Real Part of Bulk Modulus.

If a fenomenological approach is made [4], [5], it is habitual to work with the complex effective density and the complex compressibility of the equivalent fluid. It is also possible an experimental study of the samples by means of the measure of the impedance of samples of simple and double thickness [6], but their results can have problems if the

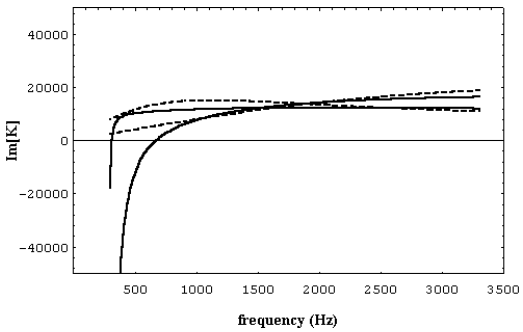

FIGURE 2. Theoretical Imaginary Part of Bulk Modulus

existent differences in the measure of impedance of the samples are small. The previous approaches can help to make a measure of the compressibility or their inverse one the bulk modulus of the samples, using the results of the measure of the flow impedance. In this work differences are observed among the theoretical results of the bulk modulus according to different formulations and they are compared with the procedure experimental employee.

Theoretical approaches of the Compressibility

In a fenomenological approach the effective complex compressibility and their inverse the complex bulk

modulus of the porous samples by the formulation of several authors can be approximate. In a thermodynamic approach [7] the bulk modulus is function of the inverse thermal constant of time. By

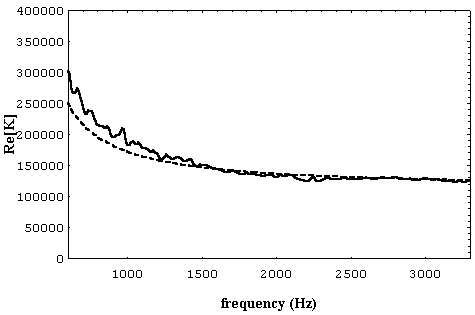

FIGURE 3. Experimental real part of bulk modulus

means of acoustic approach based on the electric analogy [6], [7], it is possible to express the compressibility in function of the characteristic impedance and of the propagation constant, being able to determine these properties by empiric approach. And finally from an approach of microscopic properties of the samples the formulation of Allard [5] can be used. In the Figures 1 to and 2 the dashed lines represent the thermodynamic and microscopic approaches [6], [5]. The continous bold lines represent empiric approaches [1], [2]. Important differences can be observed in low frequencies.

Experimental approach

The model experimental is based the acoustic measure of the specific dynamic flow impedance that one can make by a variant [3] of the method of Ingard and Dear [9], and the value of the elastic module or its inverse one the compressibility can be obtained that follows:

$$\breve{Z}_f = \phi + j\omega\rho_p = j\omega\,\breve{\rho}_e \qquad (1)$$

Where ϕ is the flow resistance, ω is the circular frequency, ρ_p is the density of air in the pores and $\breve{\rho}_e$ is the effective density of an equivalent fluid. With the results of this measurement and using the formulation of Morse [4] the complex bulk modulus $\breve{K}$ of the equivalent fluid can be expressed as a function of the complex characteristic impedance $\breve{Z}_c$ or the propagation constant of the medium $\breve{\gamma}$:

$$\breve{K} = \frac{j\omega\,\breve{Z}_c^{\,2}}{\breve{Z}_f} = \frac{j\omega\,\breve{Z}_f}{\breve{\gamma}^2} \qquad (2)$$

Where both values are function of the experimental flow impedance and calculable characteristic parameters. The complex fluw impedance was measured with a experimental setup shown in the reference [3].

RESULTS

The analyzed rigid samples were of rockwool of density $175\,kg/m^3$. The Figures 3 and 4 indicate a good adjustment between theory and experiment. The obtained results have been gotten comparing the theoretical value of the complex bulk modulus obtained by means of two empiric expressions [1], [2] into eq.(2).

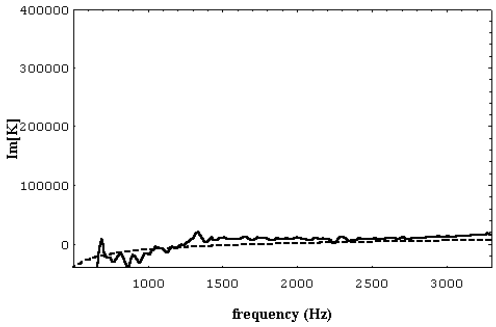

FIGURE 4. Experimental imaginary part of bulk modulus

REFERENCES

1. M. E. Delany and E. N. Bazley, *Applied Acoustics* 3, 105-116 (1970).
2. Miki Y., *J. Acoust. Soc. Jpn.* 11, 1 18-24 (1990).
3. M.A. Picard, P. Solana and J.F. Urchueguía, *Journal of Sound and Vibration* 216, 495-505 (1998).
4. P. M. Morse and K.U. Ingard, *Theoretical Acoustics*. (Princeton University Press. Princeton. New Jersey 1968) .
5. J. F. Allard, *Propagation of Sound in Porous Media Modelling. Sound Absorbing Materials.* Elsevier Science Publishers, (1993). Chap. 4, Chap. 5.
6. Smith C.D., Parrott T.L., *J. Acoust. Soc. Am.* 74 (5), 1577-1582, (1983).
7. L. L. Beranek, *Noise and Vibration Control Engineering* (Jhon Wiley & Sons 1992), p. 205.
8. R. F. Lambert and J. S. Tesar, *J. Acoust. Soc. Am.* 76, 1231-1237 (1984).
9. K.U. Ingard and T.A. Dear, *Journal of Sound and Vibration* 103, 567-572 (1985).

Experimental investigation about possible sources of uncertainty for sound absorption measurements in reverberation chambers

M. Nabuco[a], R. A. Tenenbaum[b] and A. Schmitz[c]

[a]*Laboratório de Ensaios Acústicos,-INMETRO, Av. N.Sra. das Graças, 50, Xerem, 25250-020-Brasil*
[b]*Laboratório de Acústica e Vibrações-Dep. Eng. Mecânica, Universidade Federal do Rio de Janeiro-Brasil*
[c]*Applied Acoustics Section-PTB-Germany*

The precision of ISO 354 for sound absorption measurement in reverberation chambers is still under investigation. Up to now most Inter-Laboratory Tests have furnished a variety of spread results. These inter-laboratory differences can be attributed to the distincts states of diffusion in the chambers, mainly when the sample is inserted in. Up to now the required state of diffusion in the reverberation room shall be reached installing diffusers devices. No "diffusiness" criterion is available up to now. This paper presents the data obtained in an experimental investigation of the reverberation time spatial standard deviation as a possible descriptor for the degree of diffusion in reverberation chambers for sound absorption measurements. The uncertainty of the method with respect the variance of the most significative variables that take part of the sound absorption coefficient measurement is discussed. The reproducibility standard deviation was calculated from data obtained in two different ILT carried on among Germany and South American laboratories and the results obtained during a repeatability test performed for a mineral wool sample using interrupted noise technique.

INTRODUCTION

Among all techniques used to evaluate the sound absorption coefficient, the reverberation chamber method [1] is the only standardized one that allows to test larger samples areas of material under a sound field closer to practical situations.

It is known [2, 3] that the magnitude of differences found in inter-laboratory comparisons (ILT) for reverberation chamber sound absorption measurements are very large. The most reported reason is the differences on sound field diffusion degree among participating laboratories.

To measure and calculate the sound absorption coefficient for diffuse sound field incidence using Sabine or any other equivalent formula, means to work with spatial average values for the reverberation time in the room. Although a lot of investigation were made in the past no reliable results of precision concerning the measurement method can be given. Therefore even the new draft standard of ISO 354 (2001) [1] does still not deal with precision data.

This paper is a contribution to enhance the knowledge about precision. Therefore next sections present some statistical data obtained during a repeatability investigation involving two different reverberation rooms and samples of mineral wool. The spatial reverberation time standard deviation showed to be potentially a possible diffuse field indicator, maybe for reverberation chambers qualification.

DIFFUSE SOUND FIELD INDICATOR

In order to investigate the sound field diffusion, the sound absorption coefficient of a mineral wool sample (45 kg/m^3) 100 mm thick was tested in the reverberation room of PTB which has a volume of approximately 230 m^3 . The rotating diffuser was either switched on or off. Fig. 1 shows the curves for sound absorption coefficient.

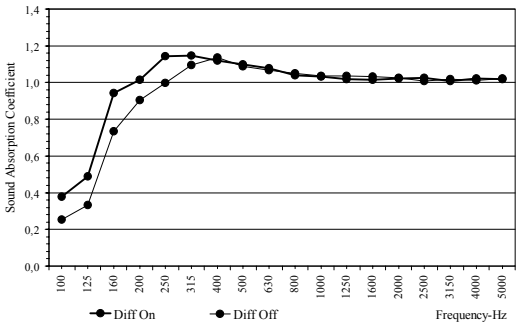

Figure 1. Sound absorption coefficient for a mineral wool sample measured with the rotating diffuser either switched on or off

Although it is possible to observe an expected difference between the curves for the two diffuse field condition, it can not be identified any significant difference between 500 Hz and 5000 Hz, exactly the frequency range recommended by ISO 354 to evaluate the room with qualification purposes (static diffusers installation-Annex A [1]).

The Spatial Reverberation Time Standard Deviation was investigated in four diffuse field degrees: the most diffuse field condition is associated to the empty room with rotating diffuser on. A second stage is attributed to the empty room without the diffuser operating. A third and fourth condition were associated to the same rotating diffuser operation state but with the sample in the room (Fig. 2).

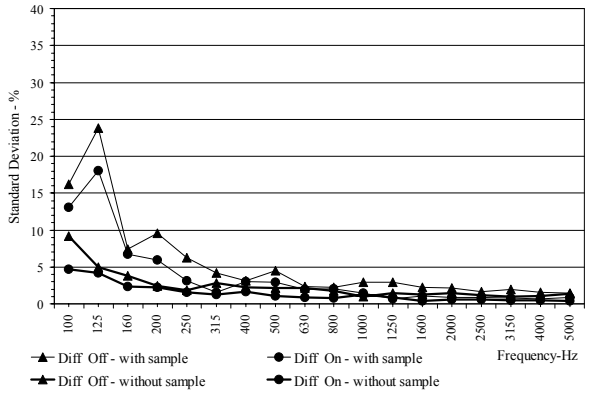

Figure 2. Spatial Reverberation Time Standard Deviation

If the diffuse field hypothesis were correct it would be possible to see a relationship between the spatial reverberation time variation and the different degree of "diffusity" in the room.

UNCERTAINTY DEVIATIONS

The reproducibility value [4] is defined as the range of values in which the difference between two single results on identical test material reported by two laboratories should be. It is calculated from the repeatability and reproducibility variances.

Figure 3 shows curves for the repeatability, reproducibility and spatial reverberation (room with sample) time standard deviations performed using the same sample material.

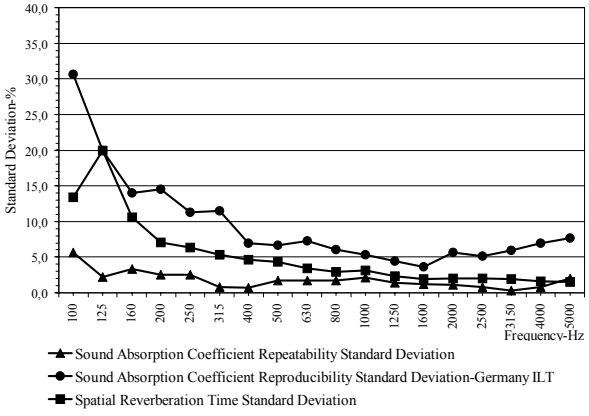

Figure 3. Repeteatability, Reproducibility and Spatial Reverberation Time Standard Deviation

While the repeatability standard deviations values remained at stable low values, the reproducibility and the spatial reverberation time standard deviations showed high values for frequencies below 500 Hz.

FINAL COMMENTS

All curves showed to be interesting to extend the frequency range for reverberation room adjustment for sound absorption coefficient measurements for frequencies lower than 500 Hz.

Spatial Reverberation Time Satandard Deviation

The spatial reverberation time standard deviation appears as a possible powerful parameter to qualify reverberation rooms for sound absorption measurements. Unfortunately, up to now, the experiments allowed only qualitative analysis once there is no absolute sound absorption value to be compared. With a reference artefact, as PTB is developing, it will be possible to establish a limit for the spatial reverberation time standard deviation that could assure high reliability for the measurements.

Inter-Laboratory Testing ILT

For future ILT experiments it would be the best to use preferably a reference sound absorber. A new ILT will be started in Brazil in collaboration with PTB. The laboratories will be invited to test five times two different reference absorbers using their own methods, equipment and sound source. The samples will also be tested with a standard method using backward integration technique and a sound source as directional as possible (as recommended by ISO 354).

ACKNOWLEDGEMENTS

The authors would like to acknowledge the Physikalisch Technische Bundesanstalt – (PTB) Braunschweig Germany to have sponsored this research and gently enabled its facilities for all measurements.

REFERENCES

1. ISO 354-"Acoustics-Measurement of sound absorption in a reverberation room", *Int. Org. for Standardisation* (1985)
2. Kosten, C.W., *Acustica* **10**, pp 400-411 (1960)
3.Malte, K., "Vergleichbarkeit von Absorptionsgrad-messunge im Hallraum", Diploma Thesis Technischen Universitaet Braunschweig, Germany, 1994
4. ISO 140-2 Acoustics-Measurement of sound insulation in buildings and of building elements - Part 2: Determination, verification and application of precision data, *Int. Org. for Standardisation* (1991)

Sound Absorption Characteristics of Microperforated Absorbers for Random Incidence

L. Ke, M. Dah-You
Institute of acoustics, Academia Sinica. 100080 Beijing, P.R.China

Based on previous work on "Statistics absorption coefficient of microperforated absorbers", in which it was shown that theoretical results agree well with experiments on the absorption characteristics of microperforated absorbers (MPA) for random incidence. Further work was carried out in this investigation of the statistical absorption coefficients of MPA in random fields by computation, in order to find the best structure of MPA. It is established that ordinarily the absorption curves of MPA for random incidence and that for normal incidence are quite alike, only that the absorption coefficients are more or less reduced and the whole curve is shifted to higher frequencies without any change of shape. But when the perforate constant is reduced below 2, say, secondary absorption bands start to play more important role. Pretty soon, they merge with the main absorption band and form a long tail of the latter, extending the absorption far into high frequencies, raising the resulting absorption band to three, four or more octaves. The behavior of the secondary absorption bands is discussed.

INTRODUCTION

In a recent work[1], it has been shown that the computed statistical absorption coefficients agree well with experiment, thus the behavior of the MPA in diffuse sound field can be predicted as well. This leads to global survey of the acoustical behavior of the MPA in diffuse sound field. This relation is very important, because the computation of statistical coefficient of MPA is much more involved than the computation for normal incidence, and may be replaced by the latter, when their exact relations exist. It is found when the value of k is reduced they become more and more significant and pretty soon they start to play an important role in absorption, as the perforate constant is reduced to a low value, and the absorption is extended far into high frequencies. Thus the MPA may be used as a general absorber or absorber for specific purposes[2].

Theory

The absorption coefficient of MPA at normal incidence[3] [4] [5]

$$\alpha_n = \frac{4r}{(1+r)^2 + (a\xi - ctg(b\xi))^2}. \qquad (1)$$

The absorption coefficient of the MPA when sound is incident on it at an angle θ to its normal is given by

$$\alpha(\theta) = \frac{4r\cos\theta}{(1+r\cos\theta)^2 + (\omega m\cos\theta - ctg(\frac{\omega D\cos\theta}{c})^2)} \qquad (2)$$

In a diffuse sound field, the statistical absorption is the average of all angles of incidence and equal to[6]

$$\alpha_{stat} = \int_0^{90}\alpha(\theta)\sin 2\theta d\theta \qquad (3)$$

Substituting Eq(3) into Eq(2) and writing x for cosθ and ξ for f/f_0, it yields

$$\alpha_{stat} = \int_0^1 \frac{8rx^2\cdot dx}{(1+rx)^2 + (\omega mx - ctg(\frac{\omega Dx}{c}))^2} \qquad (4)$$

Thus the acoustical behavior of MPA, either for normal incidence or in diffuse sound field depends on the values of perforate constant k and the resistance ratio r. Among the two parameters k is the most important one, because the value of r is rather limited, considering its effect on the magnitude of maximum absorption. An investigation of the acoustical behavior involves only the computation on measurements of MPA over parameter values of k and r.

Results

It was decided to work first on a fixed intermediate value of the perforate constant k, and change the value of r to see its effect in general.

MPA with larger values of k in random field

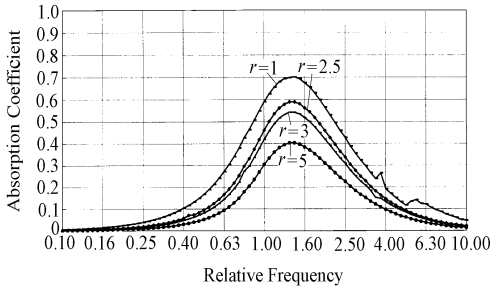

FIGURE 1. Absorption curve in diffuse field for k=2.5

As value of k is increased to 2, 2.5, to 3, the absorption curves for different values of r in random field are quite alike. When k=2.5, the absorption curves for different values of r in random field is shown in Fig.1. The secondary absorption band for k=2.5 become a ripple on the absorption curve and negligible in absorbing sound. The secondary band essentially disappear.

Small k

It is evident that better absorption requires smaller values of the perforate constant k. First try the extreme, k=0.5, lower than which the behavior of MPA does not change significantly.

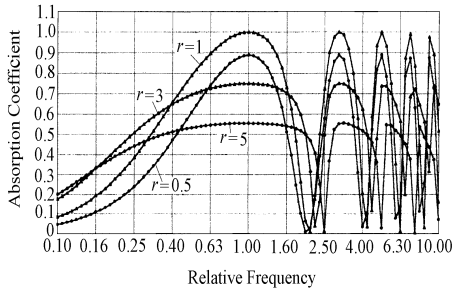

FIGURE 2. Absorption curves for k=0.5 at normal incidence

The situation is entirely different from that for large k. Normal incidence absorption curves are shown in Fig.2 for different values of r. The main absorption bands are exactly what were predicted in a previous work[2], but the absorption curves for higher values of r are no more entirely under the ones for lower values of r. The band interval increase rapidly with the value of r. The rise of secondary absorption bands are tremendous, having comparable band widths and essentially the same maxima as the main bands.

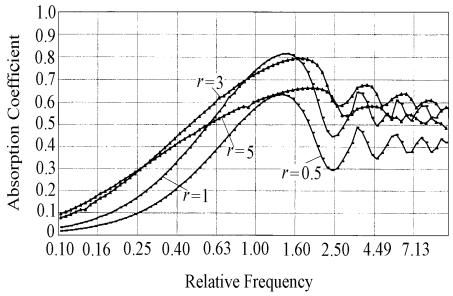

FIGURE 3. Absorption curves for k=0.5 in diffuse field

All these improvements of the frequency characteristics for normal incidence are reflected to the acoustical behavior of the MPA in diffuse sound field (Fig.3). The secondary absorption bands have merged with the corresponding main absorption band to make it greatly extended.

Variation of maximum absorption

The value of α_m, the maximum absorption coefficient at random incidence is usually lower than that at normal incidence. Butα_m may equal to or even greater than α_0, as k is smaller than 1.6, especially when r is large.

Discussion

The perforate constant k and resistance ratio r have been taken for computation to make a survey of acoustical behavior of microperforated absorbers for random incidence, and it has been established that under specific conditions of k and r, the absorption of the MPA may be extended to higher frequencies tremendously by emphasizing the contributions of the secondary absorption bands. This makes the MPA entirely different from what one can imagine heretofore. The relation of the behavior of MPA in random field to that at normal incident, as described by maximum absorption α_m and frequency shiftξ_m , as well as the absorption of the secondary absorption bands make it a straight forward process to design the MPA from the desired characteristics. To realize the absorber, its structure constants, say d, f_0, b, t, D are easily determined through the Eq. with known values of k and r . Among these, t and d or f_0 may be arbitrarily chosen to suit the purpose, within some reasonable limits. The board material may also be freely chosen from metal, wood, plastics, paper board or films.

ACKNOWLEDGMENTS

The project is supported by national nature science foundation of China.

REFERENCES

1. Nocke, Christian, LIU Ke, MAA Dah-You, *Chin. J.Acoustics.*, **19**(2), 97-104 (2000).

2. H.V.Funchs, X Zha, *Acustica*, **81**, 107-116 (1196).

3. Maa Dah-You, *J.Acoust.Soc.Am.*, **104**(5), 2861-2866 (1998).

4. Maa Dah-You, *Noise Control Eng. Journ.,* **20**(3), 77-84 (1987).

5. Maa Dah-You, *Chin.J.Acoustics,***16**, 193-202 (1997).

6. Morse,P.M.,Bolt R.H., Rev.Mod.Physics (1944) 16,65-150

The acoustic location detection of the defects in in-homogeneous material by tapping on the surface

R. Shimoyama and K. Yamazaki

College of Industrial Technology, Nihon University, 1-2-1 Narashino Chiba, Japan

The acoustic location detection of the inner cave in the wood board as a sample of the in-homogeneous material with the automatic tapping system is discussed. The time-dependent sound pressure, which was radiated by tapping the wood on the surface at many points, was measured. The relations between the distribution of the sound pressure amplitude radiated by tapping the wood on the surface at the frequency, which gives the space differential of the amplitude maximum and the cave location, were shown. It was found that the peak of the sound pressure amplitude appeared close to the inner cave and its level abruptly changed across the surface above the inner cave at higher frequency.

INTRODUCTION

The sounding method of tapping with the hammer and of listening the radiated sound is frequently used to detect the inner defects in the material. This method which is available to check the material without any information about the material constant, the shape and the boundary condition depends on the human ability for sound recognizing. We have proposed the acoustic method to detect the location of the backside holes on the wood plate [1]. The sound pressures radiated by tapping on the surface at many points were measured. The specific frequency, which gave the space differential of the sound pressure amplitude maximum, was searched. The amplitude of the sound pressure radiated by tapping on the surface near the holes remarkably depended on the tapping position at the searched frequency. In the present paper, The relations between the sound pressure amplitude distribution at the searched frequency and the inner cave location in the wood board are shown.

METHOD AND PROCEDURE

The flat board of Japanese Judas tree (W0.25 × L0.30×D0.030, Unit : m) was mechanically tapped on the surface at a lot of points with the automatic tapping system in Figure 1. The compressed air (0.2MPa) actuated the air cylinder (0.01φ) to tap on the surface with the iron hammer rounded at the tip. The air cylinder could be positioned with a precision of 0.0001(m) in x, y and z direction. The radiated time-dependent sound pressure (up to 6.4kHz) was detected with the microphone which was set and fixed at the coordinate (0.150, -0.125, 0.10) and was recorded and analyzed with Pulse 3560C. The wood board was made of double plates(W0.25×L0.30×D0.015)bonded each other with the epoxy adhesive, in which each plate had a groove in face-side at the corresponding position. The board surface was tapped on two regions

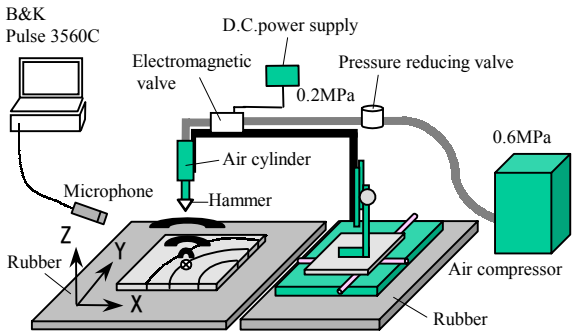

Figure 1. Measuring system

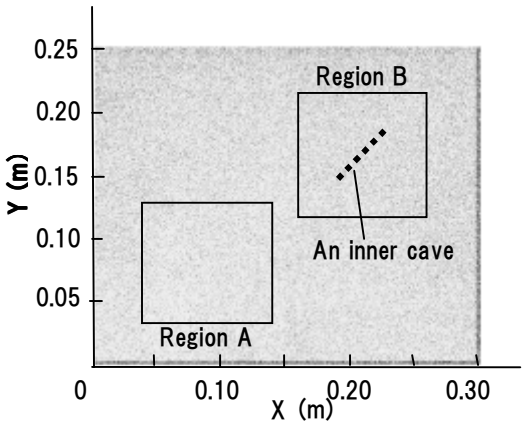

Figure 2. A wood board apparatus and two tapping regions on the surface

A, B in Figure 2. Region A has no artificial defects and region B includes an inner cave (W0.013×L0.073 × D0.022, surface thickness 0.003). As the sound radiated by tapping might depend on the surface condition, the sound data recording were repeated 3 times at the same position after 20 times tapping in advance. Three recorded data were averaged after FFT transformation. The wood surface was tapped at 11 ×11 points in x, y direction with constant interval Δx, Δy in each region (Figure 2.). The space differentials $d^{(x)}_{i,j}$, $d^{(y)}_{i,j}$ of the sound pressure amplitude were

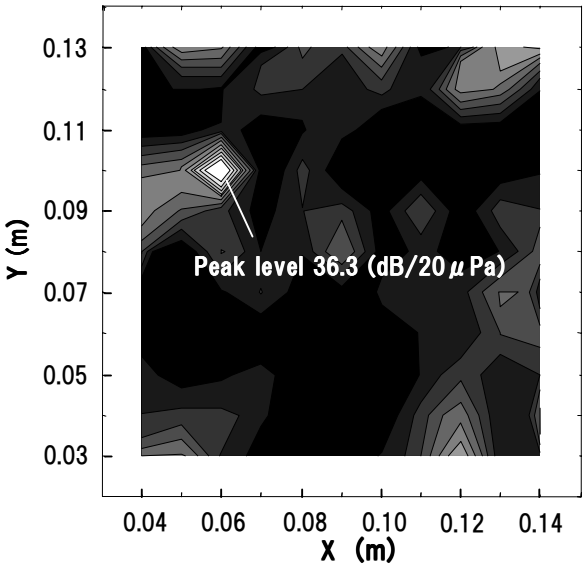

(a) Region A with no defects at 5320Hz

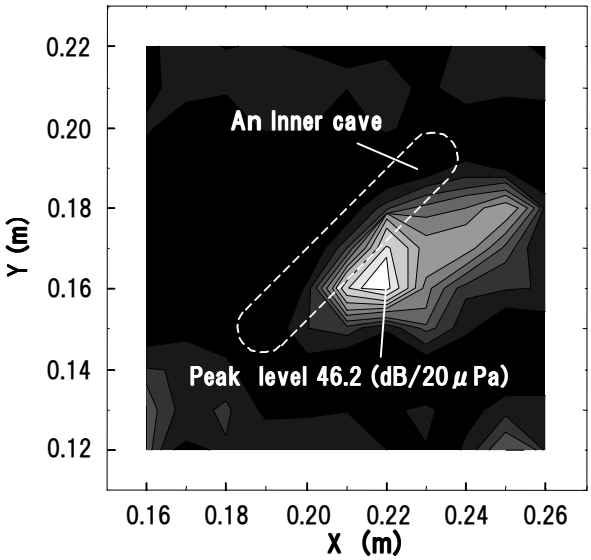

(b) Region B with an inner cave at 5472Hz

Figure 3. The relative sound pressure amplitude distributions in two regions

numerically approximated in x, y direction at the position (i, j) as follows.

$$d^{(x)}_{i,j} = \frac{S_{i+1,j} - S_{i,j}}{\Delta x} \qquad (1)$$

$$d^{(y)}_{i,j} = \frac{S_{i,j+1} - S_{i,j}}{\Delta y} \qquad (2)$$

Where i = 1 to 10, j = 1 to 10, $S_{i+1,j}$, $S_{i,j+1}$, $S_{i,j}$: the sound pressure amplitudes at the arbitrary frequency. While the frequency was swept from f_L to f_H, the maximum of $|d^{(x)}_{i,j}|$ or $|d^{(y)}_{i,j}|$ was numerically searched at all of the measured points. Then the sound pressure amplitude distribution was obtained at the searched frequency in which the space-differential was max.

RESULTS

Figure 3 show the relative amplitude distributions of the sound pressure measured for tapping (a) in the region A with no defects and (b) in the region B included an inner cave. Each frequency was obtained by searching from 4.2kHz(f_L) to 6.4kHz(f_H). The high sound pressure level is shown in white and the lower level in darker. The sound pressure peak appeared close to the inner cave in Fig. 3(b). The peak level of the sound pressure in Fig. 3(b) was 46.2 (dB/20 μ Pa) which was higher about 10(dB) than the peak level in Fig. 3(a). The sound pressure levels along x direction corresponding to Fig. 3(b) for five times tapping at the same position are shown in Fig.4. It was found that the sound pressure level abruptly changed about 20(dB) across the surface above the inner cave at 5472Hz.

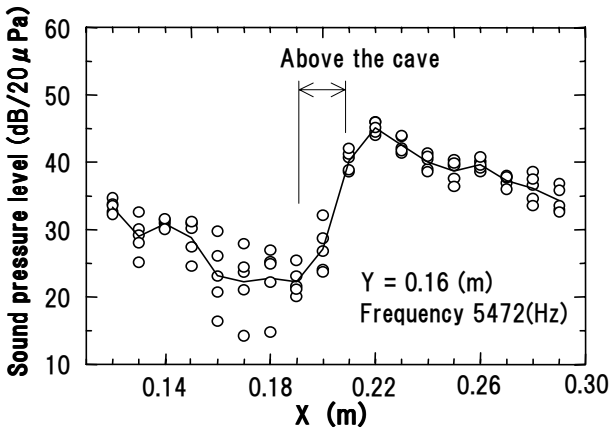

Figure 4. The sound pressure amplitudes along x direction for five times tapping at the same position

SUMMARY

The time-dependent sound pressure (up to 6.4kHz) radiated by tapping on the wood board surface with an inner cave were measured at a lot of points. The relations between the sound pressure amplitude distribution and the inner cave location were investigated. It was found that the sound pressure peak appeared close to the inner cave and its level abruptly changed about 20(dB) across the surface above the inner cave at 5472Hz.

REFERENCE

1. Shimoyama, R. and Yamazaki, K.," Nondestructive acoustic detection of material discontinuities by hammering on the surface" in Proceedings of WESTPRAC VII, ASJ, Japan, 2000, pp. 349-352.

Dynamic and Acoustic Properties of Orthotropic Sandwich Structures

E.M. Nilsson

MWL (The Marcus Wallenberg Laboratory for Sound and Vibration Research),
Department of Vehicle Engineering, KTH, 100 44 Stockholm
e-mail: eva@fkt.kth.se

The number of applications for lightweight sandwich structures is steadily increasing. For any type of optimisation of a sandwich structure with respect to strength, weight and acoustics the material parameters determining the dynamic response of the structure must be known. For sandwich structures the dynamic properties are strongly frequency dependent. A 6th order wave equation is used to describe the vibration of the structure. Based on the calculated results and measurements on beams the dynamic properties of the beam can be calculated in the entire frequency range. The bending stiffness can be determined at the first few eigenfrequencies, determined using simple FRF measurements.
The eigenfrequencies for orthotropic panels are predicted based on the Rayleigh-Ritz technique. The frequency dependent dynamic parameters of the plate are determined based on measurements on beams representing the two main and perpendicular axes of the plate. Measured and predicted results are compared.

PREDICTION OF EIGENFREQUENCIES FOR BEAM

Using Hamilton's principle a 6th order equation is derived as shown in [1]. The wavenumber $k_x = \kappa_1$ for the first propagating wave can be written as $k_x^4 = \omega^2 \mu / D_x$ where D_x is the apparent bending stiffness of the structure. The wave equation can then be rewritten as

$$\left(\frac{G_e H}{\mu^{1/2}\omega}\right)\left[\frac{D_x^{3/2}}{D_1} - D_x^{1/2}\right] + D_x - 2D_2 = 0 \qquad (1)$$

when neglecting the moment of inertia. The parameters are defined according to Figure 1 where μ is mass per unit area and D_1 is bending stiffness of the entire beam, D_2 is bending stiffness of one laminate, and G_e is the effective shear stiffness of the core.

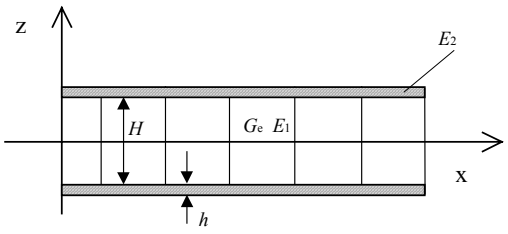

FIGURE 1. Structure of sandwich panel

Consequently D_x can, as a first approximation, be defined as the bending stiffness of a simple homogeneous beam which at a certain frequency has the same dynamic properties as the honeycomb structure. The laminates are assumed to move in phase. As $\omega \to 0$, the first part of the equation dominates why $D_x \to D_1$. The bending stiffness is consequently determined by pure bending of the beam. When $\omega \to \infty$ $D_x \to 2D_2$. D_1 and D_2 are defined as $D_1 = E_1 H^3/12 + E_2(H^2 h/2 + Hh^2 + 2h^3/3)$ and $D_2 = E_2 h^3/12$.
For a beam with boundary conditions well defined, the bending stiffness can be determined by means of simple measurements. The apparent bending stiffness D_{xn} for mode n having the eigenfrequency f_n is for a beam, length L and mass per unit area μ, given by

$$D_{xn} = 4\pi^2 f_n^2 \mu L^4 / \alpha_n^4 \qquad \text{for } n = 1,2,3\ldots. \quad (2)$$

where for a free-free beam α_n=4.73; 7.85; 11.00; 14.14; 17.2; ….; nπ. Measurements reveal the first few eigenfrequencies of the beam. The bending stiffness of a composite structure is strongly frequency dependent as given by equation (1). Equation (1) can be written in a more general way as

$$\frac{A}{f} D_x^{3/2} - \frac{B}{f} D_x^{1/2} + D_x - C = 0 \qquad (3)$$

where

$$A = \frac{G_e H}{\mu^{1/2} 2\pi D_1} \quad ; \quad B = \frac{G_e H}{\mu^{1/2} 2\pi} \quad ; \quad C = 2D_2 \qquad (4)$$

Within the frequency range of interest, here up to 4 kHz, the parameters D_1, D_2 and G_e in equation (4) are assumed to be constant for the structures investigated. Using the measured data the parameters *A, B* and *C* can be determined by means of the least square method.

EIGENFREQUENCIES FOR PLATE - PURE BENDING

An expression defining pure bending of an orthotropic plate can be written as

$$\left[D_x \frac{\partial^4 w}{\partial x^4} + 2\alpha \sqrt{D_x D_y} \frac{\partial^4 w}{\partial x^2 \partial y^2} + D_y \frac{\partial^4 w}{\partial y^4} \right] \cdot \left[\frac{1}{1 - \nu_{xy} \nu_{yx}} \right] + \mu \frac{\partial^2 w}{\partial t^2} = 0 \qquad (5)$$

where the parameter α is defined as $\alpha = (D_{12} + 2D_{66}) / \sqrt{D_x D_y}$. For an orthotropic honeycomb structure the parameter α can be as low as 0.06. Whenever the shear modulus G_{xy} is approximated by $\sqrt{E_x E_y} / \left[2\left(1 + \sqrt{\nu_{xy} \nu_{yx}}\right) \right]$, α is an integer.

The bending of a plate with α=0.06 is consequently dominated by the bending stiffness in the *x*- and *y*-directions. In general $(1 - \nu_{xy} \nu_{yx})$ in equation (5) can, as a first approximation, be set to equal unity. This is equivalent to saying that the test beams used are modelled as narrow plates. The parameters D_x, D_y and μ are frequency dependent.

For a plate with free or clamped edges and satisfying equation (5) the eigenfrequencies can be estimated by means of the Rayleigh-Ritz method. By using simple beam functions satisfying the proper boundary conditions the eigenfrequencies f_{mn} for a rectangular plate with free edges are determined according to [2], here as a function of α. As before D_x, D_y and μ are frequency dependent and should be evaluated at $f = f_{mn}$.

EIGENFREQUENCY MEASUREMENTS FOR PLATE

The first few eigenfrequencies for a plate were measured for free boundary conditions. The eigenfrequencies for the plate with free edges are now predicted. The parameter α is adjusted to give a good agreement between the predicted and measured eigenfrequency for mode (1,1). The parameter α is here set to equal 0.3. If all the material and geometrical parameters are well defined the quantities D_x, D_y and μ can be calculated as functions of frequency. The first few measured and predicted eigenfrequencies for the plate are compared in Figure 2. The bending stiffness for the strongest direction of the plate in Figure 2 is in the low frequency range about 2 times the bending stiffness of the weak direction.

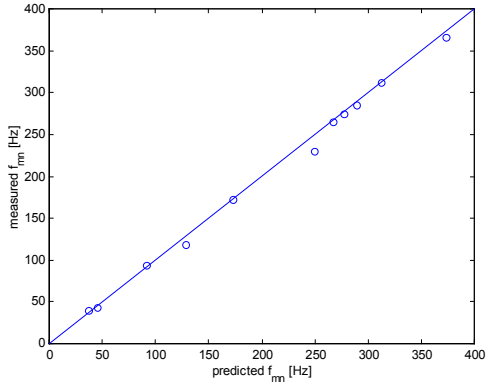

FIGURE 2. Measured and predicted natural frequencies for a plate plotted against each other.

CONCLUSIONS

The theory for the bending stiffness of honeycomb beams is here applied to an orthotropic plate structure. The frequency dependent bending stiffness is introduced in the ordinary wave equation for plates. Using this, the eigenfrequencies for the plate are predicted using the Rayleigh-Ritz technique. For comparison the first few eigenfrequencies are measured for a free plate. The comparison shows that using the frequency dependent bending stiffness for the two main perpendicular directions only and inserting it into the plate equation gives very good agreement to the measured result.

REFERENCES

[1] E.NILSSON 2000, *Some dynamic properties of honeycomb structures*, TRITA-FKT 2000:30, Department of Vehicle Engineering, KTH, Sweden

[2] R.D.BLEVINS 1984, *Formulas for natural frequency and mode shape.* Krieger Publishing Company, Malabar, Florida.

Sound Velocity Measurement by Acoustic Microscope with Additional Refraction Surface

S. Berezina[a] and J. Slabeycius[b]

[a]*Department of Physics, University of Zilina, 01026 Zilina, Slovakia*
[b]*Faculty of Material Engineering, University of Trencin, 02032 Puchov, Slovakia*

Large impedance mismatch between the coupling liquid and hard specimen reduces the fraction of the acoustic energy transmitted into the specimen and creates the difficulties with registration of the acoustic response. To overcome this problem we have bonded a part of steel sphere on the specimen's face. Refraction of converging beam at the spherical surface transforms the aperture angle. Fitting the distance between the lens and steel element (transformer) we can create in transformer's volume the narrow quasi-collinear beams of both the longitudinal and shear wave as well. Beam of shear waves arose due to mode conversion on the spherical surface has the cylindrical radial polarization. So, the acoustic energy of the wide collinear beam from the transducer can be concentrated by large aperture lens and spherical surface into the narrow beam incident normally on the specimen face. The steel element serves also as impedance transformer between coupled liquid and the object..

INTRODUCTION

The acoustic investigation of the small objects with high sound velocities is complicated due to weak sound penetration and high aberration inside the object. Strong mismatching the coupled liquid and object (both of velocities and impedances) decrease drastically the energy of the transmitting beam.

Wickramasinghe [1] suggested to use the solid hemisphere as an additional refraction surface to decrease the beam aberration inside the solid objects. The application of such element for image formation is complicated since it involves to upkeep the constant thickness of contact layer between the hemisphere and object during the scanning. Nevertheless the strong decreasing the aberration by use of it was attractive for quantitative problems [2].

We show that solid hemisphere gives the additional possibility of measuring the sound velocity in acoustic microscope.

METHOD AND EXPERIMENT

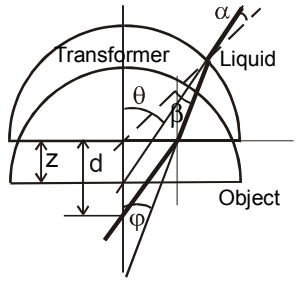

FIGURE 1. Ray diagram in transformer-object system

The ray diagram on the Fig.1 shows the transformation of the beam on the spherical refraction surface when the object is displaced from the focal plane by z towards the lens. The ray from the lens with aperture angle θ has after refraction the angle $\varphi = \alpha + \theta - \beta \le \theta$. Fig.2. presents the dependencies of the maximal beam aperture angle in transformer body φ_0 for both longitudinal and shear waves on the shift z.

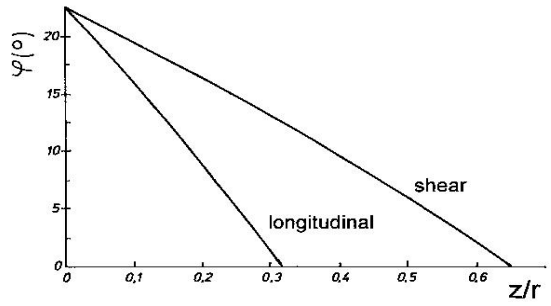

FIGURE 2. Dependencies maximal aperture angle in transformer on the normalized shift z, r – radius of transformer. Calculation were made for refraction boundary mercury-steel

The beam with $\varphi = 0$ propagates along the geometric axis of the lens that means the refraction surface creates the narrow quasi-collinear beam. The waist of such beam is less than the size of transformer and its minimal value can be limited by diffraction effects.

The divergence of such quasi-collinear beam of longitudinal waves in steel transformer with radius R = 3 mm for lens aperture angle $\theta_0 = 30^{\circ}$ and mercury as the immersion liquid was less than 2°. The ray diagram of the lens system in this case is analogous to the reversed telescope's one.

It is possible to create also the quasi-collinear beam of shear waves which arise on the spherical surface due to mode conversion. Note should be taken that this

beam has the radial polarization and it has a structure of the tube with minimal energy on the axis.

Acoustic response of the plan-parallel sample on normally incident collinear beam is typical pulse train with time interval determined by sample's thickness and velocity

Experimental verification of the possibilities of the transformer was made on the thick (5,68 mm) glass plate at frequency 13,5 MHz. Transformer - a half of steel ball with radius r = 3,36 mm was bonded on the front surface of the plate. Mercury provided good acoustic contact between the Si-lens (R = 6 mm, $\theta = 22^0$) and steel.

The pulse trains obtained at frequency 13,5 MHz for longitudinal and shear waves by quasi-collinear beams in 5,68-mm glass plates are presented in Fig.3 *a,b*. The velocity values calculated from the measured delay times and known thickness were 5,8 km/s for longitudinal and 3.4 km/s for shear wave and complied with known data.

The transformer was then successfully applicated for measuring the longitudinal sound velocity in small hard samples (∅3mm×2mm) of fullerene ceramics [3,4]. These new phases of carbon created from C60-powder at pressure 8÷13 GPa and temperatures up to 1800 k are distinguished by outstanding mechanical properties. The steel hemisphere bo provided good acoustic impedance matching between mercury and hard sample. It was possible to use the lens with rather big aperture angle $\theta = 23^0$ since the angles of incidence on spherical surface were smaller than critical one within a broad interval of the specimen shift z. So, the energy of the whole aperture beam transmitted into transformer.

Fig. 3 *c* represent the pulse train of longitudinal waves in the C60-sample sintered at 9,5 GPa and temperature 700 K. The measurement was carried out by acoustic microscope with operating frequency 25 MHz, pulse duration 100 ns. The pulse train containing a lot of echoes of longitudinal waves in sample (L – signals) was obtained at the shift $z = 0{,}31r$ correspondent to the creation of collinear beam of these wave. The time distance between the L – signals (τ_L = 360 ns) gave the velocity value 11,7 km/s. The same value of τ_L we measured for turned out sample. The accuracy of measurement was not high (about 2%) it can be enhanced by use of the shorter pulses.

CONCLUSION

The presented here experimental results show that application of the solid element with additional spherical refraction surface can be helpful for acoustic investigation of small samples with high sound velocity. It provides enhanced transmission of the sound into the sample and gives the possibility to evaluate the sound velocities both for longitudinal and shear waves. Such angle transformer could be interesting for crystalloacoustic experiments where a source of shear wave beam with radial polarization is needed.

ACKNOWLEDGEMENTS

This work was supported by Slovak Grant Agency VEGA (project No. 1/6072/99).

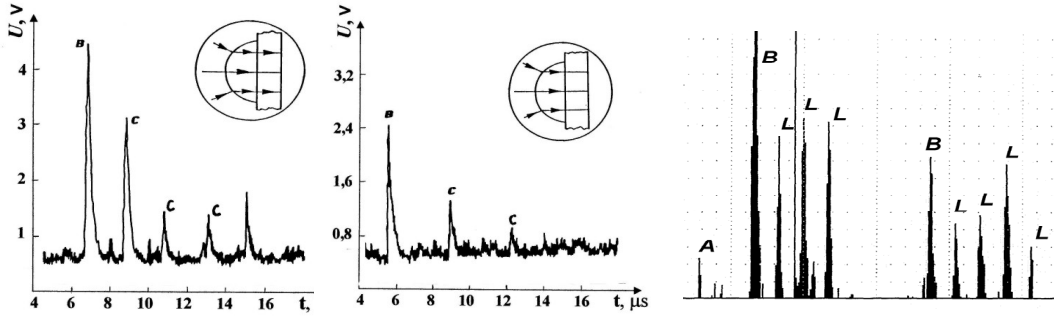

a *b* *c*

FIGURE 3. Pulse trains obtained by creating the quasi-collinear beams in 5,68-mm glass plate for longitudinal (*a*) and for shear (*b*) waves; *c* – pulse train obtained with transformer for longitudinal waves in hard C_{60}-ceramics. *B* – echo-signal from the front surface of transformer.

REFERENCES

1. H.K.Wickramasinghe, Appl. Phys. Lett. **39** (1981), 305
2. S.Berezina, I.Turek. Acta Phys.Slovaca **46** (1996), p.677-681
3. V.D. Blank et al, J. Exp. Teor. Phys. (JETPh) **87,** 741, (1998).
4. S.Berezina, V.Blank, V.Levin, V.Prokhorov, Ultrasonics, **38,** 327, (2000).

Assessing Acoustical Two-Port Properties of High Impedance Objects

P. Hiselius

Department of Engineering Acoustics, LTH, Lund University, P.O. Box 118, SE-22100 Lund, Sweden

The paper presents an experimental setup for objective measurements of high impedance objects in ducts, yielding the acoustical two-port properties of the object. The setup has been applied on earplugs. A frequently used experimental setup for measuring objective acoustical properties of earplugs is the use of artificial ears. Great effort is spent duplicating the outer ear of a person. The insertion loss is considered to give the acoustical properties of the object. Such a setup, however, gives a ratio of "the response of a system" to that of another system. The actual properties of the object is thereby embedded in a complicated artificial response. By instead fitting the test object in a duct its two-port parameters can be assessed, given the sound pressure level at both sides of the object for two sufficiently different termination impedances.

THE EXPERIMENTAL SETUP

A linear system that can be described by a two-port can, in turn, be described by an equivalent electrical circuit. Volume velocities are however difficult to measure for a wide frequency range, especially on the driving side, u_1, for high impedance objects [1]. By describing a reciprocal two-port as an admittance circuit, fig.1, the problem can be reduced to only two unknowns, Y_{121} and $Y_{22}+Y_{121}$, later denoted as impedances Z_b and Z_c.

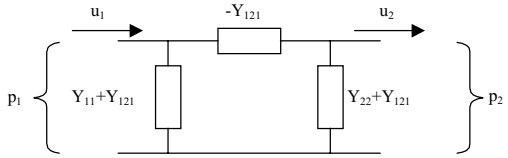

FIGURE 1. Equivalent electrical circuit.

Given the sound pressure levels at both sides of the object for two known, and sufficiently different, termination impedances the two-port parameters, Z_b and Z_c, can be solved for, fig.2.

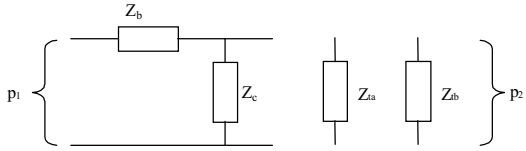

FIGURE 2. Reduced equivalent electrical circuit, including two termination impedances, Z_{ta} and Z_{tb}.

For unsymmetrical objects $Y_{11}+Y_{121}$ can be assessed by simply placing the object backwards. If, however, the input impedance of the object is much larger than the back radiation impedance, the driving sound pressure will be close to that of the blocked pressure, and thereby independent of $Y_{11}+Y_{121}$. In cases where $Y_{11}+Y_{121}$ is of interest the setup must allow the object to be positioned forwards and backwards without being refitted, fig.3.

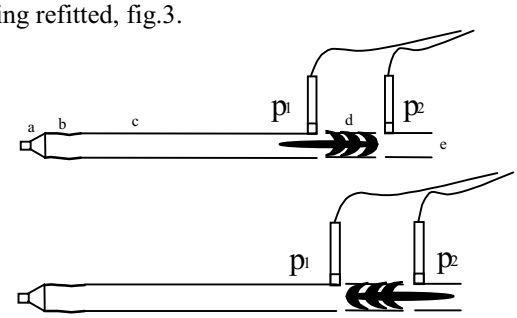

FIGURE 3. Setup allowing the object to be positioned in two directions without being refitted.

The setup comprises a loudspeaker (a), loosely coupled (b) to a duct (c). The object is fitted in a cylinder (d) with a microphone closely fitted at each side. At the end of the setup (e) various termination impedances can be fitted. For high impedance objects, and for acoustically symmetrical objects it is not necessary for the object to be fitted backwards. This allows a more realistic setup e.g. for earplugs, fig.4.

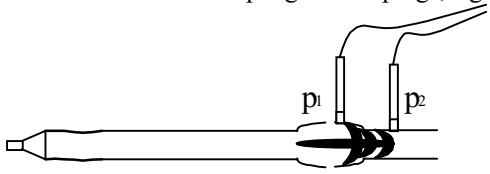

FIGURE 4. Alternative setup for earplugs.

Termination Impedances

As first (high impedance) termination a small cavity can be used. If the test object is an earplug the cavity is preferably of a size similar to that of the inner volume of an occluded ear canal. For numerical reasons it is advantageous to treat this termination as

an infinite impedance. The compliance due to the cavity will thereby be included in the two-port, but can easily be subtracted numerically at a later stage.
As second (low impedance) termination one can use a reflection free termination, e.g. by means of absorption, a *ρc-lid* [1,2], or virtually by using a truncated impulse response.

Assessing the Two-Port

Given the sound pressure at first and second microphone, p_1 and p_2, for the two termination impedances Z_{ta} and Z_{tb}, the reduced two-port can be solved for:

$$Z_b = \left(\frac{p_{1ta}}{p_{2ta}} - \frac{p_{1tb}}{p_{2tb}} \right) \Big/ \left(\frac{1}{Z_{ta}} - \frac{1}{Z_{tb}} \right) \qquad (1)$$

$$Z_c = \left(\frac{p_{1tb}/p_{2tb} - 1}{Z_b} - \frac{1}{Z_{tb}} \right)^{-1} \qquad (2)$$

EXPERIMENTAL RESULTS

Using the described setup measurements have been carried out on an earplug called EAR Ultratech, a plug where the attenuation provided is limited by sound transmission through a small canal via a resonator and an acoustically resistive "filter". The specific impedances of the reduced two-port, compared to the characteristic impedance of air and the specific acoustic impedance of 10mm of air, are given in fig.5.

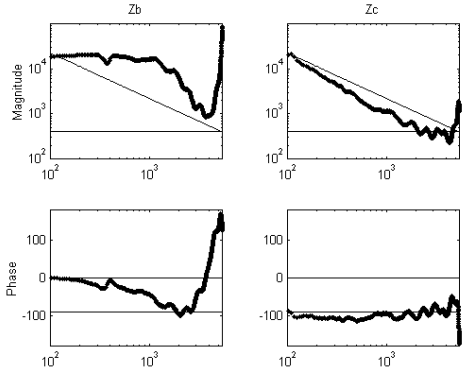

FIGURE 5. Specific impedance, magnitude [Ns/m^3] and phase [degrees], as a function of frequency [Hz].

Insertion loss prediction

By numerically couple the two-port of the earplug to that of an ear [3,4] the insertion loss of the earplug can be predicted, fig.6. The prediction is compared to third-octave band REAT (real ear attenuation at threshold) measurements [5], presented as mean attenuation +/- one standard deviation at octave band center frequencies. The result is surprisingly good considering the uncertainties and limitations of REAT measurements.

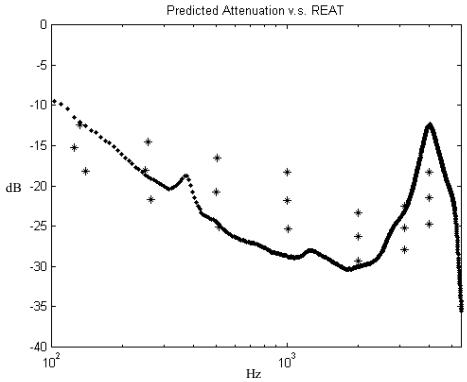

FIGURE 6. Predicted attenuation as a function of frequency, compared to REAT measurements.

SUMMARY

The proposed experimental setup can advantageously be used to assess the two-port parameters of high impedance objects for a wide frequency range. It has also been shown that if the two-port parameters of an earplug are known its insertion loss can be predicted. It is, however, important for such a prediction that the inner shape and surface of the duct, at the position of the earplug, is similar to that of an ear canal.

REFERENCES

1. Hiselius, P., "An experimental set up for assessing acoustical properties of earplugs", in *proceedings of Inter-Noise 99*, 1999, Vol.1, pp. 645-650.

2. Lindblad, S., "Insertion loss measurements on silencers with a lumped matching resistance in the open tube end", in *proceedings of Inter-Noise 85*, 1985, Vol.1, pp. 531-534.

3. Kringlebotn, M., *Scandinavian-Audiology* **17 no.2**, 75-85 (1988).

4. Hudde, H. and Engel, A., *Acta-Acustica* **84 no.6 Nov.-Dec.**, 1091-108 (1998).

5. ANSI S3.19-1974.

Acoustic Wave Sensing in Liquids: Features, Tendencies, Perspectives

I.V.Anisimkin, Yu.V.Gulyaev

RAS-Institute of Radioengineering and Electronics, Mokhovaya str., 11, 101 999 Moscow, Russia,
e-mail: ivanis@mail.cplire.ru

A state-of-art in acoustic wave liquid sensing is reviewed on the basis of sensing mechanisms and wave type employed. The presence of liquid at liquid-solid interface and changes in liquid properties are detected as velocity and/or amplitude changes of the wave propagating along the interface. Proper selection of the probing wave and sensing mechanism are key points for any application. Mass loading mechanism is attractive for studying interaction between different bilogical substances (protein binding, etc) and for measurements of the substances' concentrations at ng/mL level. Viscoelastic interaction mechanism is useful for measurements of the liquid viscousity, density, solidification, association and dissociation kinetics and their constants values. By use of electroacoustic mechanism dielectric permittivity, electric conductivity and ion concentration in liquids can be measured. Thermal mechanism is fruitful for calorimetric measurements for detecting exo/endothermal (bio)chemical reactions and obtainig such information, as temperature, density, rate, heat and kinetics of a droplet evaporation. Technques for choosing proper sensing mechanism, advatages and drawbacks as well as perspectives of acoustic wave sensing are also discussed.

INTRODUCTION

Modern chemistry, biology, medicine and food industry are in a great need of effective, dimunitive and reliable sensing devices suitable for detecting properties of liquids and (bio)chemical processes. Among different available techniques developed so far an acoustic wave sensing is one of the most promising. It is compatible with Integral Circuits fabrication. The output of acoustic sensors (frequency) provides an ideal input for digital signal conditioning circuits. Acoustic wave sensing possess inherent flexibility originated from variety of available acoustic waves, such as Rayleigh, Surface-Skimming Bulk Waves (SSBW), Surface Transwerse Waves (STW), leaky Shear Horizontal (SH), Gulyaev-Blustein Waves (GBW), acoustic plate modes (APM), and of sensing mechanisms, such as mass, viscoelastic, thermal and electroacoustic. Adsorption of liquid species on solid surface and changes in liquid properties are detected by a probing wave, propagating along a solid-liquid interface, through one of the sensing mechanisms. Acoustic measurants for the sensing are the changes in velocity and/or amplitude of the wave.

Present paper offers an analytical review of the state-of-art in acoustic wave liquid sensing based on available prototypes. The most suitable types of acoustic waves, different techniques for selective sensing by desirable mechanisms as well as applications of the sensors are presented.

VISCOELASTIC MECHANISM

Viscoelastic coupling produced by the penetration of the probing wave into adjacent liquid layer, 1-10 μm above the interface, is mainly applied for viscousity measurements within this layer. The probing is usually accomplished by Raileigh, SSBW, leaky Surface Acoustic Waves (SAW), STW, SH-APM and Love waves, propagating in ST-, YX-, 30^0, 33^0, 36^0, 42.75^0 and YZ- quartz, YZ-, 41^0 YX- and 36^0-YX-$LiNbO_3$ and 36^0 YX-$LiTaO_3$ substrates. Typical acoustic measurant for this mechanism is attenuation of the wave rather than its velocity. Selective emploing of viscoelastic sensing mechanism with respect to thermal one is provided either by thermal isolation of the test structure or by use of dual delay line configuration. The selective use towards electric loading is ensured either by screening electric fields of the wave with a metal film or by choosing substrate material with dielectric properties close to that of liquid. Though elastic coupling is hardly separated from mass loading, it is enhanced by increasing wave frequency and decreasing liquid quantity. It can also be deduced by special experiment (usually vacuum mass deposition) estimating the mass contribution separately. Minimal sensitivities towards viscousities are 50 dB/√(Pa·s) [1], 1.5 dB/√(kg/m^3·Pa·s) [2], 80 Hz/cP [3], 3.3 dB/√(kg/m^3·Pa·s), 2500 ppm/√(Pa·s) [4] and $4\cdot10^{-8}$ m^{2}s/ kg [5] in the range 0.3 - 1500 cP. Apart the measurements of viscoelastic coefficient, this mechanism is useful for studying kinetics of ion-molecular dissociation in acids and dissociation/ association constants in the range of $10^{-3} - 10^{+3}$ [6]. Solidification processes and liquid density are also monitored by viscoelastic mechanism, using SH-APM [7] and flexural plate modes [8], respectively. Though it is mentioned that density values measured together with viscousity are rather rough.

MASS LOADING MECHANISM

Mass mechanism produced by mechanical loading of a substrate by a liquid offers unique opportunity to detect (bio)chemical processes in solutions of low concentrations when thermal, electric and viscoelastic variations in the solutions are negligibly small. It is useful for studying interaction between different biological substances, such as protein binding, Deoxyribose nucleic acid molecules hybridization, etc. As compared with SSBW, Love, Lamb, SH-plate modes usually employed for the studies, STW

appeared to be the most sensitive as located in vicinity of the liquid-solid interface. The threshold sensitivity of the mass mechanism for antigen-antibody binding is estimated as 10 kHz/(mg/mL) [9], while that for detectable mass is at picogram level [10]. Typical acoustic substrates used for these measurements are ST,X-, ST,X+90^0- and YZ-quartz, YZ- and ZX-$LiNbO_3$, 36^{0}YX-$LiTaO_3$, SiN and SiO_2. Common guiding layers and metal films are SiO_2, ZnO, polimers and Au, Au/Cr, Au/Cu, respectively.

ELECTROACOUSTIC MECHANISM

While propagating along a surface of a piezoelectric substrate, mechanical wave is accompanied by a travelling electric field. The field interacts with charge carries in adjacent liquid, producing changes in acoustic wave velocity and attenuation. The electroacoustic interaction is well suited to measure dielectric permittivity (precision ±10 %), electric conductivity (precision ± 0.1 S/m) [11] and K^+ ion concentrations (in the range 1.49-4) [12] of the liquids. The best results are achieved for acoustic waves and piezoelectric substrates with large coupling constants, such as leaky SAW in 36^{0}YX-$LiTaO_3$. For Love waves in polyvinylcloride/ST-quartz structure and SH-APM in ST-quartz having small electromechanical coupling the electroacoustic sensing is less attractive [13].

THERMAL MECHANISM

Thermal mechanism based on dependence of acoustic wave velocity on temperature is usually considered as a parasitic effect. Applied for sensing, it becomes useful for some calorimetric measurements. In [14] an acoustic thermometer (sensitivity 17 Hz/^{0}C) implemented on a layered structure with Lamb modes propagation is developed. In [15] this mechanism is exploited for calorimetric sensing with liquid microsamples 1 nl-10 μL in volume. Substrate cooling produced by evaporating droplet is detected by Rayleigh, bulk SH and SSBW waves at the same time. As a result, the measurement of mass and temperature of the droplet, together with time, velocity, heat and kinetics of its evaporation are provided.

CONCLUSIONS

The frequency output, possibility to measure several liquid parameters at the same time, extremely high surface sensitivity and reduction of bulk effects are advantages of the acoustic wave sensing. Relative small mass sensitivity (usually parts of ng/L) as compared with modern clinical diagnostic methods (pg/L), necessity of preliminary calibration towards each component of a liquid mixture and impossibility to detect properties of liquids in the bulk are disadvantages of the available prototypes.

In our mind, the nearest tasks to be solved in SAW liquid sensing contain: enhancing adsorbed mass sensitivity of the method up to pg/L level together with possibility of operation not in pure buffer, but in real biological solutions; increasing sensitivity for viscousity measurments in liquids of less than 10 cP and elaboration of theory for large viscousity liquids (>1000 cP) to be in agreement with experiments; making possible to measure viscousity and density simultaniously wherever viscous liquid is; increasing sensitivity towards electric properties of liquids; further development of multiparameter sensing and thermal sensing for (bio)chemistry. These are some important problems for future investigations.

REFERENCES

1. Kostial, P., Machalikova, J., Kaniok, J. *Acta Phys. Slov.* **43**, **3**, 169-172 (1993).
2. Martin, S.J, Ricco, A.J., Hughes, R.C. "Title of the paper", in *Proceedings of 4th Conference on Solid-State Sensors and Actuators*, edited by hhhh, Publisher, City, 1987, pp.478- .
3. Nomura, T., Yasuda, T. "Measurement of Acoustic Properties of Liquids Using SH-type SAW", in *Proceedings of Ultrasonics Symposium*, edited by B.R. McAvoy, IEEE, New York, 1990, pp. 307-310.
4. Moritake, H., Inoue, M., Toda, K. *Jpn.J.Appl.Phys.* **36**, 6088-6096 (1997).
5. Herrmann F., Weihnacht, M. „Sensors Based on SH-SAW in Layered quartz/SiO_2 and $LiTaO_3$/SiO_2 Structures", in *Proceedings of Ultrasonics Symposium*, edited by M. Levy et al., IEEE, New York, 1999, pp. 413-416.
6. Kostial, P., Machalikova, J., Cernobila, F. *J.Phys. III France* **3**, 355-361 (1993).
7. Hughes, R.C., Martin, S.J., Frye, G.C., Ricco, A.J. *Sensors&Actuators* **A21-A23**, 693-705 (1990).
8. Martin, B.A., Wenzel, S.W., White, R.H. *Sensors&Actuators* **A21-A23,** 704-711 (1990).
9. Rapp, M., Moss, D.A., Reichert, J., Ache, H.J. "Title of paper", in *Proceedings of 7th Conference on Solid-State Sensors and Actuators,* edited by hhhh, Publisher, City, year, pages.
10. Schikfus, M.V., Welsch, W., Weiβ, M., Hunklinger, S."Title of paper", in *Proceedings of 7th Conference on Solid-State Sensors and Actuators,* edited by hhhh, Publisher, City, year, pages.
11. Kondoh, J., Yogi, S., Hayashi, S., Shiokawa, S. "Title of the paper", in *Proceedings of World Congress on Ultrasonics*, edited by hhhh, Publisher, City, 1997, pp. 94- .
12. Caliendo, C., D`Amico, A., Verardi, P., Verona, E. "K^+ Detection Using SH Acoustic Modes", in *Proceedings of Ultrasonics Symposium.*, edited by B.R. McAvoy, IEEE, New York, 1990, pp. 383-387.
13. Martin, S.J., Ricco, A.J., Niemczyk, T.M., Frye, G.C. *Sensors&Actuators* **20**, 253-259 (1989).
14. Wenzel, S.W., White, R.M. *IEEE Transactions* **ED-35**, **6**, 735-739 (1988).
15. Anisimkin, I.V., Anisimkin, V.I. *Radioeigineering & Electronics*, **45**, **7**, 893-897 (2000) (in Russian).

Mechanical Properties of Plastic Foams - Experimental Validation of Frequency-Temperature Superposition Principle

M. Etchessahar[a], L. Benyahia[b] and S. Sahraoui[a]

[a]*Laboratoire d'Acoustique de l'Universite du Maine, UMR CNRS 6613*
[b]*Laboratoire Polymère, Coloides, interfaces, UMR CNRS 6120*
Avenue Olivier Messiaen, 72085 Le Mans cedex 9, France

Plastic foams are widely used for passive sound absorption. In the low frequency range the frame can be considered elastic, the acoustic propagation in the porous material is then described by the Biot Allard theory which necessitate the knowledge of both the acoustical and mechanical prarameters of the foam. The mechanical parameters of the skeleton are temperature and frequency dependant making their experimental determination difficult. One way to make acurate measurements on a wide frequency range is to use the frequency-temperature superposition principle. In this paper, we measured the complex shear modulus of a PU open-cell foam on a frequency range 0.1-1000 Hz using the frequency-temperature superposition principle. This principle is experimentaly validated on the frequency range 1-100 Hz for the tested foam.

INTRODUCTION

Polymeric open-cell foams are widely used in sound absorbing applications, the response of such materials with elastic frame to harmonic excitation can be predicted by the Biot model [1][2]. The model needs several parameters which caracterise the solid phase, the saturing fluid and the coupling between them. Among these parameters, the mechanical properties of the skeleton are required.
Open-cell foams made of polymers are viscoelastic materials, consequently their mechanical properties depends on both frequency and temperature. Therefore experimental characterisation of such materials must be done on a wide frequency range. Quasistatic [3] and dynamic [4][5] measurements of Young modulus E and poisson's ratio ν were made on a narrow frequency range only. One way to expand the measurement frequency range is to use one of the polymer's properties : the frequency-temperature superposition principle.
We propose in this article to validate the frequency-tempereature superposition pinciple for polymeric foams. We present some properties of viscoelactic materials and the method of reduced variables, its limitations and applicability. Then two methods to measure the shear modulus $G^\star$ are presented and results are compared.

DYNAMIC EXCITATION OF VISCOELASTIC MATERIALS

Viscoelastic tests are generally performed in the viscoelastic range, where the Boltzmann superposition principle is satisfied [6]. Several types of mechanical deformations for viscoelastic tests can be used such as creep, relaxation or dynamic measurements. When testing materials in the linear viscoelastic range, in strain dynamic load, the strain response can be decomposed in two components: one in phase and one out of phase leading to a complex modulus $G^\star$,

$$G^\star(f,T) = G'(f,T) + jG''(f,T) \tag{1}$$

where $G'(f,T)$ represents the elastic part and $G''(f,T)$ the viscous part.

FREQUENCY-TEMPERATURE SUPERPOSITION PRINCIPLE

In the transition zone, between glasslike and rubberlike consitency, the material behavior can exhibit complex viscoelastic response due to a strong dependance on both frequency and temperature. The frequency-temperature superposition principle is the graphical traduction of the method of reduced variables which take its origin in the flexible chain theories. For viscoelastic modulus $G^\star$, the link between $G^\star_{T_0}$ (modulus at temperature T_0) and $G^\star_{T_i}$ can be written for real and imaginary parts as [6]:

$$G'(T_i,f) = \frac{\rho_0 T_0}{\rho T_i} G'(T_0, f a_{T_i/T_0}) \tag{2}$$

$$G''(T_i,f) = \frac{\rho_0 T_0}{\rho T_i} G''(T_0, f a_{T_i/T_0}), \tag{3}$$

where ρ_{T_0} and ρ are the material densities at temperatures T_0 and T_i respectively, a_{T_i/T_0} is the slidding parameter of both curves. From measurements at several temperatures on a narrow frequency range, a master curve is built at

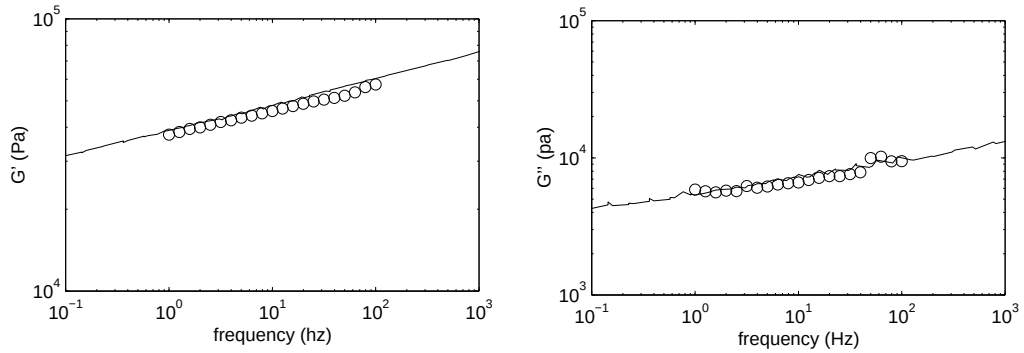

FIGURE 1. Real and imaginary parts of the shear modulus of foam samples measured with two measurement methods. In plain lines: measurements with Rheometric apparatus, the presented master curve is built with the frequency-temperature principle by slidding the isothermal curves. In circles : reference curve on the frequency range 1-100 Hz.

temperature T_0 on a wide frequency range by slidding the isothermal curves. Three criterias for applicability of this method are requireed : the exact matching of the slopes of adjacent curves, the same values of a_{T_i/T_0} must superpose all the viscoelastic functions, the temperature dependance of a_{T_i/T_0} must have a reasonable form consitent with experience [6].
When testing a foam, the response is a contribution of the responses of both the structure and the material from which the structure is made. The microstructure is a network of cells made of beams [7]. Under loading, those beams present bending and shearing such as deformations in the microstrucure are not equals. The frequency-temperature superposition principle is defined for homogenous materials under homogenous stress, the applicability of this principle to polymeric foams is then not defined.

EXPERIMENTS AND RESULTS

Two shearing experiments were made on the same PU foam samples (Recticel) on two different apparatus in the linear viscoelastic range.
On the first apparatus, working in tranlation shearing, only frequency can be controled. Experiments were made under quasistatic mode at ambiant temperature on a wide frequency range 1-100 Hz. All measurements were made in the linear viscoelastic range.
The second apparatus is a typical rheometric apparatus where the testing frequency range is fixed but where the temperature can be controled. The shear modulus was measured under quasistatic hypothesis on a narrow frequency range 0.1-16 Hz at different temperatures. For our experiments, the temperature varied from 10°C to 25°C every 5°C. Using the fequency-temperature superposition principle, a master curve was built at temperature 20ŏC on the frquency range 0.1-1000 Hz with care of the three criterias.

Figure 1 shows the real and imaginary parts on the shear modulus of the samples for the two experiments on the frequency range 0.1-1000 Hz. The same frequency dependance of the shear modulus is noticed.

CONCLUSION

In this study we measured the complex shear modulus of a PU foam over a wide frequency range 0.1-1000 Hz with the frequency-temperature superposition principle. In addition, on the frequency range 1-100 Hz, we validated the frequency-temperature superposition principle for the sudied foam.

REFERENCES

1. M. A. Biot, J. Acoust. Soc. Am **28**, 168-191 (1956).
2. J. F. Allard, *Propagation of sound in porous media: modeling sound absorbing materials* Chapman and Hall, London, 1993.
3. S. Sahraoui, E. Mariez, M. Etchessahar, Pol. Test. **20**, 93-96 (2001).
4. T. Pritz, J. Sound Vib. **178**, 315-322 (1994).
5. A. Sfaoui, J. Acoust. Soc. Am. **97**, 1046-1052 (1995).
6. J. D. Ferry, *Viscoelastic properties of polymers* Wiley, New York and London, 1961.
7. L. J. Gibson and M.F. Ashby, *Cellular solids : structure and properties* Perganom Press, Oxford, 1988.

Theorethical Estimate of the Tortuosity Governing the Acoustical Absorption Factor of Open Graded Asphalts.

G. Licitra[a], M. Losa[b], and M. Cerchiai[a]

[a]*Environmental Physics, Departm. of Livorno, A.R.P.A.T., 57126 Livorno, Italy E-Mail: fisica.li@arpat.toscana.it*
[b]*Department of Civil Engineering, University of Pisa, 56126 Pisa, Italy E-mail: losa@ing.unipi.it*

Acoustical absorption properties of open graded asphalt depend on the tortuosity of void paths, the specific resistance to air flow and the porosity of connected voids. While the last two parameters can be measured easily by laboratory tests, the tortuosity of void paths can be determined only indirectly by the measurement of the acoustical absorption factor.
In order to evaluate the tortuosity of void paths theoretically, as a function of the grain size distribution of mineral aggregates, a simulation procedure based on the Monte Carlo method has been proposed.
The model has been validated by using the results of tests performed on asphalt specimens composed of mineral aggregates with different grain size distribution. The values of the tortuosity, theoretically estimated in function of the grain size distribution of the mineral aggregates, have been compared with that ones indirectly obtained by performing experimental measurements of the acoustical absorption factor on the asphalt specimens.

INTRODUCTION

The improvement of acoustical properties of a road pavement can be reached mainly by means of two different kinds of action:

- to reduce the rolling noise emission due to the tyre-pavement interaction;
- to optimise the acoustical absorption properties of the pavement;

In order to hit this targets, other pavement characteristics bound to security, such as the friction, and bearing capacity, have not to be penalised.

All these properties depend on mineral aggregates characteristics such as grain size distribution and shape.

In this paper the optimisation of the acoustical absorption properties of the open graded asphalt has been studied by investigating its dependence on the shape and the grain size range of the mineral aggregates used in the pavement mixture.

ACOUSTICAL ABSORPTION OF AN OPEN GRADED ASPHALT MIXTURE

The open graded asphalt mixtures in which voids make connected paths (void channels) are able to dissipate acoustical energy. This happens when the connected voids form a rigid and fixed structure within which waves of air compression and rarefaction can grow.

Obviously, this phenomenon is linked both to the air viscosity and to the thermal exchange between air and void channels surfaces, and to the intrinsic acoustic properties of the mixture such as the propagation constant (complex wavenumber) and the complex characteristic impedance.

At the present, some models using the physical parameters of the porous asphalt material allows to calculate its acoustical properties. These, in turn, let us describe schematically the system composed by the porous asphalt material and the air in the void channels as an equivalent compressible lossy fluid. This, at last, let us model the sound field using the formalism of sound propagation in air.

In this work the phenomenological model by Hamet and Berengier [1] is used in order to evaluate the acoustical intrinsic characteristics of the porous open graded asphalt.

The main parameter used for evaluating these properties is the acoustical absorption factor α.

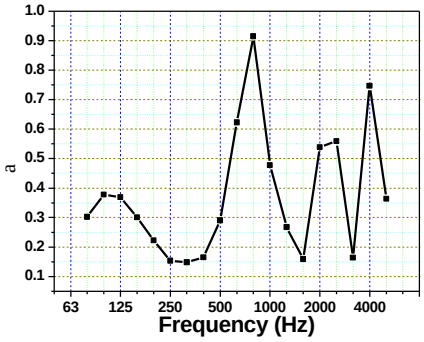

FIGURE 1. values of measured α on the sample used to tune the model here proposed.

As for the other parameters describing the porous asphalt pavement performance, it's very important to have a model that should predict the value of α as a function of frequency; so one is able to produce a pavement with desired acoustical absorption, in order to reduce traffic noise emission. In figure 1 a graph is shown of the α values, measured *in situ*, to tune the model here proposed [2].

The acoustical absorption factor α is a function of the complex acoustic impedance Z, which in turn is a function of the intrinsic characteristic acoustic impedance Z_C of the porous layer, of its thickness l,

of the acoustic impedance Z_T of the layer below and the wavenumber *k*. *Z* may be calculated (see [1]) as a function of both the acoustic properties of the porous asphalt material (airflow resistance *r*, the percentage of connected voids Ω, the void channels inner tortuosity index) and the parameters connected to air thermal effects and air viscosity (frequency *f*, specific heats ratio γ, air density ρ_0, Prandtl number N_{Pr}, air pressure P_0).

The tortuosity may be associated to a growth of the airflow resistance by an exchange in momentum of the air particles between themselves and connected void surfaces. The tortuosity, together with geometrical variations of the void section defines a parameter $q^2 \geq 1$ (*shape factor*) connected to the acoustical energy absorption. This may be considered as an increasing of the static air density, too.

All the physical parameters may be measured with ordinary laboratory investigations on asphalt mixture samples, with the exception of the tortuosity q^2. Actually, there are not experimental techniques that allows the direct measurement of the shape factor. This can be indirectly obtained by the acoustical absorption curve of the open graded asphalt, measured in the impedance tube [3].

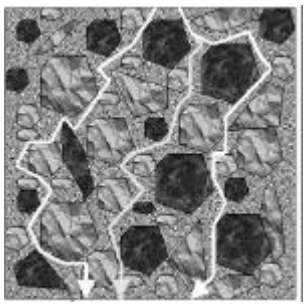

FIGURE 2. An example of the calculation of the tortuosity

MODELLING THE TORTUOSITY WITH A MONTE-CARLO METHOD

The movement of air particles, as they follow along their tortuous path through the open graded asphalt, dictated by the solid matter that marks the connected voids, gives rise to more or less jagged jumps and a very irregular pattern (see Fig. 2). Upon close examination, it would appear that the fluctuations of individual particles of air along the paths of flow are random. Consequently, we appeal to a probabilistic formulation to make predictions about the overall flow.

We assume that the air travels an incremental distance at each step in the direction of flow before colliding with a solid particle. In order to simulate the incremental distance and the direction of flow at each step we use two series of random outcomes, that are interpreted as distances and directions, selected by the Monte Carlo method to conform respectively with a log-normal and a uniform distribution.

The values of distances are selected by setting their mean value and their variance in function of the grain size distribution of the mineral aggregates; the values of directions are included in the range between 0 and 360°.

The simulation stops when the path has been passed through the layer and the tortuosity of the void path can be calculated. The tortuosity of the material is calculated as the mean of the values obtained by a great number of simulations. In figure 3 the results obtained during a run of the simulation model based the Monte Carlo method are shown for the mean tortuosity as a function of the number of performed iterations.

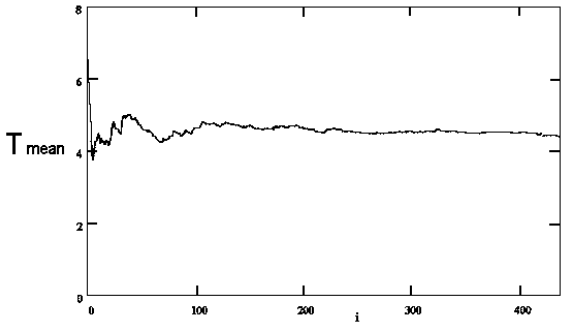

FIGURE 3. Mean tortuosity as a function of the number *i* of iterations.

CONCLUSIONS

In order to optimise the acoustical absorption factor of the open graded asphalt pavements, their characteristic parameters, such as the shape factor, should be carefully estimated. Here a model based on the Monte Carlo method is used for the prediction of the tortuosity is proposed.

This model however should be carefully tuned, so our efforts will be directed to validate the theoretical approach in order to define other parameters that influence the shape factor governing the acoustical absorption.

REFERENCES

1. M. Bérengier, J. F. Hamet, "Étude acoustique des milieux poreux. Application aux revêtements drainants." Bulletin des Laboratoires des Ponts et Chaussées, **212**, 65-74 (1997).
2. M. Losa, G. Licitra, M. Bérengier, M. Cerchiai, "Physical characteristics of road pavements and noise emission", Proceedings of Inter.noise 2001, The Hague, The Nederlands, to be published (2001).
3. France Regulation NFS 31-065 "Acoustique: détermination du facteur d'absorption acoustique et de l'impédance acoustique en incidence normale par la méthode du tube." (1980).

Reflection of plane acoustic waves from a layered elastic bottom

M.S. Fokina

Institute of Applied Physics, Russian Academy of Science, 603950, 46 Ulyanov Str. N.Novgorod, Russia,
E-mail: fok@hydro.appl.sci-nnov.ru

An exact expression for the reflection coefficient is obtained with the Thomson-Haskell technique for the geoacoustical model of an ocean bottom consisting of an elastic homogeneous sediment layer overlying an elastic half-space. Characteristic equations for explicit determination of the position of each individual resonance contribution to the reflection coefficient are derived. Analytical expressions for the angular and frequency resonance positions are found. The resonance expression for the reflection coefficient is written in the form of a sum of resonance terms. Comparison between resonance theory and exact calculations for the elastic layer covering the elastic half-space is presented. The results of resonance formalism show excellent agreement with exact theory in all the cases. For development of resonance method for bottom properties determination this expression was transformed to the Breit-Wigner form. The dependence of the resonance positions, half-width of resonances and it's amplitude from two layered elastic bottom model parameters was investigated in resonance approximation and comparison with computations was done. Resonance properties of inhomogeneous gradient elastic layer was investigated by using characteristic matrix of layer in the form of routinely convergent series.

INTRODUCTION

Studies of the acoustical properties of layered elastic media are of interest to researchers in hydroacoustics, geophysics, and design of layered composite materials. An approach based on the use of "propagator" matrices has been employed by many authors. Calculated reflection coefficients for acoustic signals reflected from a stratified ocean bottom exhibit, in general, a complicated structure consisting of fairly regular sequences of peaks and dips. Such features can usually be attributed to resonance phenomena of some sort, and it is often found that the resonance structure, i.e., the distribution and widths of the resonance peaks contain all relevant information about the interacting medium involved [1,2].

EXACT REFLECTION COEFFICIENT

The physical model used in the study of resonances is an elastic layer covering elastic half-space. The parameters associated with the water column and substrate are identified by subscripts 0 and ∞, respectively: c, ρ, d, are the velocities of sound waves, density and thickness of the elastic layer (sediment). The liquid half-space and the elastic half-space are assumed to be homogeneous and semi-infinite. If only waves of vertical polarization are taken into account, then the displacement fields $U=U(U_x,U_y=0,U_z)$ can be written in the terms of the scalar and vector potentials φ and ψ. For an incident plane wave of unit amplitude the system of linear algebraic boundary equations can be obtained.

The solution of linear algebraic boundary equations for the reflection coefficient V can be obtained by Kramer's rule. Due to radiation conditions, we have $\varphi_\infty^- = \psi_\infty^- = 0$. The exact expression for the complex reflection coefficient may be written as

$$V = \frac{Q_{21}^{-1}(D_{21}D_{33} - D_{23}D_{31}) - Q_{22}^{-1}(D_{43}D_{31} - D_{41}D_{33})}{Q_{11}^{-1}(D_{21}D_{33} - D_{23}D_{31}) - Q_{12}^{-1}(D_{43}D_{31} - D_{41}D_{33})} \quad , \quad (1)$$

where Q, D –matrices of liquid and elastic layered half spaces. The problem has already been solved in the literature, and the reflection coefficients was calculated by Brekhovskikh (1980). The reflection coefficient is a function of properties of the media and of the angle-frequency-thickness variables δ=αd and η=βd. The results of calculation of the modulus of the reflection coefficient in the frequency-grazing angle plane has a complicated structure consisting of regular sequences of minima and maxima. These features are connected with the reflection coefficient resonances. Absorption in the layer reduces the height of the resonance peaks due to energy dissipation. Thus, it is reasonable to use the knowledge of the resonance structure obtained from measurements to gain access to properties of the seabed [1].

RESONANCE FORMALISM

We analyze the exact expression for the reflection coefficient using the elastic layered seabed model. The resonance behavior appears when the real part of the denominator in Eq.(1) vanishes, i.e., when the characteristic equation for resonance positions is satisfied [1]. Characteristic equation can be solved with respect δ and η. The roots of the characteristic equation can be found as $\delta_r = 2\mathrm{arctg}(X)$, $\eta_r = 2\mathrm{arctg}(X)$, where X are the roots of the addition quartic equations. The solutions for δ_r and η_r determine two types of reflection coefficient resonances for compression and shear waves, respectively. Finally the solutions of characteristic equation can be written as: $\delta_{nr}=\delta_r+2\pi n$, $\eta_{nr}=\eta_r+2\pi n$, where n is the number of resonance (n=0,1,2,…).

The variables δ and η are functions of the frequency and the incidence angle. For a constant angle or frequency, the positions of the frequency and angular resonances can be written separately for compression and shear waves:

$\delta = \frac{2pFd\cos(q_\ell)}{c_\ell}$, $\eta = \frac{2pFd\cos(q_t)}{c_t}$.

RESONANCE APPROXIMATION OF THE REFLECTION COEFFICIENT

The basic assumption of the resonance formalism is that in the vicinity of the resonance the amplitude of a process is described essentially by the Breit-Wigner resonance form with the addition of a slowly varying background [1]. Following this idea, the exact expression for the reflection coefficient in Eq.(1) can be expanded in a Taylor series with respect to the powers $(\delta-\delta_{nr})$ and $(\eta-\eta_{nr})$ around the resonance positions δ_{nr} and η_{nr} Thus, the resonance expression for the reflection coefficient can be obtained as the sum of resonance terms, both in the frequency and angular variables. The sum over resonances must be taken only symbolically since the expansion is assumed to be valid only in the immediate vicinity of each resonance position. After the usual manipulations, the reflection coefficient may be written in the suggestive form:

$$R(x,\varphi) = \sum_{n=1}^{\infty} \frac{a + b(x - x_n) + ic\frac{G_n}{2}}{x - x_n + i\frac{G_n}{2}}, \qquad (2)$$

where G_n is the width of resonance. For two layer elastic model the coefficient are cumbersome and is not given here. The analytical and numerical investigations of interdependence of G_n and material parameters of two layered model was performed. In whole reflection coefficient has a rather complicated dependencies from the material parameters of bottom. This fact illustrated in Fig.1,2. which also show resonance behavior of reflection coefficient on the bottom parameters plane.

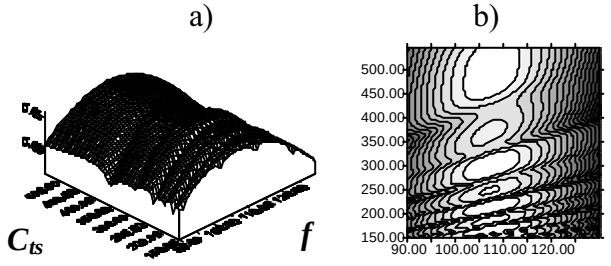

FIGURE 1. . Reflection coefficient on the frequency - shear waves velocity in the layer plane: a) in the form of surface, b) in the form of contours.

INFLUENCE OF SEABED PARAMETERS ON RESONANCES

Investigation of seabed parameters influence on characteristics of sound reflection coefficient resonances was performed for the bottom models consist from one

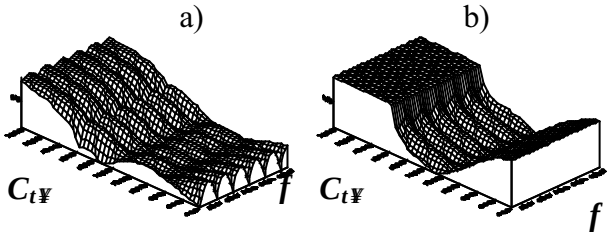

FIGURE 2. . Reflection coefficient on the frequency - shear waves velocity in the substrate plane for different $c_{\ell\infty}$, and ρ.

elastic (liquid) damping layer covering an elastic halfspace. Dependences of sound reflection coefficient resonance positions, half-width and amplitudes from different parameters of model were considered consecutively. Consideration of resonances behaviour was performed on frequency - bottom parameter plane. All other parameters of model were fixed at that time. From the beginning resonance characteristics was analysed for the model of liquid layer covering an elastic halfspace (□-resonances). Then resonances connected with elasticity in the sediment (t-resonances) were analysed.

Behavior of resonances on the frequency – bottom parameter plane are shown in the Fig. 3. Characteristics of resonance are taken for the fixed resonance minima. On Fig.3. markers + shows the position of resonance minima. The solid lines above and below indicates positions of maximums in the reflection coefficient, closest to marked minima. Markers * shows dependence of half-width for selected resonance from bottom parameter. Axe of frequency is in the left side of graph. One more solid line indicates resonance amplitude. Amplitude axis is in the right side of the graph.

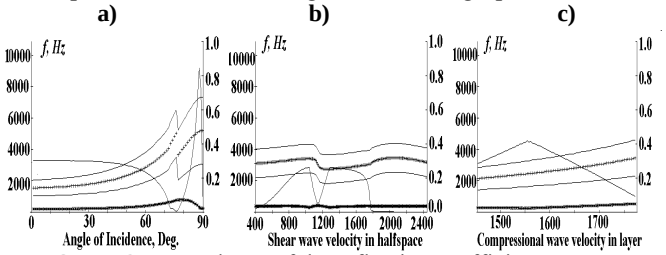

FIGURE 3. Dependence of the reflection coefficient resonance characteristics from: a) angle of incidence; b) $\tilde{n}_{t\infty}$; c) c_{ℓ}.

Unique dependence of resonance positions from values of compression and shear waves velocity in the layer may be used for development of methods for determination of parameters of layered media by resonance characteristics.

ACKNOWLEDGMENTS

The work was supported in part by the Russian Foundation for Basic Research (Grant No 00-05-64956).

REFERENCES

1. Nagl A., Überall H., and Hoover W.R. Resonances in Acoustic Bottom Reflection and Their Relation to the Ocean Bottom Properties in *IEEE TGRS*, GE-20, 1982, pp.332-337.
2. Fokin V.N., Fokina M.S. Acoust. Phys. **46**, 690-697 (2000).

Prediction of the Intrinsic Acoustical Properties of Loose Granular Materials by Fitting Measurements with a Theoretical Model

G. Iannace[a], C. Ianniello[a], L. Maffei[b], R. Romano[a]

[a]*DETEC – University of Naples FEDERICO II, P.le Tecchio 80, 80125 Naples, Italy*
[b]*DISPAMA – Second University of Naples, Borgo S. Lorenzo, 81031 Aversa, Italy*

The propagation of sound waves in air-saturated granular materials has drawn the attention of researchers in different areas of acoustics. The authors are engaged in a study aimed at characterizing sands and gravels as cheap porous-materials for sound absorption in the audible frequency range. The results reported in this paper refer to a loose granulate obtained by sieving limestone chips and to lead balls. An impedance tube was used to measure the input impedance of layers of granulates backed by a hard surface. Measured impedance data were found in an acceptable agreement with the corresponding values predicted by a theoretical model. Predicted values were obtained by combining a phenomenological model for the calculation of the complex characteristic impedance and the complex wave number of porous materials having a rigid skeleton with a standard formula for the calculation of the input impedance of a layer of material terminated with an acoustically hard surface. Non-acoustical parameters needed by the phenomenological model were measured and fitted into the above-mentioned model.

PHENOMENOLOGICAL MODEL

It's a long time that various theories and mathematical models have been proposed in the scientific literature in order to describe sound waves in porous materials. Particular attention has been dedicated to materials that can be considered as having a rigid skeleton saturated by air. For these materials the concept of equivalent dissipative gas has been established. This assumption allows the use of the formalism of sound wave propagation in the air once the complex characteristic impedance Z_m and complex wave number k_m are determined for the equivalent gas. In this respect, empirical, phenomenological and microstructural models are available. Each model requires a number of non acoustical parameters for the porous material. In this work a model given by Hamet et al. [1] was found suitable for characterizing the intrinsic acoustical properties of some loose granular materials. For the sake of brevity only final formulas are reported for k_m and Z_m:

$$k_m = k_0 (s\gamma)^{1/2} \left(1 - j\frac{f_\mu}{f}\right)^{1/2} \left[1 - \left(1 - \frac{1}{\gamma}\right) \Big/ \left(1 - j\frac{f_\theta}{f}\right)\right]^{1/2} \quad (1)$$

$$Z_m = \frac{\rho_0 c}{Y} (s\gamma)^{1/2} \left(1 - j\frac{f_\mu}{f}\right)^{1/2} \left[1 - \left(1 - \frac{1}{\gamma}\right) \Big/ \left(1 - j\frac{f_\theta}{f}\right)\right]^{1/2} \quad (2)$$

where $k_o = \omega/c_o = 2\pi f/c_o$ is the wavenumber in ambient air (m^{-1}); ω is the angular frequency (s^{-1}); f is the frequency (Hz); c_o is the speed of sound in ambient air (m/s); s is the structure factor; $\gamma = c_p/c_v$ is the ratio of the constant-pressure specific heat to the constant-volume specific heat of air ($\gamma = 1.41$ for ordinary air); ρ_o is the ambient air density (kg/m^3); Y is the porosity; f_μ and f_θ are defined below:

$$f_\mu = \frac{1}{2\pi} \frac{R_1 Y}{\rho_0 s} \qquad f_\theta = \frac{R_1}{2\pi \rho_0 N_{Pr}} \quad (3)$$

N_{Pr} is the Prandtl number ($N_{Pr} = 0.71$ for ordinary air).

The non acoustical parameters that appear in Eqs. 1 ….3 are the resistivity R_1, the porosity Y and the structure factor s. Their definitions and measurement methods used can be found in Ref. [2]. It is worth to point out that the non acoustical and acoustical intrinsic properties of loose granulates depend on the grain size, the grain size distribution and grain settlement. Although the average non acoustical parameters had been measured previously, their values were adjusted slightly to ameliorate the comparison of the measured input impedance of samples backed by a rigid termination with the corresponding predicted values.

MEASUREMENTS AND FITTING PROCEDURE

A test rig based on an impedance tube, held vertical by a framework, was used to measure the input acoustic impedance of a sample of granulate. The material was poured like water into a sample holder obtained from a length of tube coaxial with the measurement tube. The measurement technique was based on the sound pressure transfer function between two points in front of the sample surface, as reported by Fahy [3]. It can be shown that the normalised

specific acoustic impedance ζ at the sample surface is linked with the ratio of the sound pressures at two close locations along the axis of the tube by equation:

$$\frac{Z}{\rho_0 c} = \zeta = \frac{H\sin(k_0 x_1)\sin\phi + j[\sin(k_0 x_2) - H\sin(k_0 x_1)\cos\phi]}{H\cos(k_0 x_1)\cos\phi - \cos(k_0 x_2) + j[H\cos(k_0 x_1)\sin\phi]} \quad (4)$$

where $H = |p_2/p_1|$ is the modulus of the ratio of the sound pressure p_2, at the larger distance from the sample face x_2, to the sound pressure p_1, at the smaller distance x_1; $k_o = 2\pi f/c_o$ is the wavenumber in free air; ϕ is the phase angle of p_2 minus the phase angle of p_1. An MLS-based system was used to for the acquisition of data needed by Eq. 4. The theoretical input impedance Z of a porous sample (thickness = d) backed by a hard surface is:

$$Z = -jZ_m \cot(k_m d) \quad (5)$$

Available experimental values of R_1, Y and s were inserted into Eqs. 1…3 in order to calculate the input impedance of each tested sample through Eq. 5. These values were compared with the corresponding values measured by processing the experimental sound pressure signals according to Eq. 4. A slight adjustment of the measured non-acoustical parameters was required for a better fitting between predicted and measured input impedance. As an example of results Fig. 1 reports the comparison between the real part and the imaginary part of the input impedance of a layer

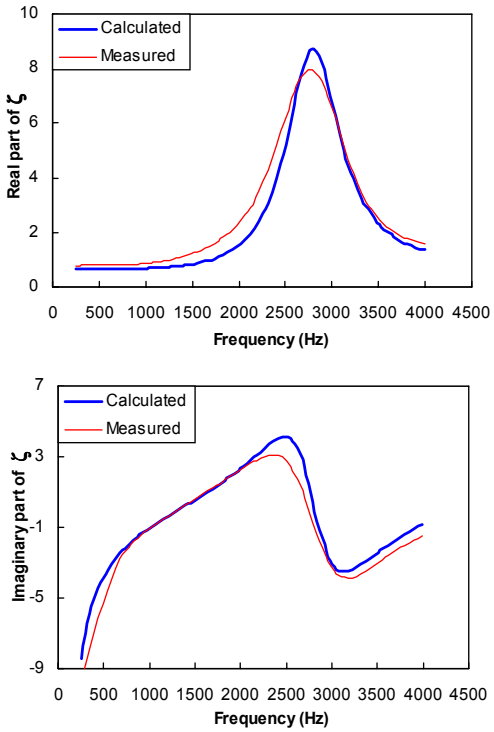

FIGURE 1. Real and Imaginary parts of the normalized acoustic impedance vs. frequency. Limestone chips, d=40 mm.

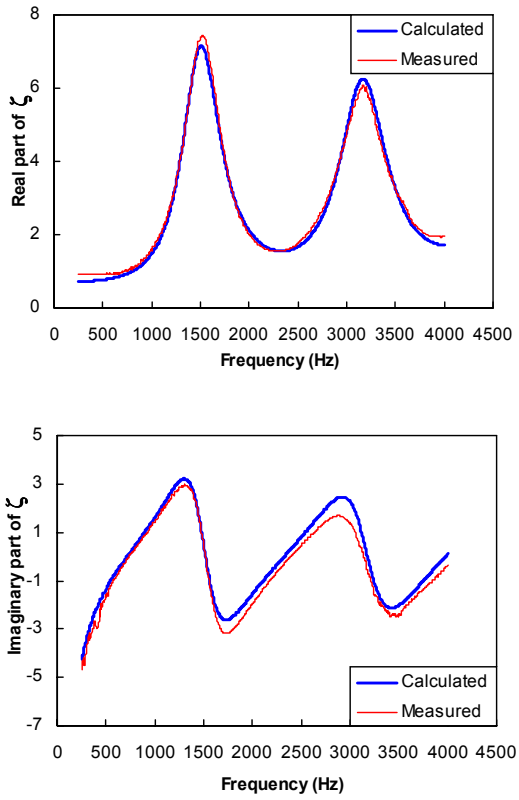

FIGURE 2. Real and Imaginary parts of the normalized acoustic impedance vs. frequency. Lead balls, d=80 mm.

(d = 40 mm) of limestone chips sieved in the range of gauge 1.6-2.0 mm. Analogous data is reported in Fig. 2 for a layer of lead balls having a diameter of 1,9 mm. Table 1 reports the relevant non-acoustical parameters.

Table 1. Non-acoustical parameters

	R_1 (Pa s/m^2)	Y	s
Limestone chips	1,7x10^4	0,45	2,58
Lead balls	6,0x10^3	0,40	1,75

CONCLUSION

The results presented herein, and other results as well, suggest that the considered theoretical model describes the intrinsic acoustical properties of loose granulates with an acceptable confidence.

REFERENCES

1. J. F. Hamet, and M. Bérengier, *Proc. Internoise 93*, Leuven, Belgium, 641-646 (1993).

2. G. Iannace, C. Ianniello, L. Maffei and R. Romano, *Proc. Euronoise 2001*, Patras, Greece (2001).

3. F. J. Fahy, *Journal of Sound and Vibration*, **97** (1), 168-170 (1984).

Investigation of medium's acoustic properties, utilising the measurements of quasi-continuous waves phase

M. Piszczek[b], M. Szustakowski[a] and L. Jodlowski[a]

[a] *Institute of Optoelectronics, Military University of Technology, 2 Kaliskiego Str., 00-908 Warszawa, Poland*
[b] *Department of Electronics, Military University of Technology, 2 Kaliskiego Str., 00-908 Warszawa, Poland*

The properties of real objects are described by a row of materials' parameters. The phase velocity of an acoustic wave, for acoustic, is one of the most important parameters. Its evaluation with high precision is possible with using phase analysis. This work describes a measuring method based on measurement of phase relations of the acoustics signals. Using high stable signal generator (*f ~ 1,5MHz*), A/D conversion, and digital data processing gives the resolution of transit time measurement *Tp* in a range of a few hundredths of the period of used probing wave *(~ 5ns*). Sensibility and simplicity of measuring system makes the proposed solution a very attractive tool for investigations. It can be applied for measurement of different changes of material properties in the automatic systems and medicine. This work shows the first measurement results for neurology (brain stroke).

BASIC INFORMATION ON MEASURING METHOD

In many applications typical pulse methods do not offer required measuring resolution and solutions based on analysis of continuous wave are limited.
Using short wave packets and analysis of the phase dependencies *R* between waves gives solution easy to performed in practice, and moreover it ensures higher resolution.

$$R = j(t_1) - j(t_2) \qquad (1)$$

Proposed measuring process consists in determination of temporal relations between transmitted and received acoustic signals thanks to phase analysis of these signals. *Phase method* [2] is based on analysis of the phase relations *R* between transmitted and received signals for one probing frequency f_1. *Time method* [4] is a developed phase method that employs two suitably selected frequencies f_1, f_2 and determines the transit time of a probing signal *Tp*
Both methods are aimed at elementary phases determination [1]. It is possible to find the signal parameters, including the phase value *ö,* using solutions of the problem approximation of *n* samples performing equation of a harmonic wave.

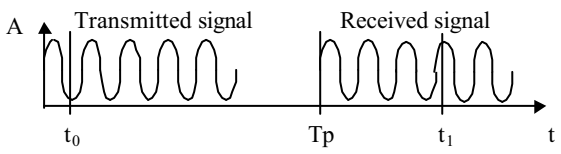

FIGURE 1. Measurement of phase relations of acoustic wave packets.

$$Tp = (t_1 - t_0) + \frac{1}{4p}\left(\frac{R_1 + 2pP_1}{f_1} + \frac{R_2 + 2pP_2}{f_2}\right) \qquad (2)$$

$$P_1 = integer\left(\frac{R_{12} f_1}{2p(f_1 - f_2)} - \frac{R_1}{2p}\right) \qquad (3)$$

$$P_2 = integer\left(\frac{R_{12} f_2}{2p(f_1 - f_2)} - \frac{R_2}{2p}\right) \qquad (4)$$

$$R_1 = j(t_1) - j(t_0) \quad \text{for } f_1 \qquad (5)$$

$$R_2 = j(t_1) - j(t_0) \quad \text{for } f_2 \qquad (6)$$

$$R_{12} = R_1 - R_2 \qquad (7)$$

For the measurement of an oscillations phase, the steady oscillations of ultrasound transmitter are used. It is enough to get several samples to determine the phase of a signal, so the generated signal is called a quasi-continuous wave.

RESULTS OF TECHNICAL AND MEDICAL TESTS

Using the measuring system consists of transmitting - receiving module and a computer with A/D converter card. An acoustic transducer with the following parameters was used: the diameter *D = 20 mm*, the resonance frequency f_o = *1.43 MHz* and the quality factor *Q ~ 5* During test was used acoustics waves packets with pulse duration t_i = 45 [ìs]. The test results are presented in Table 1.

Table 1. Measuring resolution

Phase relations R	$2{,}5^0$
Transit time T_p	5ns
Shift	3,75μm
Acoustic wave velocity	1,12(m/s)/cm
Temperature	$0{,}45^0$C/cm
Density	0,09(kg/m^3)/cm

Analysis of the developed measuring method was based on laboratory system, including glass cell with a movable barrier. Precise shift of the barrier was done by means of a micrometer screw (with 10-*ìm* scale). Distilled water was a measuring medium in the cell. During tests measurements the temperature of liquid T and the measuring space L was precisely hanged. The tests were aimed at verification of measuring possibilities the devices used for investigation of physical and structural properties of media.

New approach in acoustic research of brain blood supply has been made. Vascular diseases in a nerve tissue cause edema or haemorrhage of brain. Thus, physical parameters of brain are changed (the density ρ, the elasticity K, and the velocity of acoustic wave $c = \sqrt{K/\rho}$). Changing the velocity Dc causes the change of the transit time DTp. The best area for acoustic probing is between temporal bones because majority of brain structures are parallel to each other and perpendicular to an acoustic beam. Human brain is 15-cm long (between temporal bones) and it consists of soft tissues (density of about 1000 kg/m^3, sound velocity of about 1530 m/s). The transit time of an acoustic wave (between temporal bones) is about 100 μs. In a diseased brain, this time can change by $< 1mc$.
The measuring device called *Encephalodensometer* and used for monitoring pathological changes of blood circulation in blood vessels was elaborated in co-operation with Prof. Roman Mazur from the Neurology Clinic of Medical Academy in Bydgoszcz (Poland).
The obtained results show possibilities of investigation of this kind of brain blood vessels pathology [3] what is confirmed in Figure 3.

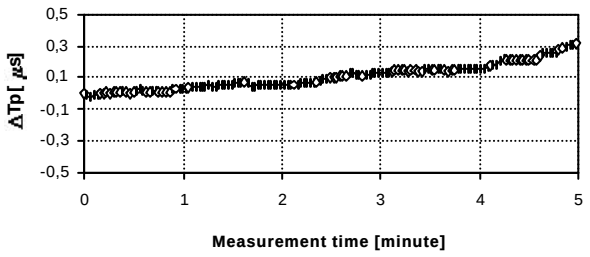

FIGURE 2. Example result for patients with diagnosed brain stroke.

CONCLUSIONS

The proposed measuring method is an innovative one:

1. It is a solution including elements applied in the methods based on a continuous wave and elements used for pulse technique.
2. Steady oscillations of piezoelectric receiver are used for measuring process, both for transmission and receiving the signals, what ensures a very good quality of harmonic signal and finally diminishes the error of phase determination.
3. The phase relation analysis, for a single frequency of an acoustic probing signal (phase method), is suitable for the measurements of relative signals (phenomena monitoring). Using two different and appropriately optimised probing frequencies make possible determining the transit time.
4. The measuring method, based on phase relations analysis, ensures resolution of the range of a few hundredths of a period of the used probing wave.

The above presented features make this method attractive for applications. It does not employ any sophisticated equipment. The obtained results show that the method can be applied in fundamental research of materials, sensors, and for medical diagnosis.

REFERENCES

1. Jodlowski, L., "Measurement of harmonic signal phase using low sampling frequency", in *27th Winter School on Molecular and Quantum Acoustics*, Ustroñ (Poland), 1998, pp. 111-117.
2. Szustakowski, M., Jodlowski, L., and Piszczek M., "Measurements of changes of phase velocity in a fluid using digital signal processing", in *27th Winter School on Molecular and Quantum Acoustics*. Ustroñ (Poland), 1998, pp. 271-280.
3. Szustakowski, M., Jodlowski, L., and Piszczek M., "First experience by using ultrasound in measurement of change brain density", in *1st Interdisciplinary Forum of Stroke,* Wroc³aw (Poland), 1998.
4. Szustakowski, M., Jodlowski, L., and Piszczek M., "Passage time measurement of medium probe signal with the use of phase method with quasi-continuous wave", in *28th Winter School on Molecular and Quantum Acoustics,* Ustroñ (Poland), 1999, pp. 279-289.

Back-Scattering of Ultrasonic Waves by Composites

I.S.Koltzova[a], A.Y.Mikhalev[a]

[a]Institute of Physics, St.-Petersburg State University, Ulyanovskaya st. 1, 198504 St.-Petersburg, Russia

The subject of this paper was experimental study of ultrasonic waves (USW) back-scattering and definition wave impedance, velocity of USW and composite elasticity by the samples reflectivity. The composites under research were 10% gelatine solution (composite 1) and epoxide resin (composite 2), used as polymeric matrices and filled with glass spheres. The average size of particles was 10 mcm, wall thickness 1 mcm, USW frequency 3 MHz, measurements accuracy 1%.

The subject of this paper was experimental study of ultrasonic waves (USW) back-scattering and definition wave impedance, velocity of USW and composite elasticity by the samples reflectivity. Back-scattering and reflection coefficients have been measured with method developed at the Saint-Petersburg State University; it allowed for the first time in the world to discover and measure scattering of USW by particles in biomatrix [1,2].

The parallelepiped sample has been positioned in the center of a cuvette filled with distilled water in the transducer ray-zone. The transducer worked in pulse regime, it's quartz was both emitter and receiver of USW. The transducer could move in plane parallel to the samples surface and rotate around of the sample's center. The sample could turn around itself. In Fig. 1 is shown the concentration dependence of reflection coefficient for composites formed by glass spheres in 10% gelatine solution and for composites formed by glass spheres in epoxide resin . It can be seen from the graph that reflection coefficient increases with growth of particles concentration.

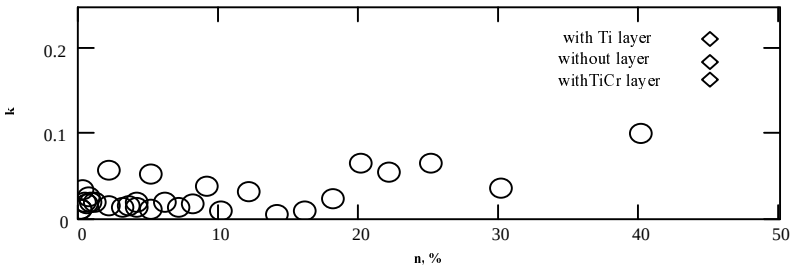

FIGURE 1. Dependence of reflection coefficient for composites 1 (○) on particles concentration (n) and values of reflection coefficient for composites 2 (◊) at volume concentration 50%.

The variation of glass spheres surface properties by titanium (Ti) or titanium-chrome (TiCr) monolayers changed the value of reflection coefficient. The fluctuation of reflection coefficient for composites 1 at volume concentrations n less then 50% appeared to be connected with variations of the particles mutual localization inside the samples. This fact has been proved by measurements of reflection coefficient for composites, where the particles localization varied by remelting of the sample. Let us consider the formula for reflection coefficient k:

$$k = (Z_k - Z_1)/(Z_k - Z_1)\,, \qquad (1)$$

where $Z_k=\rho_{eff}c_k$ – the composite wave impedance, $\rho_{eff}=(1-n)\rho_1+n\rho_2$ – the composite effective density, c_k – velocity of USW in composite, Z_1 – the water wave impedance. By measured reflection coefficient and effective density of composite one can calculate the USW velocity in composite. In Fig 2 the values of USW velocity in composite under research are presented. From this graph the smooth growth of USW velocity with that of concentration can be seen. In the same Fig.2 the values of USW velocity for composites "epoxide resin – glass spheres" at 50% concentration of inserted particles are presented. As one can note according to these data the variation of particles surface properties changes the USW velocity value.

It has been shown by calculating effective compressibility of composites

$$\beta_{eff} = 1/(c_k^2\,\rho_{eff}), \qquad (2)$$

that its value was little differs from that for composites, where inserted particles were glass globes [3].

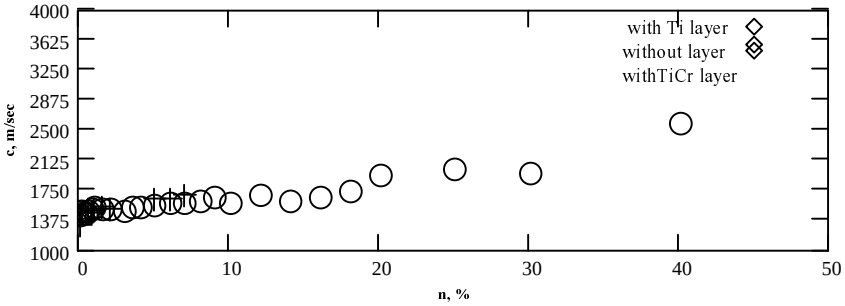

FIGURE 2. Dependence of USW velocity on volume concentration of inserted particles n for composites 1 (○) and composites 2 (◊), calculated by reflection coefficient and for composite 1 (+), measured with pulse-phase method.

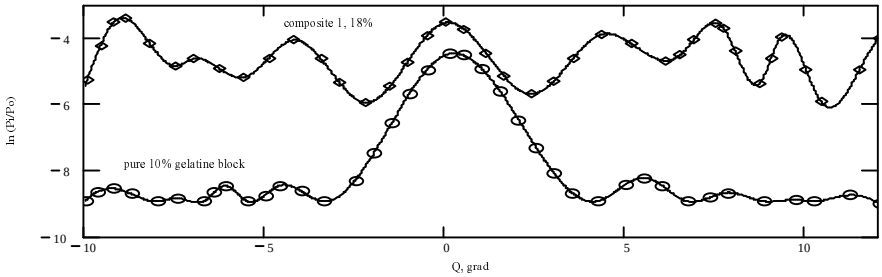

FIGURE 3. Back-scattering of USW by pure 10% gelatine solution block (○) and by composite 1 (◊) with 18% particles concentration

Fig. 3 shows the results of studying back-scattering of USW by the pure 10% gelatine solution block and composite 1 with 18% concentration of glass spheres. It can be seen from the graphs that inserting particles into the matrix increases the level of back-scattering and disturbs the regularity of interferention maximums and minimums which is in agreement with results presented in paper [4]

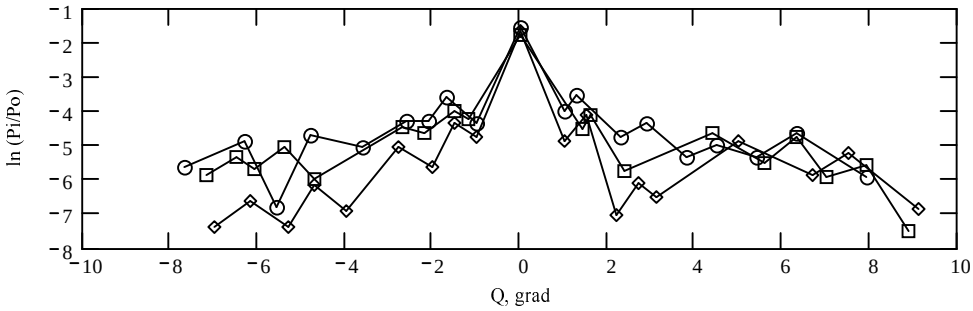

FIGURE 4. Back-scattering by composites 2: ◊ - without layer, □ - with TiCr layer, ○ - with Ti layer.

Fig. 4 presents graphs of back-scattering by composites 2, where particles produce some fractal structure [5]. It can be seen from these graphs that at small angles of back-scattering the tendency to interferention regularity is conserved but it breaks with growth of the angle. The variation of surface properties doesn't influence this tendency.

REFERENCES

1. Koltzova, I.S., and Michailov, Y.G., *Bulletin of the Leningrad University* **3**, 41-45 (1965).
2. Koltzova, I.S., and Michailov, Y.G., *Akust. Zhur.* **21**, 568-575 (1975).
3. Koltzova, I.S., and Mucel Mysun, *Akust. Zhur.* **43**, 362-366 (1997).
4. Quentin, G., and de Billy, M., *J. Acoust. Soc. Am.* **72**, 591-601 (1982).
5. Zosimov, V.V., and Lyamshev, L.M., *Akust. Zhur.* **40**, 703-737 (1994).

Tridimensional Representation of Acoustic Properties of Wood

Bucur V[1], Lanceleur P[2], Rogé B[3]

1 LERMAB, Université Henri Poincaré, Nancy, BP 239, F- 54506, Vandoeuvre, France
2 ROBERVAL Université de Technologie de Compiègne BP 20529 , F- 60205 Compiègne Cedex France
3 Institut for Aerospace Research, 1500 Montreal Road, Building M14, Ottawa, K1A OR6 Canada

Mechanical behaviour of wood considered as an orthotropic solid can be determined with ultrasonic technique. The wave propagation phenomena in wood are complex and theoretically are regulated by Christoffel's equation. These waves are submitted continuously to mode conversion phenomena. The polarisation angle changes when the propagation direction is out of principal directions of symmetry of the material. Tridimensional slowness surfaces were represented to illustrate the acoustic properties of wood. This approach contributes to the understanding of dynamic aspects of particle displacement associated with the wave fronts propagation.

INTRODUCTION

The propagation phenomena of ultrasonic waves in wood, considered as an orthotropic material is complex. Christoffel's equation stated that in each anisotropic plane three type of waves can be identified: one quasi-longitudinal and two quasi-shear waves; or in other words, one fast and two other slow. A review of the literature related to the ultrasonic wave propagation in wood was largely commented by Bucur (1995).
In all cases cited, the plane representation of the slowness surfaces was employed to show the velocity vectors as well as the polarisation vectors of both quasi-longitudinal and quasi-shear waves. It was noted that the denomination of quasi-longitudinal and quasi-shear waves is not convenient for anisotropic materials because during the propagation of ultrasonic waves out of principal directions, mode conversion takes place and the wave converged continuously from one type to anothers (Lanceleur, Ribeiro and al. 1998).
The waves are also referred as P wave for longitudinal waves and for shear waves S waves, rapid and slow .
Such conversion mode phenomena were also currently observed in wood.
The aim of this article is to present a tridimensional representation of the slowness surfaces in wood for a better understanding of propagation phenomena in this material.

RESULTS AND DISCUSSION

This tridimensional coloured representation allows to illustrate the continuous mode conversion of three different types of waves as can be seen from Fig1,2 and 3
The inner slowness sheets are coloured in red and exhibited a flatten ellipsoidal shape, more or less like a "shingle". In the planes X_1-X_2 and X_1-X_3 (axis X_1 being the axis corresponding to the fibres direction) the colour is more or less uniform, and, this means that the polarization is parallel to the propagation vector. In the plane X_2-X_3 the colour varies from red near X_2 to yellow in the vicinity of X_3 and this means that the polarization varies more and more when the angle approach the axis X_3.
This pattern was observed for all species from temperate zones (coniferous and hardwood species).

CONCLUDING REMARKS

Tridimensional representation of slowness surfaces in anisotropic solids is related to the dynamic aspects of particle displacement associated with the wave fronts. This representation for wood species supplies a better understanding of ultrasonic waves propagation through this material and underlines kinematic aspects of wave propagation related to progressive mode conversion.
The anisotropy of different species expressed by their acoustical behaviour is well represented in a global way.

REFERENCES

Bucur, V. 1995. Acoustics of wood. CRC Publ. Boca Raton, USA 285p ISBN 0-8493-4801-3

Lanceleur,P. J.F. de Belleval and N. Mercier. 1998. Synthetic tridimensional representation of slowness surfaces of anisotropic materials. Acustica & Acta Acustica 84,1047-1054

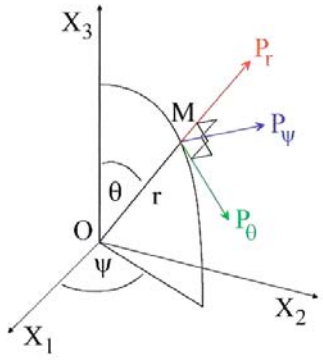

FIGURE 1 Coordinates

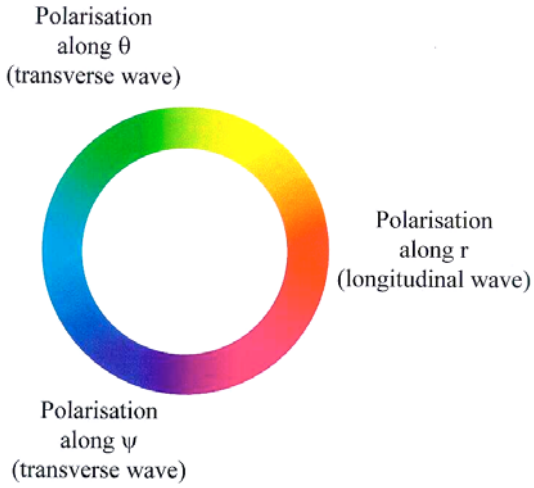

FIGURE 2 Color codeing for waves polarizations

FIGURE 3 Tridimensional representation of slowness curves

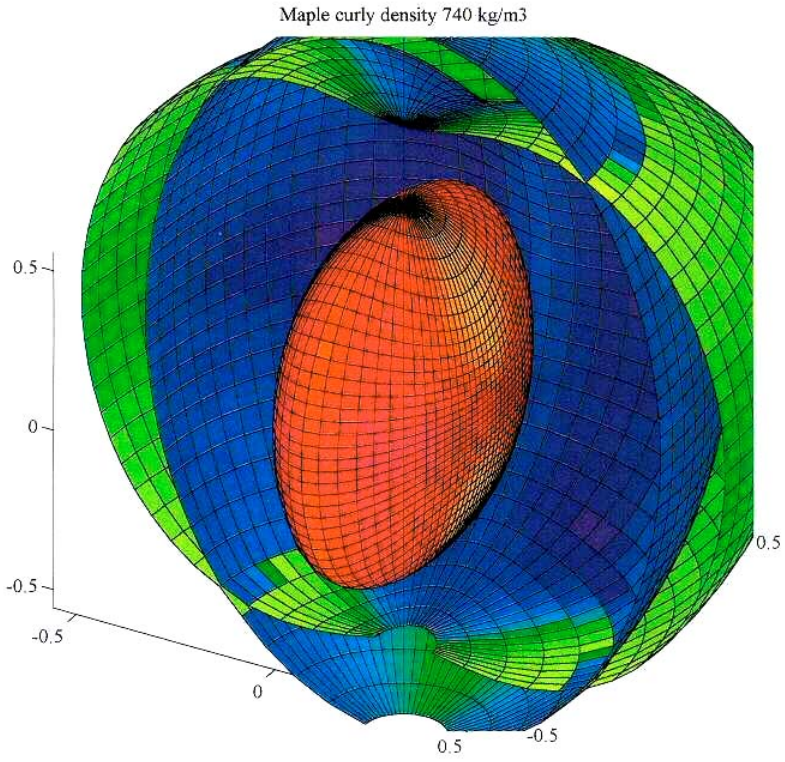

Diffusive and Normal Incidence Sound Absorption of Granular Materials

R. Bartolini[a], P. Ricciardi[a]

[a]*Dipartimento di Termoenergetica e Condizionamento Ambientale, Università di Genova, Via all'Opera Pia 15A, 16145 Genova, Italy*
ricciard@ditec.unige.it

Experimental results in superficial acoustic absorption measurements for porous materials, used as components in absorbent panels, are discussed. Normal and diffuse incident sound absorption coefficient are obtained by means of impedance tube and reverberant room methods, operating with various material layer thickness.

Theoretical approach, available in literature, on possible correlation between normal and random incidence absorption coefficients, has been examined.

A model suitable for this particular type of material has been applied. The correlation could provide diffuse sound absorption data, useful for practical applications, from laboratory results.

INTRODUCTION

In room acoustics knowledge of diffuse sound absorption coefficient of materials applied to the walls is of prime importance, and determination of this parameter is generally obtained by the reverberant room method or by in field measurements. In both cases large samples and complex procedures are needed.

In design and developing of new acoustic panels, constituted of powder beds, porous materials and multi-layer structures, that show interesting absorption properties, it is of considerable importance the possibility of determination of diffuse absorption coefficient from laboratory measurements on small samples.

The impedance tube measurement method allows to obtain acoustic impedance and normal incidence absorption coefficient of small samples.

Relations between normal and diffusive sound absorption can provide useful prediction of large acoustic panels behaviour from simple laboratory determination.

ABSORPTION COEFFICIENTS OF GRANULAR MATERIAL

In previous works [1, 2, 3] absorption coefficient measurements have been carried out by the authors on samples of granular clay with diameters of 2-3 cm, positioned in layers of 5, 10, 15, 20 cm of thickness. In [1, 2] experimental results of superficial diffusive absorption coefficient of granular media has been obtained by reverberant room method [4]. In [3] normal impedance Z_n of the material, and consequentely, superficial normal absorption coefficient have been tested by an impedance tube [5]. In figures 1 and 2 experimental results are plotted.

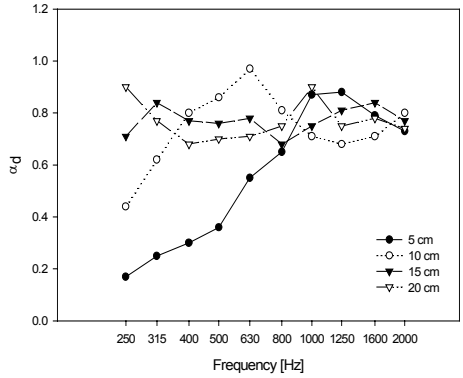

FIGURE 1: Experimental diffusive absorption coefficient versus frequency

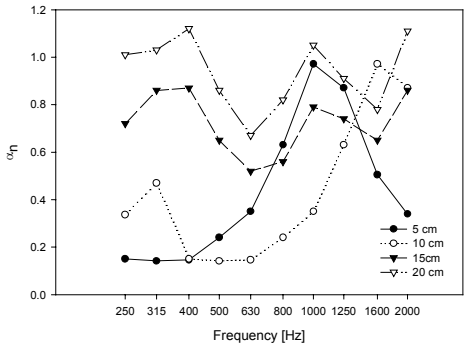

FIGURE 2: Experimental normal absorption coefficient versus frequency

STATISTICAL DIFFUSIVE COEFFICIENT

Relations between normal and diffusive sound absorption data have been theoretically derived and are available in literature [6, 7].

Sound absorption coefficient, for a wave incident at angle θ on the acoustic material, is deducted from normal acoustic impedance Z_n, obtained by the impedance tube method, by the expression:

$$\alpha_\theta = 1 - \left| \frac{Z_n \cos\theta - \rho c}{Z_n \cos\theta + \rho c} \right|^2 \qquad (1)$$

where ρc is the acoustic impedance of air.

The diffuse incident absorption coefficient can be statistically calculated by following equation:

$$\alpha_{st} = \frac{\int_0^{\pi/2} \alpha_\theta \sin\theta \cos\theta d\theta}{\int_0^{\pi/2} \sin\theta \cos\theta d\theta} = 2 \int_0^{\pi/2} \alpha_\theta \sin\theta \cos\theta d\theta \qquad (2)$$

The above considerations are valid under the assumption of local reactive behaviour of the absorbing material: this means that even if sound wave is obliquely incident, vibration inside material occurs in direction normal to the surface. This assumption is generally suitable for porous materials.

By means of equations (1) and (2) "statistical diffuse absorption coefficients" have been calculated for the examined samples from impedance values given in [3] for 4 different layer thickness.

Figure 3 shows a comparison between statistical diffusive coefficients and reverberant absorption coefficients for the 4 analysed thicknesses.

Regression coefficients have higher values for thickness of 5 and 10 cm rather than of 10 and 15, but thickness of 5 and 10 present a different trend for frequencies above 1250 Hz.

CONCLUSIONS

Examined procedure, to obtain diffused absorption coefficient from acoustic impedance values has been applied to granular material data. This method can be considered as a first prediction tool to get reverberant diffuse absorption coefficient useful in design and developing of new acoustic materials.

REFERENCES

[1]. Ricciardi, P., Bertucci, M., Di Bella, A., Magrini, U., Zecchin, R. - *Proprietà acustiche di materiali inerti porosi a struttura sferica: analisi teorica e prove sperimentali* , XXVII Convegno Nazionale A.I.A., Genova, 1999, p. 120-123.

[2]. U. Magrini, P. Ricciardi, *Surface sound acoustical absorption and application of panels composed of granular porous material"* INTER-NOISE, Nizza, France, 2000, p. 1-7.

[3]. R.Bartolini, C. Schenone –Coefficiente di assorbimento acustico ad incidenza normale di materiale granulare 28° Convegno Nazionale AIA, Bari, 10-13 June 2000, p. 197-200.

[4]. Standard UNI EN 20354-89, Acustica, Misura dell'Assorbimento Acustico in Camera Riverberante

[5]. Standard ASTM C 384-95, Standard Test Method for Impedance and Absorption of Acoustical Materials by the Impedance Tube Method, ASTM Philadelphia USA.

[6]. A. London, *J.Acoust. Soc. Am*., **22**, 263 (1950).

[7]. Y.Okudairaa, H. Ando, M. Satoh and K. Miyaanami – El. *Eng. In Japann*, **122**, (1988).

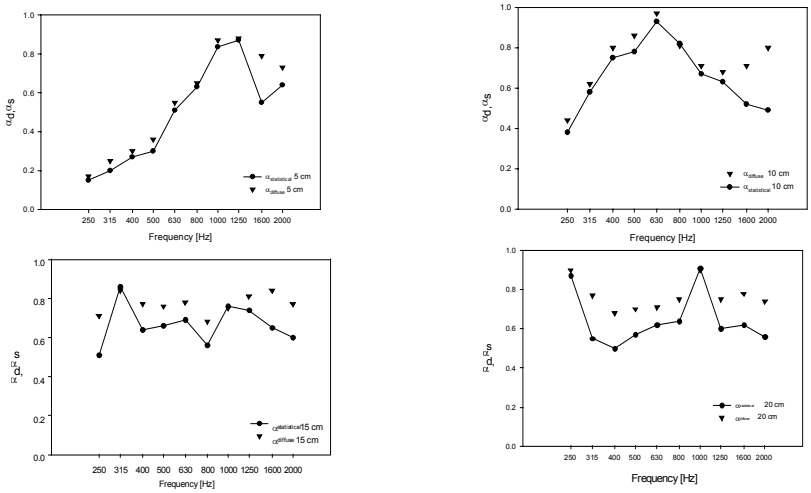

FIGURE 3- Comparison between statistical diffusive coefficient and reverberant absorption coefficient of the 4 sample thicknesses.

Reducing Artifacts of In-situ Surface Impedance Measurements

Matti Karjalainen and Miikka Tikander

Helsinki University of Technology,
Laboratory of Acoustics and Audio Signal Processing,
FIN-02015 HUT, Espoo, Finland

This paper describes developments of an in-situ measurement system for acoustic surface material measurements. It is based on the generally known 'loudspeaker plus one-microphone' technique whereby the difference of free-field calibration response and surface-reflected response is analyzed. Special attention is paid to signal processing methods in order to minimize artifacts from the acoustic setup and signal analysis (windowing) needed.

INTRODUCTION

In-situ techniques have been developed for some time [1,2], but they are found to exhibit problems that are difficult to overcome. In this paper we propose a number of methods that can improve the results of measurements when using a sound source (loudspeaker) and a microphone near the surface to be measured (Fig.1). When a free-field calibration response $h_r(t)$ is available and the response $h_m(t)$ with a microphone near a surface is measured, the reflected response is $h_m(t)$ - $h_r(t)$. When this is compensated with the reference response, in the frequency domain $H(\omega) = [H_m(\omega)-H_r(\omega)]/H_r(\omega)$, a reflection response is obtained. The surface impedance or absorption coefficient is easily obtained if the reflectance response has been reliably measured. An essential part of the technique is to apply time-domain windowing of the responses in order to exclude reflections from neighboring surfaces as well as diffraction from the edges of the surface of interest.

The method is found sensitive to any degradations of measured responses. Thus most care should be taken to obtain accurate and reliable results. An inherent limitation comes from the time-domain windowing, which restricts frequency-resolution as well, setting a practical low-frequency limit. In this paper we discuss several signal processing techniques for improving this basic in-situ technique.

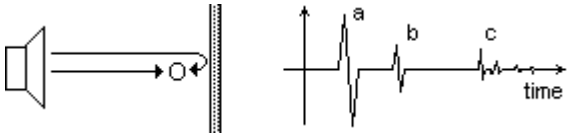

FIG. 1. On the left system setup, on the right an impulse response: a) direct sound b) reflection c) parasitic reflections.

SYSTEM IMPROVEMENTS

The in-situ setup we have developed consists of loudspeaker of spherical enclosure (ø 150 mm), an electret microphone (Sennheiser KE 4-211) 32 cm from the speaker, and a computerized data acquisition system with easy programmability. We have implemented our impulse response measurements using a fast chirp excitation (Schroeder phase sequence) and deconvolution instead of maximum length sequences (MLS), because MLS may yield distorted results when there are nonlinearities in the signal path [3], especially in the loudspeaker. As other minor experiments we tried careful time alignment of the calibration and test direct responses, continuation of the windowed responses by ARMA modeling (Prony's method), and averaging of responses obtained with different microphone distances from the surface. In practice, only minor or no improvements resulted.

Using a hard surface reference

Panel (a) in Fig. 2 plots an example of measured reflection from a surface as well as a time window (rectangular + half of hanning) to cut out parasitic reflections from neighboring walls and edges of the surface to be measured. Panel (b) depicts the result of subtracting the test response and the reference to yield the reflected signal.

Although very carefully measured, the free-field reference (corresponding to peak (a) in Fig. 1) does not yield optimal cancellation in measurement near a surface. In the example of Fig. 2 there was an absorbing material (mineral wool, 20 mm) on a hard wall and the absorption coefficient was computed as a function of frequency. Black squares in (d) indicate the measurement result obtained using impedance tube (B&K

4187) and black circles corresponding data from reverberation room measurement. Thin solid line is the resulting absorption coefficient computed from the in-situ measurement when the reference was measured in pseudo free field and the tested material was in a distance of 6 cm from the absorption material. It is in general agreement with standard techniques above approximately 400 Hz, but below that is entirely unreliable and fluctuates strongly.

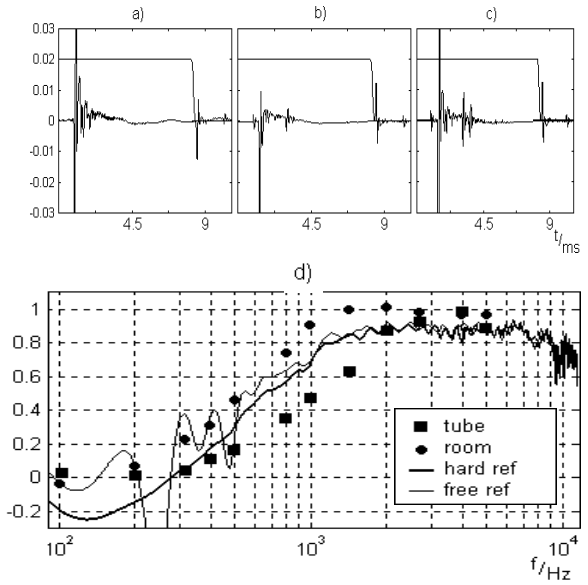

FIG. 2. a) Reference response, b) subtracted reference measurement of absorbing material, c) subtracted hard surface reference of absorbing material, and d) absorption coefficient with four different methods (see text).

As an alternative to the free-field reference, a hard surface reflection was measured and applied. This was achieved by subtracting the free-field response from the hard surface response. Otherwise the measurement technique was similar as mentioned above. The distance to the surface to be measured is kept the same in the hard surface reference measurement and in the material measurement.

As indicated by the thick solid line in Fig. 2, the absorption coefficient behaves more smoothly, although it shows also non-physical negative values at lowest frequencies. Especially when the measurement setup is exactly the same for reference and material measurement except that the material is inserted between the hard surface and microphone, the method works well (although it is not a generic in-situ method anymore).

Model-based curve fitting

Another way to obtain smooth measurement curves and material parameters is to apply model-based curve fitting. If the general behavior of the material under study is available in the form of a parametric model, (nonlinear) optimization techniques can be used. Figure 3. plots the absorption coefficient of the case discussed above and a model-based fit to the measured data. Fitting was applied to the complex-valued reflectance function as a low-order digital filter model. A model with better physical interpretation could be easily developed.

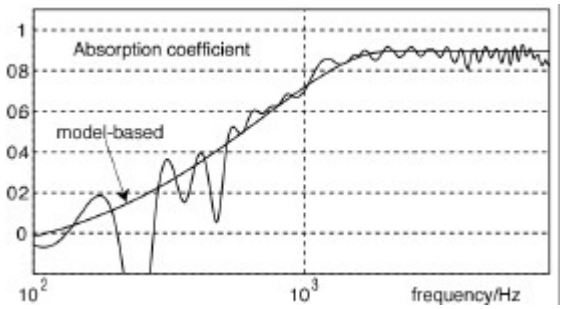

FIG. 3. Model-based curve fitting for smoothed absorption curve.

Model-based curve fitting is a useful method as far as there is evidence enough that the model used is physically valid for the case under study. On the other hand, it may easily yield inaccurate results that look reliable due to the smoothness of curves, and should therefore be used with caution.

ACKNOWLEDGMENT

This study is part of a TEKES project VÄRE/TAKU.

REFERENCES

1. Mommertz E., *Angle dependant in situ measurement of the complex reflection coefficient using a subtraction technique*, Applied Acoustics, vol. 46, 1995, pp. 251-263.
2. Garai M., *Measurement of the sound absorption coefficient in situ: The reflection method using periodic pseudo random sequences of maximum length,* Applied Acoustics, vol. 39, 1993, pp. 119-139.
3. Farina A., *Simultaneous measurement of impulse response and distortion with a swept-sine technique*. Reprint 5093. AES 108th Convention, Feb. 2000, Paris, France.

The Application of the Acoustic Interferometer to the Study of the Boundary Layers in Polymer Composite Fibers

S. P. Senchurov, Yu. F. Zabashta

Kiev Shevchenko University, Physics Faculty, Molecular Physics Dep., 03022, Glushkov Pr. 6, Kiev, Ukraine
e-mail: sergsenc@mail.univ.kiev.ua

Sound interference in polymer composite fibers with thin boundary layer at the components' interface was considered. Shape of the acoustic interferogram taken from the fiber was calculated analytically. Frequency dependence of the shape of the interferogram found. If the sound frequency is smaller than the “critical” frequency then the interferogram is a periodical function of the distance between the sound emitter and the sound detector. If the sound frequency is bigger than the “critical” frequency then the interferogram becomes non-periodical function of the distance between the sound emitter and the sound detector. The possibility of pointing out the "critical" frequency according to the shape changes of the interferogram was shown. Theoretical dependence of the “critical” frequency on the properties of the boundary layer was found. As a result a new method of the non-destructive measurement of the properties of boundary layers in polymer composite fibers based on the analysis of the shape of the interferogram can be created.

Our study deals with the widely used kind of composite fibers - composite fibers, which consist of cylindrical core (glass) and polymer cylindrical shell. It is well known fact that boundary layer appears at the border between the components of the composite. The structure and properties of this layer are significantly different from those of components. Properties of the composite material strongly depend on the properties of the boundary layer. So the possibility to measure the properties of the boundary layer in composite fibers in a non-destructive way is very important.

We suggest to use the acoustic interferometer to measure the properties of the boundary layer in polymer composite fibers. In the acoustical interferometer the fiber being studied is fastened to the sound emitter with one end. The other end of the fiber is thrown over the pulley and is pulled with the weight. The sound detector is travelling along the fiber. Incident sound wave from the emitter and reflected wave from the detector form the standing wave. Acoustical interferogram is the dependence of the sound intensity U (Y-axis in volts in figures) on the distance between sound emitter and sound detector l (X-axis in meters).

Theory of the acoustical interferometer [1] predicts that the interferogram taken from the homogeneous fiber has the shape shown in Figure 1. This shape is a periodical function of the distance between the sound emitter and the sound detector. Let us for convenience call this shape “classical”.

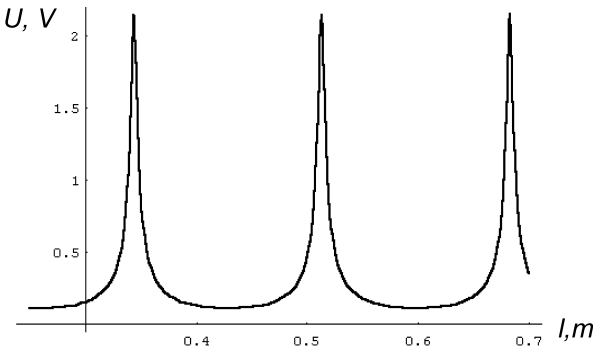

FIGURE 1. The shape of the interferogram taken from the homogenous fiber

In our previous work [2] we have shown that one or two normal axisymmetric waves can simultaneously propagate in polymer composite fiber. The cut-off frequency of the second wave is

$$\omega_0 = \sqrt{\left(\frac{1}{\rho' S'} + \frac{1}{\rho'' S''}\right)\frac{2\pi R \mu'''}{h}} \qquad (1)$$

where R is the radius of the core, ρ', ρ'' are the densities of core and covering respectively, S', S'' are the areas of the cross-section occupied by the core and the shell, μ''' is the Lame constant of interface layer (shear modulus), h is the thickness of the boundary layer. If the sound frequency ω is smaller than ω_0 then only one normal axisymmetric wave can

propagate along the fiber and if $\omega > \omega_0$ then two normal axisymmetric waves can propagate along the fiber. All the calculations in [2] were made in a long wave approximation assuming the wavelength λ to be much greater than the radius of the fiber R_{fiber} ($\lambda >> R_{fiber}$).

If $\omega < \omega_0$ then the shape of the interferogram is "classical". To obtain the shape of the interferogram for $\omega > \omega_0$ we should consider the interference of the above mentioned two waves in the fiber. We should solve the problem of sound propagation in the polymer composite fiber between the sound emitter and the sound detector. For this purpose we can use the solution of the problem of sound propagation in infinite fiber [2] and satisfy the boundary conditions at the sound emitter and the sound detector like it was done in [1].

If $\omega > \omega_0$ then two waves with different wave numbers k_1 and k_2 and different profiles $U_1(r,k_1)$, $U_2(r,k_2)$ can simultaneously propagate in the fiber in each direction:

$$U = U_1(r,k_1)\exp(i\omega t \pm ik_1 l) + U_2(r,k_2)\exp(i\omega t \pm ik_2 l) \quad (2)$$

where U is the displacement of the particles of the fiber in the direction of the axis of the fiber and "$\pm$" means that one set of waves with the wave number (k_1 and k_2) is propagating in positive direction, and the other set of waves is propagating in negative direction. The presence of the sound emitter can be taken into account with boundary condition at $l = 0$

$$U(l = 0, t, r) = u_0 \exp[i\omega t] \quad (3)$$

Boundary conditions at $l = l_{\text{detector}}$ are the continuity of displacements

$$U(l = l_{\text{detector}} - 0, t, r) = U(l = l_{\text{det ector}} + 0, t, r) \quad (4)$$

and continuity of tensions

$$\sigma(l = l_{\text{det ector}} - 0, t, r) = \sigma(l = l_{\text{det ector}} + 0, t, r) + F \quad (5)$$

before and after the detector,

$F = -\kappa U(l = l_{\text{detector}}, t, r = R_{fiber})$ is the intensity of external force from the sound detector, applied at $l = l_{\text{detector}}$. The profiles of the waves $U_1(r,k_1)$, $U_2(r,k_2)$ are not uniform over the cross-section of the fiber [2], so the conditions (4,5) cause two types of waves to exchange the energy at $l = l_{\text{detector}}$.

Substituting sets of waves, propagating in each direction (2) into (3-5), we calculated the shape of the interferogram $|U(l = l_{\text{detector}}, t, r = R_{fiber})| = f(l_{\text{detecror}})$. This shape is shown in Figure 2 and we name it "non-classical".

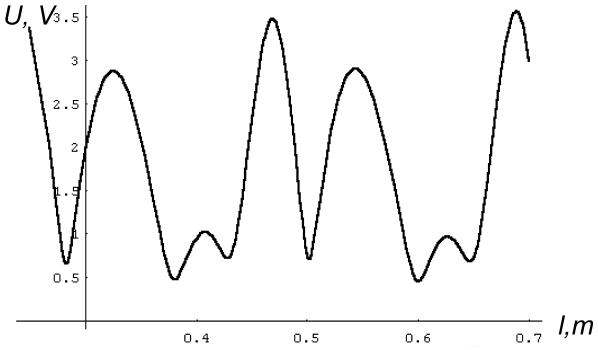

FIGURE 2. The estimated shape of the interferogram from the composite fiber if the sound frequency ω is bigger then the cut-off frequency ω_0.

So if we take a number of acoustical interferograms from the polymer composite fiber consecutively at growing frequencies and the shape of the interferogram changes from classical to non-classical, we can determine the cut-off frequency ω_0. Then we can measure the thickness of the boundary layer h in some other way, for instance, optical. If we know the cut-off frequency and the thickness of the boundary layer we can calculate the shear modulus of the boundary layer.

This is the main idea of our method of studying the boundary layers in composite fibers.

REFERENCES

1. J. W. Ballow, J. C. Smith., *J. Appl. Phys.* **20**, 493-503 (1949)

2. L. A. Bulavin, S. P. Senchurov Yu. F. Zabashta., *J. of Sound and Vibration* **231**, 1179-1187 (2000)

In Situ Determination of Acoustic Absorption Coefficient of a Barrier: Which kind of Source?

E. Crema[a], P. Martignon[b], S. Stabile[c], M. Zanolin.[d]

[a] *Studio Alfa S.r.l., Reggio Emilia (RE)*
[b] *Physical Dept., University of Parma (Italy)*
[c] *Prometeo Electroacoustic Laboratory*
[d] *MIT, Boston (U.S.A.)*

Using the basic principles of the Wave Field Synthesis it is possible, by means of linear arrays of sound sources, to generate a concave acoustic field which theoretically should represent a useful sound source to measure the reflection index of an extended area of a surface. We propose a new approach to characterise the mean properties of a non uniform surface, method which allows to reduce the number of measurements and calculations required and to simplify the post processing procedure. A future extension of this approach may lead to the possibility of separating between acoustic absorption and diffusion surface processes.

INTRODUCTION

Measurement methods for *in situ* characterisation of acoustic materials, play an important role in the case of outdoor use of acoustic devices like noise barriers.
Nowadays, some *in situ* measurement method has been proposed: between them we can mention the AFNOR NFS 31-089, translated and adopted in Italy like a project rule (UNI U20-00-050-0) and still waiting for a European Rule that overcomes the limits still present, that are:

- poor repeatability of a measurement (the source is a blank shot gun)
- high minimum frequency of applicability (350 Hz)
- validity limited to flat or quasi-flat surfaces
- operating difficulty in the case of oblique incidence.

Actually, the most credited method (still waiting for the approval of European Commission) is the "*Adrienne method*" which rises from an European project [1] and which is based on a pseudo-impulsive technique that uses a MLS signal-test and whose post-processing is based on synchronous time subtraction of the reference signal and application of particular time windowing [2,3]. The Adrienne method seems to suffer of the following limitations:

- operating difficulty in making accurate angular measurements;
- large number of measurement points, especially in the case of strongly non uniform surfaces;
- necessity to use, during the post processing, correction factors that takes account of the divergence and that, contemporary, increase the propagation error.

The Proposed Method: Basic Principles

The Wave Field Synthesis (WFS in the following) control of loudspeakers linear arrays, formally described by 2D approximation of Kirchhoff-Helmholtz integrals, allows the reproduction of an arbitrary sound field on a large area, thus representing a so called "*Volume solution*". An extremely interesting consequence of the WFS approach is the possibility to recreate the field of a virtual source placed in front of the array (sound focusing) as shown in Figure 1: this can be achieved by giving to each single speaker different signal gains and delays, according to speaker-focus distance [4,5,6].

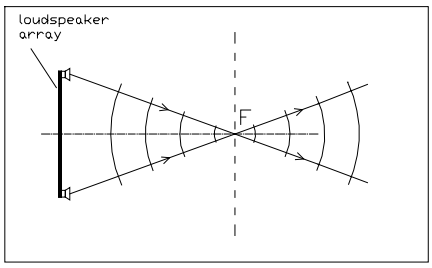

FIGURE 1: Focusing of Sound

The New Method

Our idea is to take advantage of the concave field, generated between the array and the focus (F), in order to concentrate in a single point (reflected focus, F_1) the reflection arising from an extended area of the test surface, as shown in Figure 2.

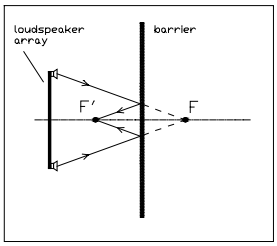

FIGURE 2: Barrier and reflected focus

Basically the proposed method consists of three Impulse Response (IR) measurements: $h_F(t)$, made in the focus in the absence of the barrier, which takes into account the free field plus, eventually, the reflection IV (see Figure 3); $h_{F'd}(t)$, made in the estimated reflected focus in the absence of the barrier too, which takes in account the free field in this new point plus, eventually, the reflection I; finally, $h_{F'b}(t)$, made in the real reflected focus in presence of the barrier, which takes in account the direct field plus the reflections III and eventually I and II.

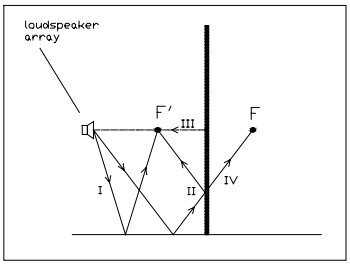

FIGURE 3: Involved reflection types

Data Processing

Synchronously subtracting the impulse response $h_{F'd}(t)$ from $h_{F'b}(t)$ only the contributions of reflection III and, eventually II remain: we call this new function, $h_{F'}(t)$. Then an appropriate time windowing, necessary to eliminate reflections II and IV, is applied and a Fourier Transform is carried out. Calling $H_F(\omega)$ the FT magnitude of $h_F(t)$ and $H_{F'}(\omega)$ the corresponding FT magnitude of $h_{F'}(t)$, we calculate the ratio:

$$R = \frac{|H_{F'}(\omega)|^2}{|H_F(\omega)|^2} \qquad (1)$$

Formula (1) represents an estimate of the mean reflection index R, that in an ideal case should be 1 over all the frequency spectrum. This index is determined by the occurrence of two distinct physical processes, absorption and diffusion whose separation is a difficult task. Considering for a moment the ideal case, i.e. an infinite array made of point sources, theoretically it should be possible to obtain a sound field that, on the focusing line, is completely concentrated in the focus being zero elsewhere on the line itself. In this case, a second set of measurements made in other points on this line than the focus, should allow to discriminate the two contributions, because in case of an ideal reflection the value of the index in these points should be zero, the residual energy thus At high frequencies this behaviour is quite well guaranteed also in the practical case [6] and the goal of separating the two contributions should be quite simple. We are currently investigating on the number of secondary measurements to be carried out in order to achieve this goal, number that should be frequency dependent.

Advantages of the New Method

The main advantages that seem to arise by using the proposed measurement method in determining the reflection index of a non uniform surface are:

1. Only three measures are necessary to determine the mean Reflection Index of the tested surface instead of the 18 required by the Adrienne Method.
2. The measurement setup is geometrically fix, thus more stable.
3. The post-processing of the measured data is faster and easier. The reflection index values arising from this procedure is the actual physical mean of all the contributions coming from a continuous portion of the surface; no mathematical meaning procedures are necessary at all.
4. Finally, increasing the number of measurements, with this approach it seems possible in principle to discriminate the two main processes that occur on the surface, i.e. absorption and diffusion.

REFERENCES

[1] European Commission, "Test Methods for the Acoustic Performance of Road Traffic Noise Reduction Devices", DGXII-SMT Project Mat1 – CT94049 Final Report, 1st Edition February 1998

[2] Garai M., "Measurement of the Sound Absorption Coefficient in situ: the Reflection Method Using Periodic Pseudo-Random Sequences of Maximum Length", Appl. Acoust. **39**, 119-139 (1993)

[3] Garai M., "Caratteristiche Acustiche delle Barriere" in Atti del Convegno Nazionale Traffico & Ambiente, Trento, 21-25 Febbraio 2000.

[4] Berkhout A.J., "An Holography Approach to Acoustic control", J. Audio Eng. Soc. (1988).

[5] Start E.W., "Direct Sound Enhancement by WFS", thesis, Delft University of Technology (1997).

[6] Martignon. P, Tesi di Laurea, Università degli Studi di Parma, Dipartimento di Fisica, (2001).